ADVANCED ENERGY MATERIALS
www.advenergymat.de

Are Polymer-Based Electrolytes Ready for High-Voltage Lithium Battery Applications? An Overview of Degradation Mechanisms and Battery Performance

Maria Angeles Cabañero Martínez, Nicola Boaretto, Andrew J. Naylor, Francisco Alcaide, Girish D. Salian, Flavia Palombarini, Elixabete Ayerbe, Mateu Borras, and Montserrat Casas-Cabanas**

High-voltage lithium polymer cells are considered an attractive technology that could out-perform commercial lithium-ion batteries in terms of safety, processability, and energy density. Although significant progress has been achieved in the development of polymer electrolytes for high-voltage applications (> 4 V), the cell performance containing these materials still encounters certain challenges. One of the major limitations is posed by poor cyclability, which is affected by the low oxidative stability of standard polyether-based polymer electrolytes. In addition, the high reactivity and structural instability of certain common high-voltage cathode chemistries further aggravate the challenges. In this review, the oxidative stability of polymer electrolytes is comprehensively discussed, along with the key sources of cell degradation, and provides an overview of the fundamental strategies adopted for enhancing their cyclability. In this regard, a statistical analysis of the cell performance is provided by analyzing 186 publications reported in the last 17 years, to demonstrate the gap between the state-of-the-art and the requirements for high-energy density cells. Furthermore, the essential characterization techniques employed in prior research investigating the degradation of these systems are discussed to highlight their prospects and limitations. Based on the derived conclusions, new targets and guidelines are proposed for further research.

1. Introduction

In the past decades, the significant advancements in Li-ion battery (LIB) technology have enabled the portable electronics revolution and the increased availability of affordable battery electric vehicles (BEVs). Consequently, the success of LIB has recently garnered additional interest towards their implementation in nonautomotive applications such as grid storage coupled with renewable energy sources.

Despite the continuous progress of LIBs, still several technical challenges should be addressed to satisfy the requirements of future applications. Thus, next-generation batteries must be cost-effective, safe, sustainable, durable, and avoid the use of critical raw materials).[1] In addition, the energy density must be further increased, especially for automotive applications.

The energy density can be increased by increasing the cell voltage. Currently, commercial LIBs exhibit a typical cell voltage

M. A. Cabañero Martínez, N. Boaretto, M. Casas-Cabanas
Center for Cooperative Research on Alternative Energies (CIC EnergiGUNE)
Basque Research and Technology Alliance (BRTA)
Parque Tecnológico de Alava
Albert Einstein 48, Vitoria-Gasteiz 01510, Spain
E-mail: macabanero@cicenergigune.com; mcasas@cicenergigune.com

The ORCID identification number(s) for the author(s) of this article can be found under https://doi.org/10.1002/aenm.202201264.

DOI: 10.1002/aenm.202201264

A. J. Naylor, G. D. Salian
Department of Chemistry—Ångström Laboratory
Uppsala University
Box 538, Uppsala 75121, Sweden

F. Alcaide, E. Ayerbe
Materials for Energy Unit
CIDETEC Basque Research and Technology Alliance (BRTA)
Paseo Miramón 196, Donostia/San Sebastián, Guipuzcoa 20014, Spain

F. Palombarini, M. Borras
Energy Storage
LEITAT Technological Centre
C/ de la Innovació, 2, Terrassa, Barcelona 08225, Spain

M. Casas-Cabanas
IKERBASQUE
Basque Foundation for Science
María Díaz de Haro 3, Bilbao 48013, Spain

of ≈3.7 V, with an upper cut-off voltage of ≈4.2 V. Recently, research efforts have focused on augmenting the operating voltage,[2–4] which constitutes a major challenge, as it can result in a premature loss in capacity.[5] This is caused by the high-voltage instability (>4.3 V vs Li/Li^+) of the organic carbonate-based solvents employed in standard liquid electrolytes. Alternatively, the cell energy density can be improved with the use of lithium metal anodes. Unfortunately, lithium electroplating in the form of dendrites can cause short circuiting, which poses serious safety issues with flammable liquid electrolytes.[6] Although several advancements have been achieved to avoid dendrite formation with liquid electrolytes,[7] solid-state electrolytes (SSEs) are regarded as the most viable solution for high voltage batteries with lithium metal anodes.[8,9]

Solid electrolytes can be broadly divided into two categories: inorganic electrolytes and polymer electrolytes, wherein the latter is particularly interesting owing to their favorable mechanical properties and processability. In general, polymer-based electrolytes include solid polymer electrolytes (SPEs), that is, complexes of a lithium salt with a polymer matrix, in presence of a plasticizer at certain instances, gel-polymer electrolytes (GPEs), which contain over 20–30 wt.% of liquid component,[10–12] and hybrid solid electrolytes (HSEs), namely mixtures of lithium-conducting inorganic electrolytes with polymer electrolytes.[13,14] Depending on the content of liquid components, composite polymer electrolytes (CPEs) containing non-conductive fillers[15] can be classified as SPEs and GPEs, because of the transport properties and charge transport mechanism of CPEs are not substantially distinct from them.

The low ionic conductivity of polymer electrolytes constitutes its fundamental weakness. At room temperature, the conductivities of semicrystalline SPEs are typically below 10^{-5} S cm^{-1}, whereas amorphous SPEs can attain 10^{-4} S cm^{-1}.[16] Thus, the ionic conductivity of SPEs is significantly less than that of commercial liquid electrolytes (5–10 mS cm^{-1} at room temperature).[17,18] Moreover, higher conductivities, between 10^{-4} and 10^{-3} S cm^{-1} can be achieved using GPEs,[12,19,20] and plasticized SPEs.[21–28]

Moreover, HSEs may attain higher conductivities than the corresponding non-hybrid SPE, because conduction occurs through both polymer and ceramic phases (ceramic phase is generally more conductive than the organic phase).[14] Unfortunately, the presence of low-conducting impurities at the interphase (e.g. Li_2CO_3 with garnet-type ceramics), and the high activation energy for the charge transfer process can produce high interfacial resistance between the two phases and in an overall conductivity that is below expectations.[29] HSEs with a gel-type organic phase can often achieve even higher conductivities, owing to the introduction of liquid components.[30]

Overall, the transport properties of polymer electrolytes are related to their mechanical properties.

In amorphous SPEs (primarily polyether-based SPEs), the charge transport relies on the segmental motion of the polymer chains (liquid-like conduction mechanism), and the ionic conductivity (σ) is related to the glass transition temperature (T_g) of the polymer electrolyte through the Vogel–Fulcher–Tamman equation $\sigma \propto \exp[-B/(T-T_0)]$,[31] where T_0 is known as the ideal glass transition temperature, with typical values of $\approx T_0 - T_g - 40$. In contrast, in semicrystalline SPEs the charge motion is decoupled from the segmental motion (solid-like conduction mechanism), and σ follows an Arrhenius dependence on the temperature $\sigma \propto \exp(-E_a/kT)$, where E_a is the activation energy and k is the Boltzmann constant. Although ionic conductivity has been demonstrated also in crystalline SPEs,[32–35] the conductivity of crystalline and semi-crystalline PEO-based SPEs is typically less than that of amorphous counterparts. In worst cases, this translates into a sudden conductivity drop below the crystallization temperature, and in best cases, in an increased conductivity activation energy in the (low-temperature) semicrystalline region. Thus, considerable effort has been invested in obtaining amorphous SPEs at room temperature and in lowering the T_g. Nonetheless, amorphous SPEs with low T_g are generally characterized by inferior mechanical properties.[36] The electrolyte mechanical stability is critical for tolerating repeated volume variation in electrodes during the cycling process[37] and inhibiting the formation of Li dendrites.[38] In principle, dendrites growth is one of the other major hurdles in the development of lithium metal polymer batteries.[39] Accordingly, several strategies can be implemented to hinder dendrite's growth. A general approach involves improving the mechanical strength of the electrolytes, for instance, by adding inorganic particles in CPEs,[40–44] crosslinking,[45,46] or developing block copolymer electrolytes.[47–49] Alternative approaches include the use of single-ion conducting polymer electrolytes (SICPEs),[50,51] the combination of various solid electrolytes in a multi-layered configuration,[52] fabricating nano-structures for the lithium anode[53–55] or electrolyte,[56] and engineering the lithium/electrolyte interface, —either by coating the lithium surface[57,58] or introducing solid electrolyte interface (SEI)-forming additives in the electrolyte.[59,60]

Despite all these issues, polymer electrolytes have been successfully applied in commercial lithium batteries for several years (e.g., LMP Bolloré batteries).[61] The cathode selected for these commercial applications is LFP ($LiFePO_4$), which operates at potentials of approximately 3.45 V versus Li/Li^+. Thus, the long-term cycling stability of SPEs in LFP-Li cells has been demonstrated. Recently, Blue Solutions from Bolloré achieved 1300 cycles.[62]

To enhance the cell energy densities, research and industrial efforts are currently focusing on the development of high-voltage lithium polymer (HVLP) batteries, by combining polymer electrolytes with 4V-class cathodes such as LCO ($LiCoO_2$), NMC ($LiNi_xMn_yCo_zO_2$) or NCA ($LiNi_{0.85}Co_{0.1}Al_{0.05}O_2$) in lithium metal batteries. The combination of high-voltage cathode materials and polymer electrolytes necessitates new requirements primarily related to the chemical and electrochemical compatibility of the cathode and electrolyte material.

Owing to the mentioned potential benefits of polymer electrolytes (safety, processability, energy density) and the current attention towards high-energy lithium batteries, polymer electrolytes are experiencing a renewed interest, with almost one thousand research articles and over 50 reviews published in only the last five years (source Web of Science). Among these, several reviews describe the general progress in SSEs,[63–70] or in specific classes of polymer electrolytes[14,71–81]

Certain reviews have specifically focused on the interfaces in solid-state batteries[82–85] and, particularly, on the issues related to the use of lithium metal anodes.[39,86–88] Correspondingly,

only a few recent reviews are focused on the cathode interface and the possible application in HVLP batteries.[89–92] To broadly summarize the conclusions of prior research, the compatibility of polymer electrolytes with 4 or 5V-class cathode materials can be deemed as satisfactory, but the long-term cyclability with high-voltage materials has not yet been proved. More importantly, no single class of SPEs or GPEs can be explicitly singled out for high-voltage applications, and the understanding of the electrolyte degradation mechanism at the electrodes' interfaces is still limited. In general, the control of the cathode-electrolyte-interphase (CEI) is suggested as one of the most critical objectives of further development.

Altogether, the development of high-voltage compatible SPEs and GPEs is a major technical route towards advanced-generation batteries, but the applicability of polymer-based electrolytes for HVLP batteries is still debated. In this paper, we aim to answer this question by providing a clear perspective on the status of research on HVLP cells, at a time corresponding to tremendous scientific and financial efforts devoted to this subject. Herein, we first present an overview of the degradation mechanisms of polymer electrolytes in HVLP batteries, by comparing the results of theoretical and experimental works, and the corresponding mitigation strategies proposed to date. Second, we analyze the current status of cell performance of HVLP batteries, thereby yielding a statistical overview based on parameters such as the cell voltage, the electrochemical stability window (ESW) of electrolyte, cell components (cathode, anode, salt, polymer types), capacity retention, temperature effect, mass loading, and current densities. Thereafter, we cover the advanced characterization techniques employed for studying the degradation of HVLP batteries. Ultimately, we provide an outlook of the topic with several guidelines for future research directions toward high voltage polymer-based batteries.

2. Chemical and Electrochemical Stability of HVLP Cells

The electrochemical stability of polymer-based electrolytes is of paramount importance for developing HVLP batteries. The oxidation of the polymer electrolyte increases the cell resistance, mechanical instability, and gassing, thereby impacting the battery performance and causing safety problems.

2.1. Intrinsic Oxidative Stability of Polyether Electrolytes

Poly(ethylene oxide) (PEO) is the most commonly used polymer matrix in SPEs, but PEO-based electrolytes have been primarily used mainly with 3V-class cathode materials, such as LFP and V_2O_5. This is because of their limited oxidative stability,[93,94] that is predominantly attributed to the presence of the labile lone pair on the ether oxygen atom of the PEO chains.[95] An oxidation mechanism of dimethoxyethane (DME)/lithium bis(trifluoromethanesulfonyl)imide (LiTFSI), wherein DME is used as a model for PEO, was initially proposed by Faglioni et al.[96] (**Figure 1**). In the first electron transfer, an electron is removed from the ether oxygen proximate to the $TFSI^-$ anion, resulting in the formation of a radical cation, stabilized by the presence of the anion. Thereafter, a proton is transferred to the $TFSI^-$ anion, forming a neutral HTFSI coordinated to the neutral radical (Figure 1a). A second electron transfer results in the formation of a carbocation, which eventually anchors a second $TFSI^-$ anion (Figure 1b). The HTFSI can further attack another DME molecule that produces a cleavage in the latter (Figure 1c). This mechanism implies that the oxidation of PEO involves a complex interplay between the polymer chain and anion. Furthermore, the oxidation of 2-methoxy ethanol follows the same route (extraction of electron from ether oxygen) indicating that the weakest point for the oxidation of PEO is the ether oxygen, also in presence of terminal hydroxyls.

The oxidative stability limit of PEO and corresponding electrolytes has been an object of study in several theoretical investigations. Pandian et al.[97] calculated the ESW of poly(ethylene glycol) (PEG) oligomers/salt complexes using density functional theory (DFT) and determined that the oxidation potential is governed by the stability of the polyether host. For ethylene oxide oligomers/salt complexes, the theoretical oxidation potential is approximately 5 V versus Li/Li^+ (**Figure 2**a,b). Chen et al.[98] evaluated the ESW of several polymers by DFT and molecular dynamics (MD) simulations, considering the influence of the polymer morphology, that is the effect of order/disorder in the chain stacking on the polymer ESW. Compared to other polymers, polyethers such as PEO and poly(propylene oxide) (PPO) display a particularly low oxidation potential that overlaps with the operation potentials of $LiMO_x$ cathodes, which is slightly below 4 V versus Li/Li^+ (Figure 2c). For instance, higher oxidative stability is exhibited by polycaprolactone (PCL), polymethyl methacrylate (PMMA), and especially poly(vinylidene fluoride) (PVdF), which are other commonly used polymer matrices for SPEs and GPEs. Interestingly, all polymers are theoretically compatible with lithium metal. Subsequently, Marchiori et al. calculated the ESW of polymer-salt complexes,[99] displaying a considerable reduction of the ESW compared to the pristine polymers, owing to the shielding of the positive charge in the polymer oxidized state by the salt anion (Figure 2d). Again, the PEO manifests the lowest oxidative stability compared to other polymers. Nonetheless, in this case, the theoretical oxidative limit for PEO/LiTFSI and PEO/$LiCF_3SO_3$ complexes was approximately 4.7 V versus Li/Li^+, whereas PEO/LiFSI (lithium bis(fluorosulfonyl)imide) displays a low oxidative limit of 4.2 V versus Li/Li^+. With regard to the impact of the terminal groups, no influence was observed by the substitution of the terminal methoxy group with hydroxyl groups (Figure 2b).

Therefore, these studies confirm that PEO-electrolytes have a comparatively limited thermodynamic stability. Furthermore, it is indicated that a) the oxidation potential in polymer electrolytes is determined by the oxidation of the polymer host, b) compared to pristine polymers, the oxidation potential is reduced by the interaction between polymer and salt anion, c) terminal hydroxyl substitution poses no influence on the oxidative stability, and d) the oxidation process occurs by loss of a single electron on the ether oxygen lone pair, possibly followed by proton transfer and loss of another electron to form an anion-stabilized carbocation (Figure 1a).[96,99] On the contrary, the theoretical studies provide various estimations of the oxidative stability limit for PEO-based electrolytes, with values ranging between ca. 4 and 5 V versus Li/Li^+, possibly because of

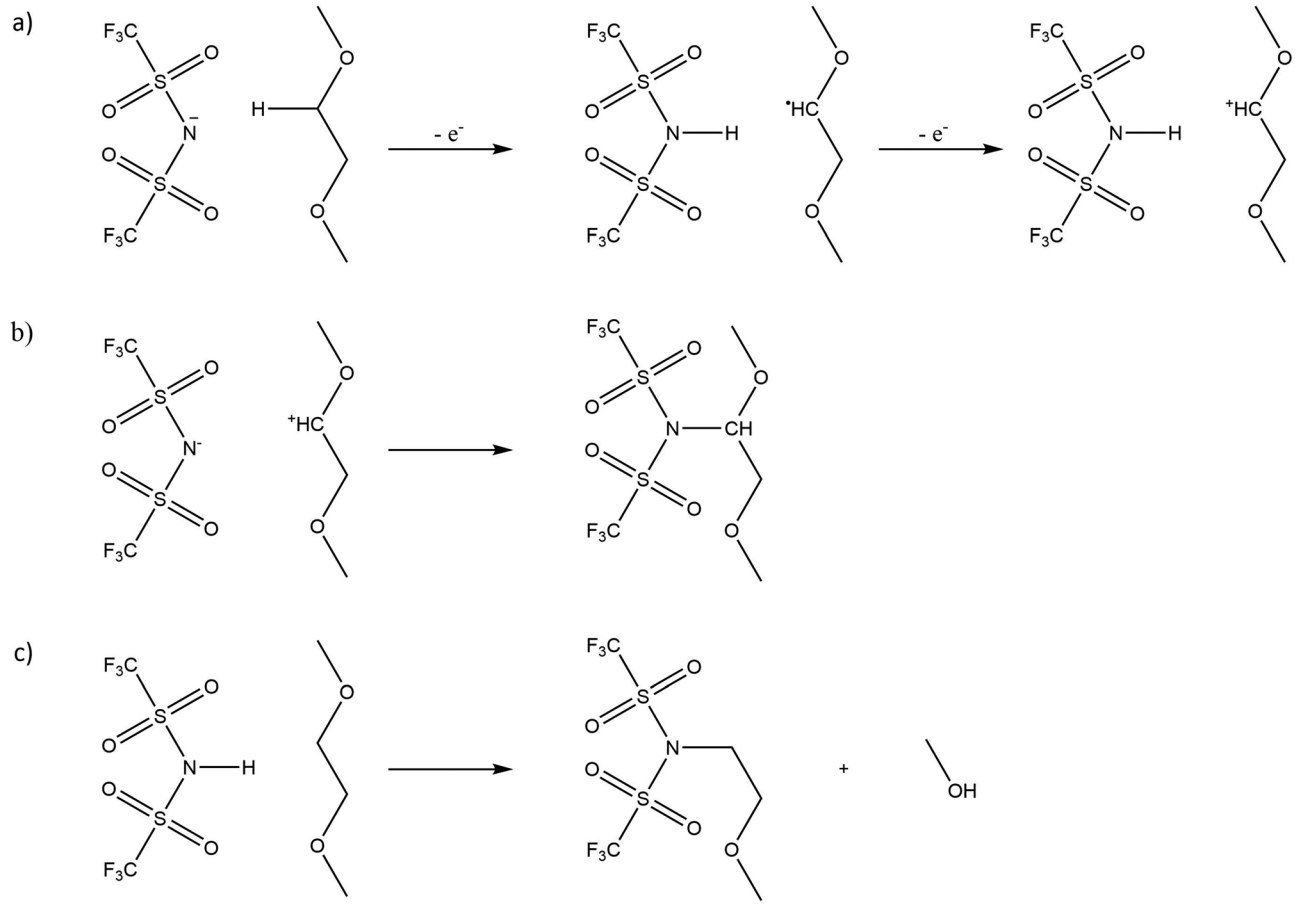

Figure 1. Simplified oxidation mechanism of DME/LiTFSI, based on the work of Faglioni et al.[96] a) Oxidation of a DME molecule with formation of a carbocation and of HTFSI; b) anchoring of $TFSI^-$ on the carbocation; c) cleavage of a DME molecule by HTFSI.

the variations in the systems considered (absence or presence of salt, salt anion type, polymer molecular weight, etc.).

Similarly, the experimental values of the oxidative stability limit exhibited considerable variation (**Table 1**). Previous reports claimed that the oxidation process potentially initiated at 3.8 V versus Li/Li^+,[100] and generally, the polyether electrolytes are oxidized above 4 V versus Li/Li^+.[93,94] Concordant with earlier voltammetric measurements,[101] Homann et al. recently reported that the primary oxidation process of PEO is initiated at 4.6 V versus Li/Li^+.[102] However, the authors did not neglect the low-intensity oxidation processes occurring at lower voltages. Crucially, the authors observed that the common fast cell failure below 4.6 V, —in form of voltage noise and infinite charge—was caused by micro-shorts resulting from dendrite growth and not the oxidative degradation of the electrolyte. Consequently, according to the authors, polyether-based electrolytes could be used with high-voltage cathodes, up to at least 4.5 V, by hindering dendrites growth, for example, using mechanically robust crosslinked polymer electrolytes.[103,104]

This finding was further challenged by Seidl et al.,[105] who coupled electrochemical and spectroscopic methods, and identified the onset for PEO/LiTFSI degradation at much lower voltages, that is, below 4 V versus Li/Li^+. In particular, they detected that the deprotonation of PEO terminal —OH groups initiates at 3.2 V, which, resulted in the formation of the strong acid HTFSI that further attacks the PEO ether main chain. The onset for the major electrochemical decomposition of the PEO chains was detected at 3.6 V, coinciding with the oxidation of the ether groups. The proposed degradation mechanism, and the emphasis on the role of HTFSI were in accordance with the previous theoretical study by Faglioni et al.[96]

In contrast, certain reports addressed the influence of terminal group substitution. Most experimental studies confirmed that the oxidization of poly(ethylene glycol) dimethyl ether (PEGDME) and glymes was initiated at ≈4 V versus Li/Li^+.[95,106] Nonetheless, a recent study reported an increase in the oxidative stability from 4.05 to 4.3 V versus Li/Li^+, for PEG and PEGDME-based electrolytes, respectively.[107] Accordingly, a higher reactivity of the terminal hydroxyls would be in agreement with the early oxidation of hydroxyls in PEO reported by Seidl et al.[105] Another recent study reported higher oxidative stability for a cross-linked polymer electrolyte containing free hydroxyls compared to PEG, which was caused by the restricted mobility and reactivity of the hydroxyls in the cross-linked electrolyte.[108]

The diverging results reported in the recent literature or their conflicting interpretation indicate that the evaluation of

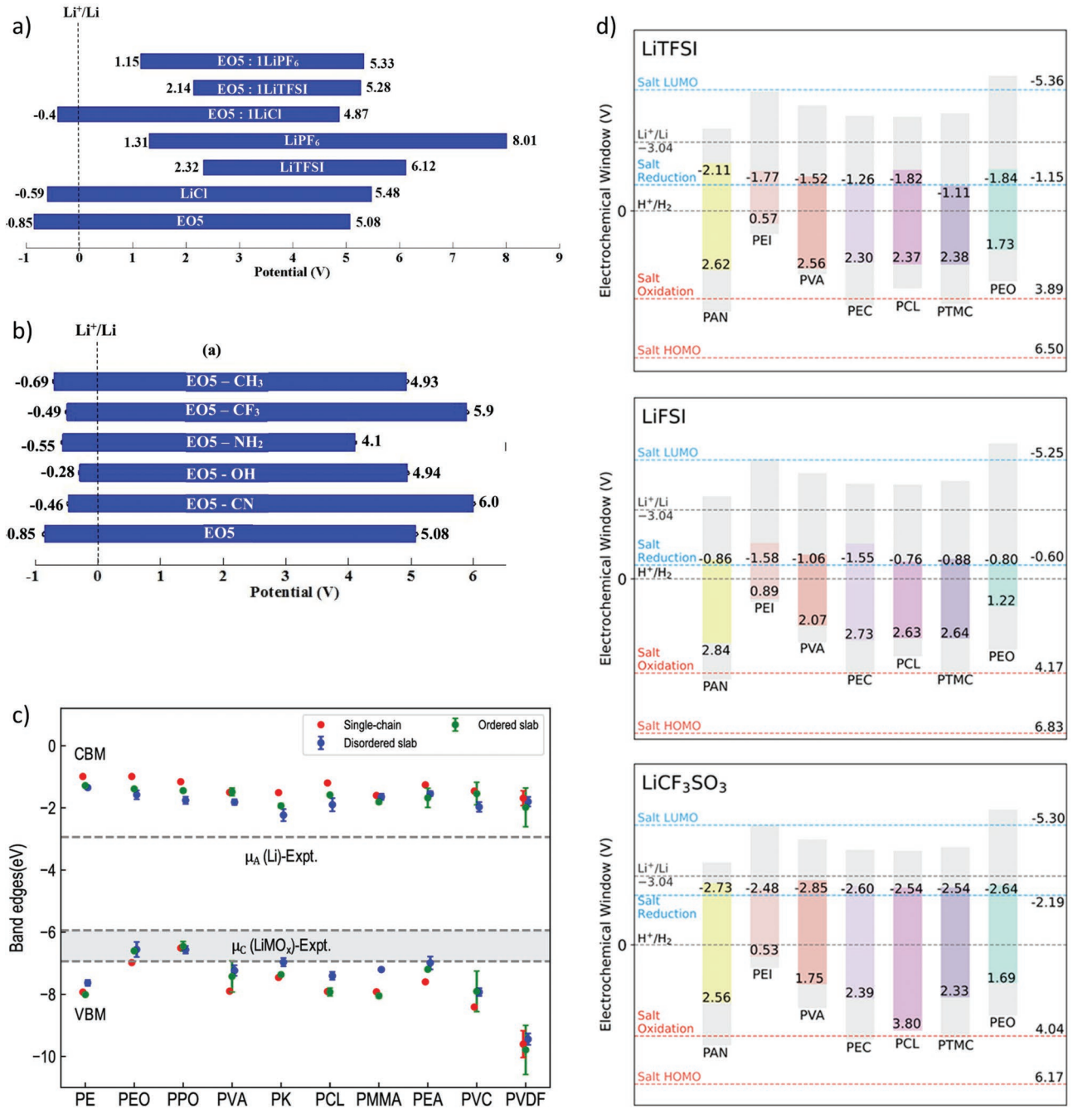

Figure 2. Theoretical calculations of the electrochemical stability of polymers and polymer-salt complexes: a) Effect of salt type on oxidation and reduction potentials of penta(ethylene oxide) (EO5). Reproduced with permission.[97] Copyright 2018, Elsevier; b) Effect of various terminal functional groups on the oxidation and reduction potentials of PEO electrolytes. Reproduced with permission.[97] Copyright 2018, Elsevier; c) ESW limits for 10 model polymers matrices for polymer electrolytes. Reproduced with permission.[98] Copyright 2019, American Chemical Society; d) ESW of polymer-salt complexes with LiTFSI, LiFSI, and $LiCF_3SO_3$ as lithium salts. Reproduced with permission.[99] Copyright 2020, American Chemical Society.

the absolute stability limit of PEO-based electrolytes is still challenging. In contrast, the relevance of this intrinsic value for battery operation is unclarified. As described in the following section, the electrolyte stability is influenced by the working electrode (or cathode) chemistry and morphology, and therefore the intrinsic stability of the electrolyte may not reflect the effective stability in real cycling conditions.

2.2. High Reactivity of Specific Electrode Chemistries

One of the major sources of confusion with polymer electrolytes is that the oxidative stability—measured by linear sweep voltammetry (LSV) with flat blocking electrodes—is consistently overestimated with respect to the electrochemical stability in HVLP cells. This indicates a specific reactivity of certain

Table 1. Electrochemical stability of selected PEO and PEG-based electrolytes, by different methods and with different electrodes.

Electrolyte	Oxidative stability/V versus Li/Li^+	Method	Working electrode	Ref.
$(EO)_5$/LiTFSI	5.28	DFT		[97]
PEO/LiTFSI	4.77	DFT		[99]
PEO/LiTFSI	4.5	CV	SS[a)]	[101]
PEO/LiTFSI	3.8	LSV	Carbon	[100]
PEO/LiTFSI	4.9	LSV	Pt	[102]
PEO/LiTFSI	4.6	LSV	Carbon	[102]
PEO/LiTFSI	4.6	GC[b)]	NMC-622, LNMO[c)], LFP	[102]
PEO/LiTFSI	3.9/4.5[d)]	LSV	Carbon	[110]
PEO/LiTFSI	4.2	GC[b)]	LCO	[110]
PEO/LiTFSI	4.5	DEMS	Carbon	[111]
PEO/LiTFSI	4.2	DEMS	LCO	[111]
PEO/LiTFSI	3.6	CV/SEC	Graphite/carbon	[109]
PEO/LiTFSI	3.6	LSV/PDV	SS[a)]	[105]
PEGDA[e)]/PEGDME/LiTFSI	4.0	LSV	SS[a)]	[106]
PEG/LiTFSI/LiFSI	4.05	LSV	Carbon	[107]
PEGDME/LiTFSI/LiFSI	4.3	LSV	Carbon	[107]

[a)]Stainless steel; [b)]Galvanostatic cycling; [c)]$LiNi_{05}Mn_{15}O_4$; [d)]Stabilized kinetically to 4.5 V; [e)]PEGDA: Poly(ethylene glycol) diacrylate.

electrode components. In particular, two factors may affect the electrolyte stability: a) an enhanced reactivity of the composite cathode electrodes, with respect to the flat blocking electrodes, caused by the high surface area of the former, and by the presence of carbon conductive additive; b) chemical reactivity of the active material. The first case can be tested by performing LSV with a carbon-coated working electrode, which usually gives a lower oxidation potential than with a flat blocking electrode. For instance, Xia et al. observed a reduction of the oxidation onset of PEO/LiTFSI from 4.5 to 3.8 V versus Li/Li^+, by replacing a stainless-steel electrode with a carbon composite electrode in LSV experiments.[100] More recently, Homann et al. observed a reduction from 4.9 to 4.6 V versus Li/Li^+ by shifting from platinum flat electrode to a conductive carbon electrode.[102] The variations in the results are probably caused by the subjective choice of the onset point in the LSV curves, which is the major limitation of this kind of experiment (refer to Section 4.1 for a detailed discussion). Nonetheless, the use of carbon-coated electrodes in LSV provides a more realistic picture of the stability of SPEs, with respect to the use of flat blocking electrodes. The addition of graphite increases the electrochemically active area and the fraction of polymer electrolytes undergoing oxidation. Li et al. determined an oxidation onset that was as low as 3.6 V versus Li/Li^+ for PEO/LiTFSI by a cyclic voltammetry (CV) reversibility test coupled with size exclusion chromatography (SEC), and by using a composite working electrode formed from PEO/LiTFSI/graphite.[109]

Particular cathode chemistries may display enhanced oxidation ability and thus promote electrolyte oxidation. This has been already observed by Xia et al. for $LiNiO_2$ (LNO) and $LiCoO_2$ (LCO).[100] This issue could be mitigated by protecting the cathode/electrolyte interface, or by using less reactive cathode chemistries. As such, Qiu et al. reported that, PEO oxidation occurs already at ≈4 V versus Li/Li^+, but the reaction products form a stable cathode-electrolyte interphase (CEI) which prevents further decomposition up to 4.5 V.[110] The poor cycling performance with LCO could be attributed to the high oxidative ability of this active material, and it was ultimately improved either by using the less reactive $LiMn_{0.7}Fe_{0.3}PO_4$ (LFMP), or by coating the LCO particles with $Li_{1.4}Al_{0.4}Ti_{1.6}(PO_4)_3$ (LATP). The high reactivity of LCO has been confirmed also by Nie et al.,[111] who studied the degradation mechanism of PEO/LiTFSI electrolyte using differential electrochemical mass spectrometry (DEMS). As observed, the hydrogen evolution initiated from 4.5 V versus Li/Li^+ with a blocking electrode, and from 4.2 V in LCO/Li cells. Moreover, the evolution of H_2 was supposedly caused by the crossover of HTFSI to the anode. According to the oxidation mechanism proposed by Faglioni et al., the abovementioned result is a consequence of the oxidative deprotonation of PEO.[96] The DFT calculations indicated that partially delithiated LCO can coordinate deprotonated PEO, thereby promoting the dehydrogenation reaction. In absolute terms, the energy of the reaction was the highest when a voltage was applied. Thus, the process can be viewed as a chemical degradation accelerated by the electrochemical process. Similar to the LCO cathodes, NMC cathodes possess a high oxidizing ability as well. This was recently confirmed by Kaboli et al.,[112] who observed a continuous thinning of a PEO-based SPE, followed by outgassing, in an NMC-622/Li cell under in situ scanning electron microscopy (SEM). This type of degradation can be attributed to a chemical decomposition at the polymer/electrode interface, which is further accelerated by the electrochemical process. A recent study on the thermal stability of PEO with LCO and polycrystalline NMC-811 demonstrated that PEO can suppress the oxygen release and thermal runaway of LCO owing to the formation of a passivation layer on the surface of the LCO particles. In contrast, the PEO cannot passivate polycrystalline NMC-811 because of the poor wettability of the NMC primary particles. This results in inferior thermal stability that is similar to or deteriorates with respect to liquid electrolytes.[113]

Summarily, the ultimate oxidative stability limit of PEO- and polyether-based electrolytes, corresponding to the oxidation of the polymer main chain, occurs at approximately 4.5–4.6 V versus Li/Li^+, but the stability is substantially reduced to 3.8–4 V versus Li/Li^+ owing to diverse factors such as a) the high reactivity of PEO/PEG terminal hydroxyls, b) increased reactivity caused by high surface specific area of composite cathodes and the presence of conductive carbon, and c) specific oxidative activity of certain cathode chemistries.

2.3. Strategies to Enhance the Electrochemical Stability of Polymer Electrolytes

2.3.1. Composite Polymer Electrolytes

Reportedly, the addition of inorganic fillers can enhance the electrochemical stability in PEO-based CPEs. This effect has been observed with several types of fillers, namely "passive" fillers such as SiO_2,[114] ZrO_2,[115] and Al_2O_3,[116] lithium-conductive fillers,[81] such as $Li_{1.5}Al_{0.5}Ge_{1.5}(PO_4)_3$ (LAGP),[41,117] garnets (e.g. $Li_7La_3Zr_2O_{12}$ – LLZO and $Li_{7-x}La_3Zr_{2-x}Ta_xO_{12}$ – LLZTO),[118–126] argyrodites

Table 2. Reported oxidative stability of various CPEs and HSEs.

Electrolyte	Inorganic filler	ESW limit/V	Method	Cathode material (cycling)	Ref.
PEO/$LiClO_4$	SiO_2	5.5	LSV	LFP	[114]
PEO/$LiClO_4$	Al_2O_3	4.8	LSV		[116]
PPO/LiTFSI/SN[a)]	ZrO_2	5.0	LSV	NMC-622	[115]
PEO/$LiClO_4$	LAGP	4.75	LSV	LFP	[117]
PEO/LiTFSI	LAGP	5.12	LSV	LFMP	[41]
PEO/LiTFSI	LLZO	5.7	LSV	LFP	[126]
PEO/LiTFSI	LLZO	4.9	LSV	NMC-622	[122]
PEO/LiTFSI	LLZO	4.8	LSV	NMC-532	[124]
PEO/LiFSI	LLZO	4.2	LSV	NMC-622	[121]
PEO/$LiClO_4$	LLZTO	4.6	LSV	LFP	[118]
PEO/LiTFSI	LLZTO	4.75	LSV	NMC-111	[119]
PEO/LiTFSI	LLZTO	4.5	LSV		[123]
PEO/LiTFSI	LLZTO	4.9	LSV	LFP	[125]
LiBFSIE [b)]	LLZO	5.7	CV	NMC/NCA	[120]
P(PEGMEA)[c)]	Li_6PS_5Cl	5.0	CV	LCO	[127]
PEO/LiTFSI	LSTZ	5.2	LSV	NMC	[128]
PEO/LiTFSI	D-UiO-66-NH_2	4.97	LSV	LFP	[129]

[a)]SN: succinonitrile; [b)]LiBFSIE: Fluoroboron-centered Li-conductive polymer framework; [c)]PEGMEA: Poly(ethylene glycol) methyl ether acrylate.

(Li_6PS_5Cl),[127] perovskites (e.g. $Li_{3/8}Sr_{7/16}Ta_{3/4}Zr_{1/4}O_3$- LSTZ),[128] and cationic metal-organic frameworks (such as D-UiO-66-NH_2).[129] In particular, the electrochemical stabilization of the CPE supposedly involves Lewis acid–base interaction, hydrogen-bonding or dipolar interactions between the PEO ether lone pairs and the filler surface groups. For instance, this mechanism was recently observed in argyrodite-containing CPEs, with a possible interaction between the ether lone pairs of the polymer matrix and filler P-atoms.[127] Nonetheless, a possible improvement of the oxidative stability by the addition of sulfides is surprising, as sulfide electrolytes are characterized by a narrow ESW.[81,130,131] With garnets, the stabilization has been attributed to the interaction between the filler and salt.[126] The binding of the salt anion on the filler surface may effectively stabilize the SPE against oxidation by hindering the interaction between the anion and polymer host. Indeed, the oxidative stability of the polymer–salt complexes is reduced with respect to pristine polymers because of the charge shielding in the oxidized carbocation by the anion. In addition, a possible oxidation mechanism for PEO-based SPEs involves anion-mediated oxidative deprotonation.[96,132]

Although most CPEs have reported stability over 4.5 V versus Li/Li^+ (**Table 2**), the stability is typically measured using voltammetric methods that could overestimate the stability with respect to real cell conditions.

2.3.2. Concentrated Polymer Electrolytes

Highly concentrated electrolytes exhibit greater electrochemical stability than the diluted ones owing to the coordination of all solvent molecules by the Li^+ cations (**Table 3**).[95,132] This effect has been reported for polyether electrolytes as well, wherein the Li^+ coordination stabilizes the ethylene oxide units.[133] Furthermore, concentrated electrolytes may inhibit the corrosion of the current collector (refer to Section 2.4.2). The fundamental limitation of using high salt concentrations is that the high solution viscosity and ion pairing pose a detrimental impact on the ionic conductivity. This is problematic, especially for SPEs as its ionic conductivity is generally low. However, a decreased conductivity may be acceptable in GPEs[134,135] and plasticized SPEs.[136,137] A specific case is represented by certain polycarbonate-based SPEs, for example, poly(ethylene carbonate)-based electrolytes, in which the conductivity reportedly increases with the salt concentration.[138,139] In this case, concentrated electrolytes may exhibit benefits both in terms of conductivity and electrochemical stability.

Table 3. Reported o xidative stability of selected concentrated polymer electrolytes.

Electrolyte	ESW limit/V	Method	Cathode material (cycling)	Ref.
$Li(DME)_{0.7}FSI$-$PEO_{0.6}$	4.5	LSV	NMC-111	[135]
P(VdF-HFP)/LiTFSI/DMC[a)]/FEC[b)]	5.0	LSV	NMC-111	[134]
$P(EO)_1LiFSI$	4.5	LSV	NMC-111	[136]
PEGDAE[c)]/VEC[d)]/PEGDME/LiTFSI EO:Li = 13	5.1	LSV	NCA	[137]
PEGDAE/LiTFSI/LiDFOB[e)]	4.6–5.0	LSV	NCA	[133]
PEC/LiFSI (120 mol%)	5	LSV	LMO[f)]	[139]
PEC/LiTFSI (> 80 mol%)	5	LSV		[138]

[a)]DMC: dimethyl carbonate; [b)]FEC: fluoroethylene carbonate; [c)]PEGDAE: poly(ethylene glycol) diallyl ether; [d)]VEC: Vinyl ethylene Carbonate; [e)]LiDFOB: lithium difluoro(oxalate)borate; [f)]LMO: $LiMn_2O_4$.

2.3.3. Alternative Polymer Hosts

Generally, the most straightforward approach for enabling HVLP cells involves the use of non-polyether polymer hosts, that exhibit higher oxidative stability. However, their utilization poses two major drawbacks: first, a weaker stability towards reduction, and second, a lower ionic conductivity compared to PEO-based electrolytes. Thus, the use of alternative hosts often relies on the addition of plasticizers, the presence of residual processing solvent, or directly on the addition of liquid electrolytes. As an advantage, a wide range of chemical structures is available, and the use of plasticizers or liquid electrolytes yields substantially higher conductivities than in SPEs.

Based on the results of DFT calculations,[98,99,140] polymers with higher oxidative stability than PEO include polycarbonates such as poly(ethylene carbonate) (PEC), poly(propylene carbonate) (PPC), and poly(trimethylene carbonate) (PTMC), polyesters like PCL, and poly(β-propiolactone), poly(acrylonitrile) (PAN), PMMA, and PVdF. The application of these and other alternative polymer electrolytes with NCA and NMC has been recently reviewed by Zhang et al.[90]

Polycarbonates and polyesters are frequently used as alternative polymer matrices in SPEs, and have higher oxidative stability than PEO.[89,98,99,140–142] For instance, PEC-based

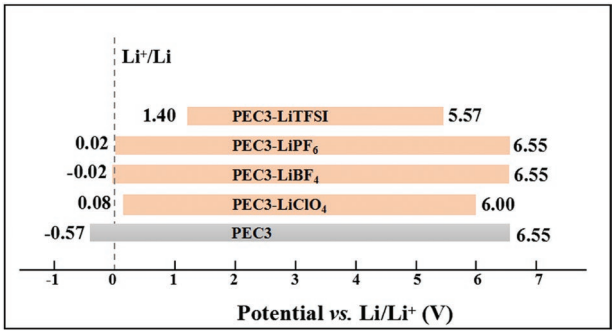

Figure 3. ESW of PEC-based polymer electrolytes with different lithium salts, with ethylene carbonate (EC) unit:Li^+ ratio of 3:1. Reproduced with permission.[140] Copyright 2021, Elsevier.

electrolytes have theoretical stability proximate to or exceeding 6 V versus Li/Li^+ (**Figure 3** and **Table 4**).[140] However, only a handful of studies have reported on the application of polycarbonate SPEs with high-voltage cathodes. Although the PEC/LiFSI electrolyte has been cycled with $LiMn_2O_4$ (LMO), the increased stability, in this case, could be attributed to the high salt concentration.[139] Moreover, PPC has been used in propylene carbonate (PC)-containing GPEs with $LiNi_{05}Mn_{15}O_4$ (LNMO).[143] However, certain reports raise conflict with the chemical/electrochemical stability of polycarbonate-based electrolytes. The low first-charge coulombic efficiency was reported for PEC, PPC, and poly(2,3-butylene carbonate) (PBC) electrolytes, wherein the LFP served as the cathode material,[144] along with the evolution of CO_2 during a galvanostatic charge below 4 V, and the reduction of Fe^{3+} after contacting delithiated LFP with PPC/LiTFSI. In another study, the evolution of CO_2 with PTMC/LiTFSI on a carbon cloth electrode, was detected from 4.25 V versus Li/Li^+.[145] An interesting polycarbonate host for HVLP applications is poly(vinylene carbonate) (PVCA),[146–148] which can be prepared in situ using the radical polymerization of VC. The inclusion of electron-withdrawing groups in the polymer host such as nitrile groups,[149–151] carbonate and urethane moieties (PCUMA: polymerized (2-(((2-oxo-1,3-dioxolan-4-yl) methoxy) carbonylamino))-ethyl methacrylate (CUMA))[152,153] may further increase the oxidative stability. The high oxidative stability up to 5.6 V versus Li/Li^+ was achieved by copolymerizing with quaternary ammonium-containing monomers (PCUMA-NPF_6: copolymer 2-(methacryloyloxy)-*N,N,N* -trimethylethanaminium hexafluorophosphate (NPF_6)).[154] Similarly, poly(vinyl ethylene carbonate) (PVEC)-based electrolytes, prepared in situ by radical polymerization of vinyl ethylene carbonate (VEC) displayed oxidative stability of 4.5 V versus Li/Li^+.[155] A higher oxidative stability of PVEC-based electrolytes—up to ca. 5.0 V versus Li/Li^+—was achieved by adding SiO_2 nanoparticles,[156,157] by copolymerizing VEC with fluorinated comonomers,[158] or by ring-opening polymerization in presence of tin(II) 2-ethylhexanoate.[159]

Additional polymer hosts (PAN, PMMA, PVdF, polymerized ionic liquids) were primarily used in GPEs and plasticized SPEs. The PMMA and its copolymers were primarily used in GPEs, especially with carbonate electrolytes.[160–163] The polymerized ionic liquids (PILs) such as poly(diallyldimethylammonium) (PDADMA) neutralized with either $TFSI^-$ or FSI^-, were fundamentally used in combination with ionic liquids and the corresponding lithium salts (LiTFSI or LiFSI). Such ternary systems, have been recently cycled with NMC, NCA,[164,165] and even with LNMO.[166] In context, PAN and PVdF (and its derivates such as P(VdF-HFP) (poly(vinylidene fluoride)-co-hexafluoropropylene) and P(VdF-TrFE) (poly(vinylidene fluoride-co-trifluoroethylene)) were also used in CPEs and HSEs (Table 4).[30,43,167–174] In GPEs, the electrochemical stability may be limited by the choice of the solvent or plasticizer. Glyme-based electrolytes bear an oxidation potential at approximately 4 V versus Li/Li^+, coinciding with the low oxidative stability of polyethers,[95] whereas carbonate electrolytes are stable up to 5 V versus Li/Li^+.[175] However, the oxidation initiates beyond 4.5 V versus Li/Li^+ with transition metal cathodes.[176] The ionic liquids have possibly even higher oxidative stability,[177] and this property is normally retained in ionic liquid-containing GPEs.[80] Alternative organic solvents with high oxidative stability include fluorinated solvents,[178,179] phosphates,[180] sulfolane,[181–183] and nitrile-containing additives, such as succinonitrile (SN).[184] Interestingly, the enhanced oxidative stability can be observed in certain GPEs containing polymer blends, which can be attributed to an intermolecular interaction between a "functional" polymer and the cathode or the additional electrolyte components.[185,186]

In addition, more exotic polymer hosts are advantageous in HVLP batteries (Table 4). The single-ion-conducting GPEs have been prepared by functionalizing partially-fluorinated poly(arylene ether sulfones) block copolymers with anionic perfluorosulfonimide moieties, which ensure high oxidative stability.[187,188] Certain cross-linked SPEs and GPEs depict enhanced oxidative stability, possibly because of the restricted mobility of the polymer chains, hindering continuous degradation of the polymer.[189] Cross-linked electrolytes with SN as plasticizer show particularly high oxidative stability.[190,191] The electrochemical stability of cross-linked electrolytes can be further enhanced by introducing specific functional groups such as nitrile and anhydrides groups. The examples of cross-linked polymers for high-voltage GPEs were poly(cyanoacrylates),[192,193] poly(methyl vinyl ether-alt-maleic anhydride),[194] and poly(acrylic anhydride).[195] Alternative polymer hosts with reported high voltage stability include poly(1,3-dioxolane) (PDOL),[196–200] poly(formaldehyde) (POM)[201] (both in situ-generated), and poly(butylene oxide) (PBO).[202] More importantly, the chemical structure modification can enhance the oxidative stability of polyether-based polymer electrolytes (Table 4).[89] In general, crosslinked copolymer electrolytes of PEO and poly(propylene oxide (PPO) exhibit greater stability than pure PEO-based electrolytes—up to 4.75 V versus Li/Li^+.[203] The copolymer electrolytes with carbonate and ethylene oxide units, such as poly(ethylene ether carbonate) (PEEC),[204] and poly(triethylene glycol carbonate) (PTEC)[205] exhibited improved oxidative stability and were cycled with NMC and LFMP, respectively. This suggests that the introduction of electron-withdrawing carbonate groups in the backbone can improve the oxidation stability of ethylene oxide moieties. The triblock copolymer electrolytes with perfluoroalkyl pendant chains and PEO blocks (poly(ethylene oxide)-block-poly(heptadecafluorodecyl methacrylate) (PFMA-PEO)) exhibited high oxidative stability up to 4.9 V versus Li/Li^+.[206] In contrast, Itoh et al. have reported breakdown potential between

Table 4. Oxidative stability of polymer electrolytes with alternative polymer hosts (non-PEO), cycled with high-voltage cathode materials.

Electrolyte	Oxidative stability/V	Cathode	Ref.
EO-copolymers			
PEO-PPO	4.75	NMC	[203]
PEEC/LiTFSI	4.9	NMC-622	[204]
PTEC/LiTFSI	4.5	LFMP	[205]
PFMA-PEO/LiTFSI	4.9	NMC-622	[206]
PEG-VC/LiTFSI	4.1–4.6		[207]
Polycarbonate electrolytes			
PPC/PC/LiDFOB	4.6	LNMO	[143]
PEC/LiFSI	5.0	LMO	[139]
PVCA/LiDFOB	> 5.0	LCO	[210]
PVCA/LiTFSI	> 5.0	NMC-111, LCO	[209]
PVCA/LiDFOB	4.8	LFMP	[146]
PVCA/LiDFOB	4.5	LCO	[147]
PVCA/LSnPS/LiDFOB	4.5	LFMP	[148]
P(VC-AN)/EC[a)]/DMC/$LiPF_6$	> 5.0	LNMO	[151]
PVEC/LiTFSI	4.5	NCA	[155]
PVEC/LiTFSI/SiO_2	5.0	LCO	[156]
PVEC/LiFSI/SiO_2	5.3	NMC-532	[157]
P(VEC-co-TFEMA)/LiTFSI[b)]	> 5.0	NMC-811	[158]
PVEC/LiTFSI	4.8	LCO	[159]
PCUMA/SN/LiDFOB/LiTFSI	5.3	LCO	[152]
PCUMA/LiDFOB/EC/DMC	> 5.0	LCO	[153]
PCUMA-NPF_6/EC/DMC/$LiPF_6$	5.6	LCO, LNMO	[154]
PAN-based electrolytes			
PAN/PVEC/PYR14TFSI/LiTFSI[c)]	> 5.0	NMC-811	[211]
PMA/LiTFSI	4.75	LCO	[213]
PAN/LiTFSI	4.5	NMC-622	[216]
PAN/LiTFSI	> 5.0	NMC-622, NMC-811	[215]
PAN/LiTFSI	4.2		[123]
PAN/LiTFSI/LLTO[d)]	4.8	NMC-622	[123]
PAN/LATP/LiTFSI	>5.0	NMC-811	[214]
PAN/PVdF/SN/LiTFSI	4.6	NMC-811	[173]
PAN/PVdF/SN/LiTFSI/LLZO	>5.0	NMC-811	[173]
PAN/LLTO/$LiClO_4$	4.6	NMC-811	[217]
PAN/BN (boron nitride)/$LiClO_4$	4.5	NMC-811	[169]
PAN/SiO_2/LiTFSI	5.0–5.2	NMC-622	[172]
PVdF-based electrolytes			
P(VdF-HFP)/PYR13TFSI/LiTFSI[e)]	4.5	LCO	[221]
PVdF/LiTFSI	4.8	NMC-811	[218]
P(VdF-TrFE)/LATP/LiFSI/PYR14FSI[f)]	5.2	NMC-811	[171]
PVdF/LLZTO/PYR14TFSI/LiTFSI	4.6	NMC-811	[30]
P(VdF-HFP)/LLZTO/LiTFSI	4.8	NMC-532	[168]
PVdF/LLZTO/LiTFSI	4.5	LMO	[174]
PVdF/LLTO/LiTFSI	4.5	NMC-811	[220]

Table 4. Continued.

Electrolyte	Oxidative stability/V	Cathode	Ref.
Other non-PEO electrolytes			
PDADMAFSI/LiFSI/PYR13FSI[g)]	> 5.0	NMC-811, LNMO	[166]
POE/LiTFSI	> 5.0	NMC-622	[208]
PBO/LiTFSI	5.2	NMC-811, LCO	[202]
PDOL/EC/$LiPF_6$	4.7	NMC-622	[196]
PDOL/AlF_3/LiTFSI	4.7	NMC-622	[200]
PDOL/$Al(Otf)_3$/LiTFSI	4.7	NMC-622	[197]
PDOL/EC/LiTFSI/LiDFOB	> 4.5	NMC-811	[198]
P(DOL-TTE)/LiTFSI[h)]	4.9	LFMP	[199]
POM/LiDFOB/SN	4.5	LCO	[201]
DAP[i)]/PETEA[j)]/FEC/FEMC[k)]/$LiPF_6$	5.5	LRO	[179]

[a)]EC: ethylene carbonate; [b)]TFEMA: trifluoroethyl methacrylate; [c)]PYR14TFSI: 1-butyl-1-methylpyrrolidinium bis(trifluoromethylsulfonyl) imide; [d)]LLTO: lithium lanthanum titanate; [e)]PYR13TFSI: 1-propyl-1-methylpyrrolidinium bis(trifluoromethylsulfonyl)imide; [f)]PYR14FSI: 1-butyl-1-methylpyrrolidinium bis(fluorosulfonyl)imide; [g)]PYR13FSI: 1-propyl-1-methylpyrrolidinium bis(fluorosulfonyl)imide; [h)]TTE: trimethylol-propane triglycidyl ether; [i)]DAP: diallyl phthalate; [j)]PETEA: pentaerythritol tetraacrylate; [k)]FEMC: 2,2,2-trifluoroethylmethyl carbonate.

4.1 and 4.6 V versus Li/Li^+ with copolymer electrolytes of poly(ethylene glycol) vinyl methyl ether and vinylene carbonate (PEG-VC), which implied that the oxidative stability, in this case, was not greater than of pure polyether-based electrolytes.[207]

Finally, polymer hosts with high oxidative stability (>4.5 V vs Li/Li^+) can be used as a cathode-contacting interlayer in multilayered configurations, typically with a polyether-based SPE acting as the main separator or anode-contacting layer (Table 4). The examples of such polymer matrices include poly(oxalate) (POE),[208] PVCA,[209,210] PVEC,[211] PPC,[212] poly(N-methylmalonic amide) (PMA),[213] PAN,[123,214–217] PVdF,[218–220] and P(VdF-HFP).[221]

Overall, the use of alternative polymer electrolytes is established as a successful approach for the development of high-voltage polymer batteries. Various classes of alternative polymer electrolytes (CPEs, concentrated polymer electrolytes, and non-PEO-based SPEs) have reported oxidative stability greater than 4.5 V versus Li/Li^+, which should be sufficient for operation with 4-V class cathodes such as NMC and LCO (Table 4). Notably, the oxidative stability in these cases is evaluated by standard voltammetric methods, which can overestimate the oxidative stability. Among the various available options, commercial polymers such as polycarbonates, polyesters, PAN, and PVdF are readily available with sufficient oxidative stability, whereas synthetic polymers with complex chemical structures may be considered highly expensive for employment on a wide scale, at least in the short term. In situ-generated polymer electrolytes such as PVCA, PVEC, POM, and PDOL-based electrolytes provide an interesting solution despite requiring an additional separator and processing similar to the liquid electrolyte (injection). The use of oxidative-stable polymers will also probably require the implantation of multilayer structures to ensure both sufficient oxidative stability and compatibility with lithium metal anode.

2.3.4. Passivation of Polymer-Cathode Interface

The polymer electrolytes can be stabilized at high voltages by forming an artificial passivating interlayer at the cathode electrolyte interface. This is called the artificial CEI, which is analogous to the anode counterpart (SEI). The ideal CEI ought to be thin, homogeneous, and ionically conductive to facilitate charge transfer between the electrolyte and active material. In addition, it should be electronically insulating, and elastic, to withstand the volumetric variations of the active material particles upon charge and discharge. An artificial CEI can be produced ex situ, either by coating the cathode particles or electrode layer. Alternatively, or complementarily, task-specific electrolyte additives may react at the cathode interface during the charging process, thereby forming the CEI in situ.

Ex Situ CEI: The coating of the cathode particles with ceramic thin layers constitutes the most classic approach for stabilizing SPEs with highly reactive cathode materials such as LCO and NMC. The increased cyclability with LCO and polyether electrolytes has been already demonstrated in 2005 by coating LCO particles with Li_3PO_4,[222,223] LAGP,[224] and Al_2O_3 (**Table 5**).[225]

More recent examples include coating with LATP,[110,111,226] LAGP,[227] Li_2CuO_2,[228] and TiO_2,[208] either with LCO or NMC. Although this method is effective, it often fails to completely stabilize the electrolyte. In particular, coatings have been conducted by mechanical powder-powder mixing, spray coating, or other wet-coating methods. The achievement of homogeneous coatings based on these methods is challenging, especially in the first case, so that the electrolyte remains partially exposed to the cathode material. Alternatively, atomic layer deposition (ALD) can be used to coat preformed electrode layers. This method is advantageous for providing a uniform and conformal coating, and the electrolyte is protected from the conductive carbon additive, which may exhibit oxidative activity. In contrast, ALD is significantly expensive and challenging to upscale, and a relatively less number of oxide compositions are available for application with this technique. The typical ALD coating materials used in combination with SPEs include lithium tantalate,[229] Al_2O_3,[230] and $LiNbO_3$.[231] The latter is a widely used coating material for high-voltage cathodes, and is particularly effective for hindering the chemo-mechanical degradation of Ni-rich layered oxides.[232–236]

An intrinsic disadvantage of ceramic coating pertains to the rigidity of the resulting artificial CEI, which may not sustain the mechanical stress owing to the expansion/contraction of the active material particles during cycling. In addition, polymeric CEIs can be designed to resolve this issue. For instance, sodium carboxymethyl cellulose (CMC) has been used for coating the NMC-111 particles.[237] The oxidation product of CMC formed during charging is lithium conductive and protects the electrolyte from oxidation. In a more recent study,[238] researchers determined that carboxyl-containing binders such as the CMC and sodium alginate can act as coating agents to cover the active material particles and protect the SPE. As hypothesis, a favorable binding morphology that uniformly acts with the binder covering the active materials' particles can be obtained with amorphous polymers, in contrast to semicrystalline binders such as PVdF.[239] These binders raise interest because they are environmentally friendly, as they are fluorine-free and water-processable. Note that in this case the functions of binder and catholyte (electrolyte within the cathode pores) remain separated in this case, that is, a SPE should be introduced either in the slurry formulation or coated on the cathode layer, to ensure the lithium-ion transport to the active material particles. In certain cases, a polymer electrolyte coated on the cathode layer can act as both catholyte and passivating layer. The typical approach resembles the multilayer-electrolyte configuration described above. Typical coating polymers include poly(ethylcyanoacrylate) (PECA)[240] and poly(vinylene carbonate) (PVCA).[209,210]

The polymeric passivating layers can be obtained by electrodeposition.[241] For instance, PVCA and PAN coatings can be obtained from vinylene carbonate (VC) and acrylonitrile (AN)-containing precursor solutions. Interestingly, another approach involves the use of lithium-conducting polyelectrolytes as protective layers and catholytes, that is, that is polymers bearing anionic groups and neutralized with lithium

Table 5. Examples of ex situ coating of high-voltage electrodes with SPEs and GPEs.

Coating method	Electrolyte	Cathode material	Coating material	Ref.
Powder-powder coating	P(EO/MEEGE/AGE)[a]/LiBETI[b]/$LiBF_4$	LCO	Li_3PO_4	[223]
Powder-powder coating	P(EO/MEEGE/AGE)/LiBETI/$LiBF_4$	LCO	LAGP	[224]
Powder-powder coating	PEO/LiTFSI	LCO	LATP	[110]
Powder-powder coating	PEO/LiTFSI	LCO	LATP	[111]
Powder-powder coating	PEO/PEGDME/LiTFSI/LiBOB[c]/$LiPF_6$	NMC-532	LAGP	[227]
Spray coating	P(EO/MEEGE/AGE)/LiBETI/$LiBF_4$	LCO	Al_2O_3	[225]
Spray coating	P(EO/MEEGE/AGE)/LiTFSI/$LiBF_4$	LCO	Li_3PO_4	[222]
Casting	P(EO/MEEGE/AGE)/LiTFSI/$LiBF_4$	NMC-111	CMC	[237]
Casting	PEO/LiDFOB	LCO	PECA	[240]
Casting	PEO/LiTFSI	LCO	LAGP	[226]
Casting	PEO/LiTFSI	NMC-111	PVCA/LiTFSI	[209]
Casting	PEG/DEGME[d]/LiBOB/$LiNO_3$/HFiP[e]	NMC	Lithion	[242]
Casting/Thermal polymerization	PEO/LiTFSI	LCO	PVCA/LiDFOB	[210]
Wet chemical coating	PVdF/PYR13FSI[f]	NMC-111	Li_2CuO_2	[228]
Electrodeposition	PEO/LiTFSI/LiDFOB	NMC-532	PAN/PVCA	[241]
ALD	PEG/LiTFSI/LiBOB	NMC-111	Al_2O_3	[230]
ALD	PEO/$LiClO_4$/LLZTO	NMC-811	$LiNbO_3$	[231]
ALD	PEO/$LiClO_4$/LLZTO	LCO	Li_2O/Ta_2O_5	[229]

[a]P(EO/MEEGE/AGE): Polyethylene oxide 2-methoxyethoxyethyl glycidyl poly(allyl glycidyl ether); [b]LiBETI: $LiN(SO_2CF_2CF_3)_2$; [c]LiBOB: lithium bis(oxalato)borate; [d]DEGME: bis(2-methoxyethyl) ether (diglyme); [e]HFiP: tris(hexafluoro-iso-propyl)phosphate; [f]PYR13FSI: N-Propyl-N-methylpyrrolidinium bis(fluorosulfonyl)imide.

Table 6. Examples of additives for in situ CEI formation, with SPEs or GPEs.

CEI-forming additive	Electrolyte	Cathode material	Ref.
LiBOB	PEG/DEGME/LiBOB/$LiNO_3$/HFiP	NMC	[242]
LiBOB	PEO/PEGDME/EC/PC/LiTFSI/LiBOB/$LiPF_6$	LCO	[227]
AlF_3	PDOL/LiTFSI/AlF_3	NMC-622	[200]
Tetramethylene sulfone	PVAC/PVdF/LLZTO/$LiClO_4$	LCO	[183]
FEC	UPyMA[a]–PETEA/FEC/LiTFSI	LMO	[251]
4-(Phenylazo) benzoic acid lithium salt	PEO/LiTFSI	NMC-532	[253]
Acrylic anhydride	Polymethacrylate	LNMO	[195]

[a]UPyMA: 2-(3-(6-methyl-4-oxo-1,4-dihydropyrimidin-2yl)ureido)ethyl methacrylate).

ions. The typical examples included lithiated Nafion (Lithion)[242] and poly[(4-styrenesulfonyl)(trifluoromethanesulfonyl)imide] (LiPSTFSI).[243] Despite exhibiting a lower conductivity than conventional dual-ion conducting electrolytes, the anion immobilization in polyelectrolytes impedes unwanted polarization effects and limits the parasitic reactions at the cathode,[244] for example, catholyte oxidation and current collector corrosion.

In Situ CEI: An in situ CEI is formed by the decomposition of electrolyte components at the cathode-electrolyte interface. In particular, a few additives are known for their stabilizing effect in liquid electrolytes, and their application is beneficial also for SPEs and GPEs.

The two most popular CEI formers are lithium salts, namely lithium bis(oxalato)borate (LiBOB) and lithium difluoro(oxalate)borate (LiDFOB), which are either used as main salts or added as secondary salts in the SPEs and GPEs (**Table 6**).[133,210,238,241,242,245–247] A possible mechanism of the CEI formation with LiBOB and diglyme-based electrolyte involves the breaking of the B—O bonds in the BOB^- anion, including a subsequent coupling reaction with the diglyme and the formation of anionic aggregates on the cathode particles surface.[242] In addition, the CEI forming ability was observed with fluorinated compounds, such as the perfluorinated anion trifluoro (perfluoro-tert-butyloxyl) borate ($TFPFB^-$),[248–250] fluoroethylene carbonate (FEC),[251] AlF_3, or even LiF.[200] However, the role of LiF in the CEI is not clearly understood. Although LiF is speculated to be a vital component in the CEI, the high concentrations of LiF on the cathode/electrolyte interface are also indicative of extensive electrolyte decomposition and may increase the interface resistance.[252] Other reported CEI-formers include azo-compounds, that form Li_3N-rich CEI,[253] anhydrides,[195] and tetramethylene sulfone (TMS).[183]

2.4. Other Sources of Degradation in HVLP Batteries

2.4.1. Transition Metal Dissolution

Transition metal dissolution (TMD) from cathode materials is a major source of capacity fade in high-energy lithium batteries and yields the well-known and detrimental phenomenon of electrode cross-talk.[254] TMD can directly cause cell capacity fade owing to the loss of active material, degradation of cathode interface,[255,256] and the deposition of the dissolved transition metal ions increases the impedance of the SEI layer.[254,257] The operation at elevated temperature and the increased upper cut-off voltage during cycling accelerates this process.[258] In addition, the presence of acidic impurities in the electrolyte, such as HF, can further promote TMD.[259]

In particular, TMD is critical for manganese-based cells, especially for those containing spinel LMO as the active material.[256,260] In addition to Mn-based spinels, TMD is relevant for Mn-containing layered oxides[261] as well as other transition metal ions. The dissolution of Co is a primary reason for capacity fade in LCO, in particular at high voltages and in presence of HF.[153,262–264] In NMC, preferential Mn dissolution is observed at low voltages,[265] but considerable Co and Ni dissolution are detected over 4.6 V.[266]

The use of polymer or GPEs may reduce TMD, because of the reduced solubility of transition metal ions in these media.[143,174] As such, lower metal-ion solubility in GPEs has been reported with other metal ions such as Co ions.[263] Most polymer electrolytes use alternative salts such as LiTFSI, which is more stable than $LiPF_6$—both thermally and against hydrolysis. This characteristic potentially reduces the presence of detrimental HF. Recently, Huang et al. demonstrated that TMD is dependent on anion chemistry, and specifically, the use of LiTFSI reduces the Mn dissolution process from LMO.[267]

Nonetheless, existing research has not clarified whether the TMD can be entirely suppressed only by substituting liquid electrolytes with SPEs or GPEs. In particular, SPEs require high operational temperatures (60 °C or higher) that may further prompt cathode structural instability and accelerate the TMD.[268] In contrast, GPEs operate at room temperature, but TMD may still be observed as these electrolytes often include the same $LiPF_6$/carbonate solutions as standard liquid electrolytes. Therefore, other strategies should be employed to achieve the suppression of TMD. The application of a coating layer on the cathode surface,[269] or the in situ formation of a protective layer[163,184,193,251] are viable approaches to improve cyclability with cathode materials prone to TMD such as LNMO and LMO.

Furthermore, TMD can be hindered through the trapping of the transition metal ions (especially Mn^{3+}) and HF scavenging by specific functional groups in the electrolyte. Moreover, chelating/scavenging activity has been reported with poly(ethylene-alt-maleic anhydride)-containing GPEs and LMO as the cathode material,[270] GPEs containing polydopamine spheres and poly(vinyl alcohol), and LMO,[271] and with poly(vinylene carbonate–acrylonitrile)-based GPE and LNMO, which can be ascribed to the chelation of transition metal ions by the nitrile groups in the polymer matrix.[151] The application of GPEs containing chelating functional groups is beneficial with layered oxides, for example, NMC-622[272] and LCO.[153] The transition metal ion trapping ability is shown also by carboxylate-containing binders, such as CMC, polyacrylic acid, sodium alginate, and poly(methyl vinyl ether-alt-lithium maleic acid) (P(MVE-LMA)).[239,273–276]

2.4.2. Current Collector Corrosion

The corrosion of the cathode current collector constitutes a major source of degradation at high voltages. For all cathode chemistries, aluminum is used as the universal substrate, and it is kinetically stabilized at high voltages via passivation. This process relies more on the salt (or salt anion) species rather than on the solvents.[175] PF_6^- can passivate aluminum at both high potentials and elevated temperatures, and this is one of the major reasons for which $LiPF_6$ is considered the most suitable salt for the LIB industry. The decomposition of PF_6^- in presence of water traces is accompanied by the formation of HF, which reacts with Al to form a passivating layer of AlF_3 or AlOF.[277] Conversely, $TFSI^-$ is the most widely used salt anion in SPEs owing to its stability, but it fails to passivate the current collector. Furthermore, $TFSI^-$ anion forms soluble $Al(TFSI)_3$ complexes, thereby prompting current collector corrosion.[278] With PEO/LiTFSI–based SPEs, Al corrosion has been observed at potentials as low as 3.8 V versus Li/Li^+.[279] In contrast, the corrosion with SPEs may be less pronounced in comparison to liquid electrolytes owing to the reduced solubility of the corrosion products.[280] The corrosion of aluminum by $TFSI^-$ can be effectively suppressed at high salt concentrations,[134,277,281] owing to the exclusion of the solvent molecule from the electrode interface or the reduced solubility of the corrosion products. In addition, certain electrolyte additives may aid in passivating the current collector. For instance, AlF_3,[282] methyl difluoroacetate (MFA),[283] and ionic liquids, reportedly decrease the solubility of $Al(TFSI)_3$ complexes, thereby shifting Al corrosion potential.[94,284]

Furthermore, other anions have been studied as potential replacements for the thermally unstable PF_6^-, which exhibit superior passivating properties compared to $TFSI^-$. These include bulkier perfluorosulfonyl imides, possibly because of the solvent exclusion effects or the reduced solubility of the Al-anion complexes.[279,285,286] FSI^- manifests improved passivating properties compared to $TFSI^-$,[287] owing to the lower stability of the fluoro-sulfonyl bond. Specifically, a high stability against corrosion has been observed at high LiFSI concentrations.[139,288]

Reportedly, difluoromethanesulfonyl)(trifluoromethanesulfonyl)imide anion ($DFTFSI^-$) suppressed the Al corrosion in carbonate solutions, owing to the decomposition of the anion that results in the formation of AlF_3 and LiF passivating layers.[289] Borates such as BF_4^- and BOB^-, passivate aluminum as well as fluorophosphates.[17] Apparently, most fluorinated salt anions, except $TFSI^-$ possess a kind of Al-passivating ability. The substitution of $TFSI^-$ with FSI^-, and the inclusion of borate-based secondary salts may be a good strategy to prevent Al corrosion at high voltages. With LiTFSI, current collector corrosion can be somehow limited by using carbon-coated aluminum current collectors.[290]

3. Statistical Overview of HVLP Batteries

To assess the current state-of-the-art cyclability of HVLP batteries, data from 186 publications reporting HVLP cells cycled from 2004 to 2022 were analyzed in this study. The total number of data entries was higher than the number of analyzed publications as several studies reported multiple long-cycling tests of the proposed polymer electrolyte using various cathode materials, cycling temperatures, or variations in the upper cut-off voltage. We considered the cycling tests with 4 V- and 5 V-class cathode materials (e.g., LCO, NCA, NMC, LNMO), excluding all cycling tests with LFP (which is considered a 3-V-class cathode material). The list of 186 articles and the collected information were compiled in the Supporting information.

The most common electrolyte materials used in the reviewed publications are presented in **Figure 4**. Among the various polymer matrices, polyethers (PEO and its low molecular weight equivalent PEG) were the preferred ones, which accounted for approximately 43% of the proportion (Figure 4a). They were used individually or in combination with other polymer types. The selection of PEO is justified by the high conductivity of polyether-based SPEs, but it is noteworthy in HVLP cells, given the instability of polyethers over 4 V versus Li/Li^+ (refer to Section 2). The second-most common polymer matrix is P(VdF-HFP), followed by polycarbonates and PVdF. In particular, PVdF-based electrolytes are usually employed in GPEs and occasionally in HSEs, which are reportedly characterized by higher oxidative stability compared to polyethers.

Prior to the assessment of the cell performance, the oxidation potential of the polymer electrolytes must be measured. In 151 out of 186 publications, this value is usually determined by voltammetric methods (refer to Section 4.1). The reported oxidation voltage versus Li/Li^+ (or upper limit of ESW-UL) of the proposed electrolytes is presented in Figure 4b based on the information from the 151 papers that reported the value of ESW-UL measured using LSV,[291] CV,[213] and/or the floating/leakage current test.[246]

The average ESW-UL of the polymer electrolytes with various polymer hosts (all values are provided in vs Li/Li^+) in descending order is: PMMA (5.14 V) > Others (5.03 V) > Polycarbonates (4.99 V) > PVdF (4.94 V) > P(VdF-HFP) (4.88 V) > PAN (4.88 V) > PEG (4.78 V) > PEO (4.77 V). The standard deviation of the obtained ESW-UL values is high in all cases (up to 0.4 V for electrolytes containing PMMA, polycarbonates, and PEG). More importantly, to highlight that the average ESW-UL value for PEO-based electrolytes is comfortably located over 4.5 V, which should be sufficient for cycling with most 4-V-class electrolytes. However, this is in contrast with most basic studies on the electrochemical stability of PEO, which indicates the onset for oxidation below 4 V versus Li/Li^+ (refer to Section 2). The discrepancy is partly caused by the inherent limitations of the standard voltammetric measurements, which tend to overestimate the oxidative stability of polymer electrolytes, as discussed earlier. Indeed, most studies employing polyether-based electrolytes employ various stabilization strategies for protecting the electrolyte from oxidation or chemical degradation. Among the 93 studies conducted on polyether-based electrolytes, 20 employed a coating on the cathode, out of which 11 used LCO as the cathode material. Overall, the most common coating material was LATP. Moreover, 24 studies used a blend with a distinct polymer or cross-linked polymer, 5 studies used a multilayer electrolyte (where the polyether was not in contact with the cathode), and 13 used composite electrolytes with varying ceramic materials.

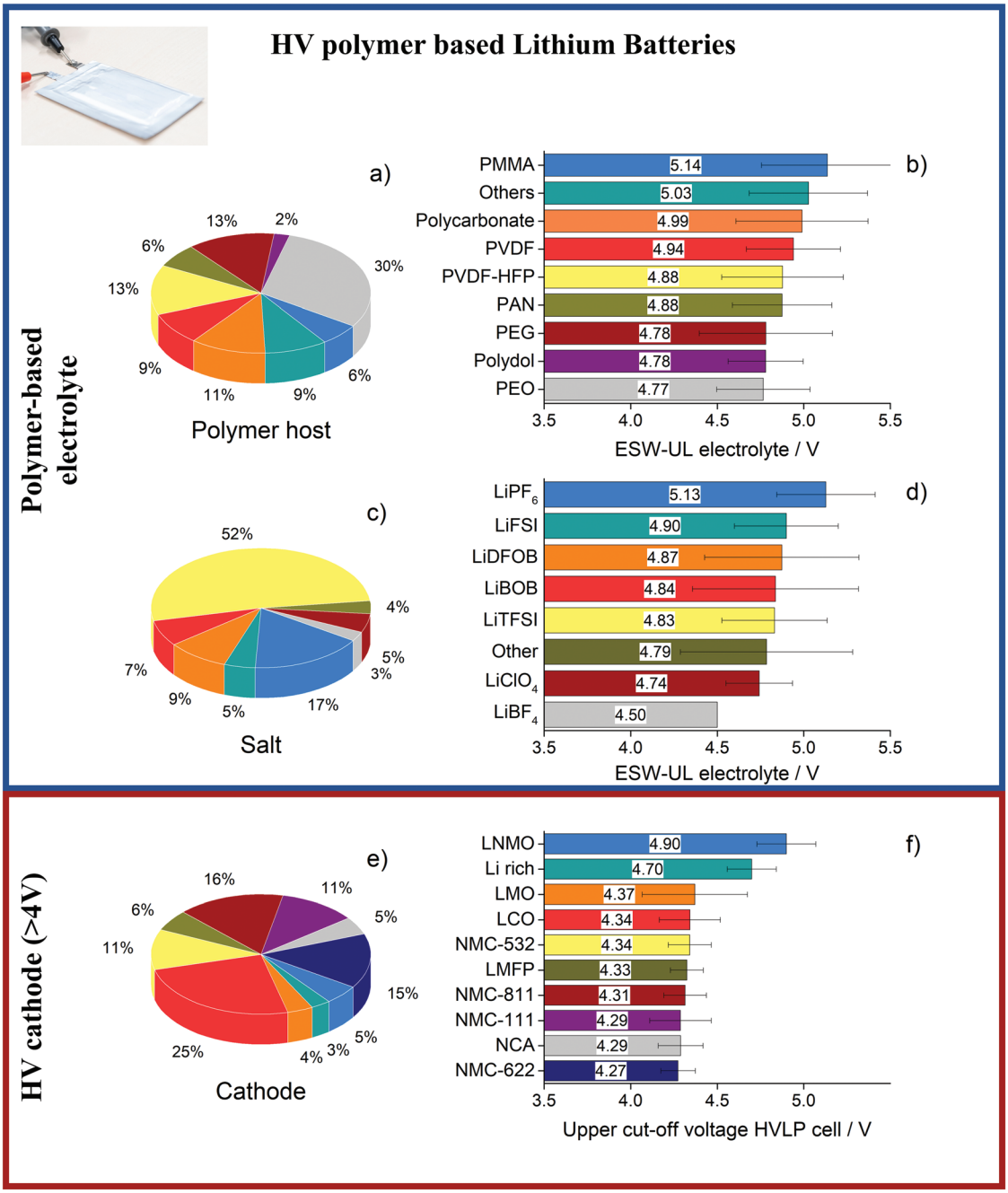

Figure 4. Polymer host in polymer electrolytes: a) employment frequency of different polymer hosts and b) average ESW upper limit (ESW-UL) with different polymer hosts. Lithium salt in polymer electrolytes: c) frequency of employment of the most common lithium salts in HVLP cells, and d) ESW-UL of electrolytes with different lithium salts. Cathode materials in HVLP cells: e) frequency of employment and f) upper cathode voltage of different cathode materials.

The average ESW-UL value of the polymer electrolytes according to the employed lithium salt is presented in Figure 4d). Polymer electrolytes with $LiPF_6$ exhibit the highest oxidation stability with an average value of over 5 V versus Li/Li^+. In general, $LiPF_6$ is mostly used in GPEs with carbonate electrolyte solutions. Therefore, the higher average stability of electrolytes containing $LiPF_6$ may indicate a higher oxidative stability for carbonate-based GPEs. Comprehensively, LiTFSI is the most popular salt used in the examined papers (Figure 4c). As LiTFSI exhibits a higher thermal and hydrolytic stability than $LiPF_6$, it is regarded as a more appropriate selection for most polymer electrolytes. The average oxidation stability of polymer electrolytes with LiTFSI, LiFSI, LiBOB, and LiDFOB was ca. 4.85 V versus Li/Li^+, although the standard deviation for LiBOB and LiDFOB was ca. 0.5 V. This variation suggests that the salt does not govern the oxidative stability of the electrolyte.

This is expected as most salts manifest higher oxidative stability than the polymer matrix (refer to Section 2). In contrast, LiBOB and LiDFOB can form stable CEI layers, and therefore, are regularly used in HVLP cells, despite providing lower ionic conductivity than LiTFSI. Both of them are used either individually as an additive or in dual or ternary salt systems.

Although a majority of the research (66%) claimed that their proposed electrolyte is stable over 4.8 V versus Li/Li^+, only 5% of the studies selected $LiNi_{0.5}Mn_{1.5}O_4$ (LNMO) or Li-rich cathode materials for the long-term cyclability test. Among the listed high voltage electrode active materials, these materials were the only ones that reversibly reacted at voltages beyond 4.7 V versus Li/Li^+.[292] This is because of the difficulty of cycling SPEs (especially, polyether-based) over 4.5 V versus Li/Li^+. As calculated from 254 data entries and illustrated in Figure 4e, the most frequently employed cathode material in HVLP cells is nickel cobalt manganese oxide (NMC) with a 53% share. The compounds with higher nickel content (NMC-811 and NMC-622) appeared more frequently because of the recent interest in these combinations, owing to their higher capacity. The second-most commonly employed material in the HVLP batteries is lithium cobalt oxide (LCO) with a 25% share. Historically, LCO was the selected material for high-voltage batteries, but in recent years the focus has gradually shifted toward cobalt-lean active materials. In the future, the share of LCO is expected to further decrease. As polymer and ceramic electrolytes are essential for a wider utilization of metallic lithium in commercial batteries, only 7 out of 186 studies use other anode materials than Li metal (6 with graphite and another with mesophase carbon microbeads, MCMB).

The upper cut-off voltage used for the HVLP cells during long-term cycling is presented in Figure 4f. The average upper cut-off voltage with LNMO and Li-rich cathodes is over 4.6 V. However, for nickel-rich-layered oxide active materials such as NMC and NCA, it is approximately 4.3 V. In comparison, the LMO and LCO exhibit a slightly higher cut-off voltage (ca. 4.35 V). An increase in the upper cut-off voltage allows for raising the average discharge voltage and the discharge capacity in layered oxides. However, this increases the risk of electrolyte and cathode degradation owing to increased irreversible phase transitions. Based on the similar average cut-off voltages employed for the four types of NMC (4.3 ± 0.3V) with different polymer electrolytes, it appears that the cathode material (and not the polymer electrolyte type) determined the upper cut-off voltage. Ultimately, the latter is mainly influenced by the structural changes (oxygen loss, phase changes)[4] and by the distinct CEI behaviors of the various cathode materials.[293]

To investigate a preferred cathode/electrolyte combination, we analyzed various combinations of polymer electrolytes versus cathode active material (CAM) utilized in 186 studies. The multiple combinations of cathode material versus type of polymer matrix are depicted in **Figure 5**a. In HVLP cells, PAN, PVdF-based materials, polycarbonates, and PMMA have been proposed as polymer hosts for Li-rich and LNMO cathode materials. Interestingly, these polymers deliver the highest ESW-UL, as measured using voltammetric methods. With other cathode materials that allow a cut-off voltage below 4.5 V, polyether-based electrolytes represent the largest share. This result hints at the possibility of using SPEs (largely polyether-based) with 4-V-class cathode materials, whereas 5-V-class cathode materials are largely confined to HSEs or GPE systems, which employ polymer matrices with higher oxidative stability.

In the case of the salt system, the various combinations of salt type versus cathode materials in HVLP cells are presented in Figure 5b. As salt is essential for the interphase formation at the cathodic and anodic side, these results can provide insights regarding the salts that could be beneficial or detrimental for CEI formation. In particular, only two salt types were proposed for LNMO systems: $LiPF_6$ and LiBOB, wherein the latter does not deliver the highest oxidative stability. However, it is often used because of its effect on interface formation (refer to Section 2.3.4). Incidentally, the most popular salt in polymer electrolytes (LiTFSI) was not selected for LNMO HVLP cells. This is primarily because the LiTFSI prompts the corrosion of the Al current collector, which is a severe issue at the high voltages. In contrast, $LiPF_6$ is the preferred salt with LNMO owing to the suitable Al passivating properties. The preferential use of $LiPF_6$ clearly indicates that LNMO is mostly cycled with GPEs containing carbonate-based electrolytes. In addition, the type of salt employed with the standard layered-oxide cathode materials

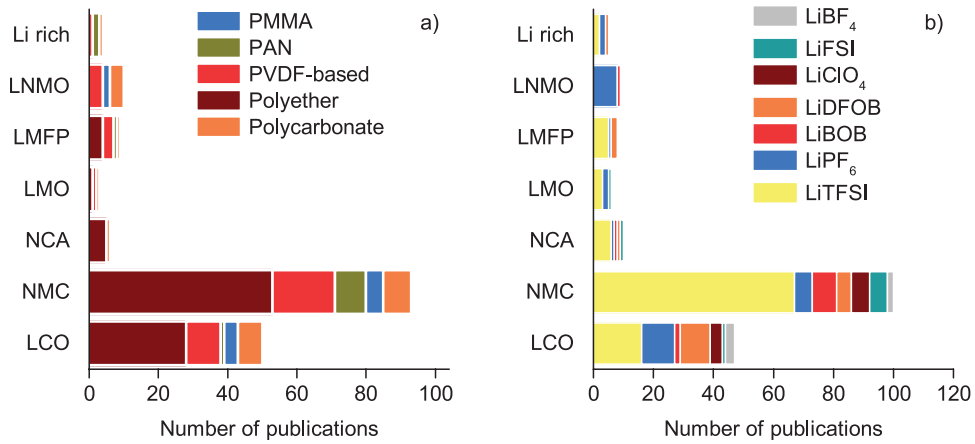

Figure 5. Cathode material–polymer electrolyte combinations. a) Number of publications with different cathode materials and polymer hosts. Number of publications with different cathode materials and lithium salts.

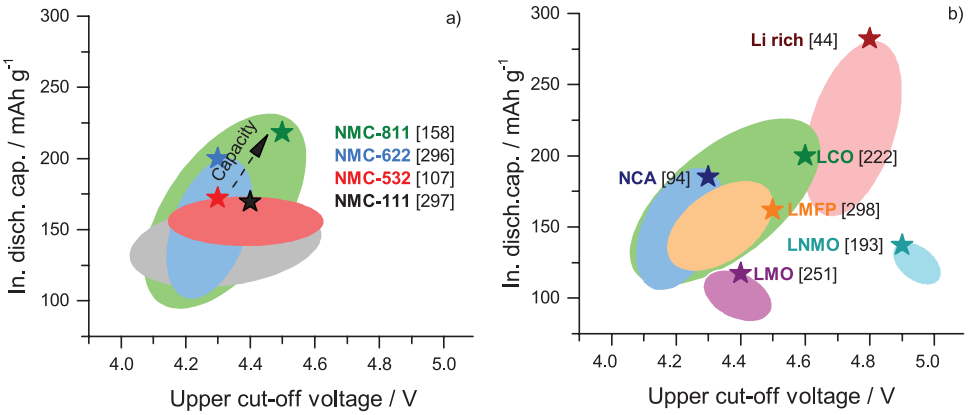

Figure 6. Initial discharge capacity of the HVLP batteries versus upper cut-off voltage in publications with a) $LiNi_xMn_yCo_zO_2$ as cathode material and b) the rest of the cathode materials. Ellipses contain the different publications using the indicated cathode materials (for information of each point see Figure S1, Supporting Information), stars correspond to the highest gravimetric energy densities for each cathode material.

(i.e., NMC and LCO) exhibited a different trend. In NMC, the majority of the studies (60%) employed LiTFSI as a single salt or in a dual-salt system. However, for LCO cathodes, the LiTFSI appears in only 33% of the research, similar to $LiPF_6$ and LiDFOB. This may have divergent explanations. In principle, the frequent use of $LiPF_6$ with LCO is indicative of its use with carbonate-based GPEs. Until recently, SPEs were used only with 3-V-class cathode materials (e.g., LFP and V_2O_5), whereas LCO was combined almost exclusively with liquid electrolytes and GPEs. The renewed interest in the high-voltage application of SPEs (typically, PEO-LiTFSI systems) is relatively recent, and is in accordance with the rise of NMC and the progressive abandonment of LCO as the standard cathode material. Moreover, the results suggested that cyclability is possibly higher with NMC than with LCO (refer to Figure 9). The frequent application of LiDFOB with LCO suggests that this cathode material requires a CEI-forming salt, whereas electrolyte degradation is possibly less severe with NMC, or at least with the low-Ni-type NMC, thereby enabling the use of LiTFSI.

As expected, the most common material combination is NMC-PEO-LiTFSI. The initial discharge capacity versus upper cut-off voltage diagram is illustrated in **Figure 6** for a) NMC-based cathodes and b) for the remaining cathode types analyzed from the 186 articles. To attain substantial improvements in the discharge energy and power densities, the average discharge voltage should be maximized. Although this parameter is related to the upper cut-off voltage, it is not directly proportional because the cell voltage varies non-linearly with the lithiation degree. As the average discharge voltage (or voltage vs capacity curve) is often not provided in the literature, the present analysis was indirectly performed based on the upper cut-off voltage.

Therefore, the maximum gravimetric energy densities achieved by the HVLP cells are located in the top-right region of the graph. The highest values of energy density were achieved by HVLP cells with Li-rich cathode material.[44,294,295] The maximum initial discharge capacity among all 186 papers was 282 mAh g^{-1}, attained by $Li[Li_{1/6}Ni_{1/4}Mn_{7/12}]O_{7/4}F_{1/4}$, with 4.8 V selected as the upper cut-off voltage.[44] However, the capacity retention of these HVLP batteries using Li-rich cathode was poor as they reached 80% SoH after 40–70 cycles. The employed composite electrolyte was PAN/Al_2O_3–triethylene glycol diacetate–2-propenoic acid butyl ester with $LiPF_6$ acting as the salt. The HVLP cells with LCO, NMC-811, and NMC-622 selected as the cathode materials reached initial discharge capacities over 200 mAh g^{-1}.[158,187,191,211,222,231,296] The nickel-rich variations of NMC (NMC-811 and NMC-622) delivered higher values of initial discharge capacities compared to the Ni-lean counterparts (NMC-532 and NMC-111).[297] However, the Ni-rich materials exhibited more variations in the initial discharge capacities when they were cycled to the same maximum voltage (i.e., NMC-811 ranges from ca. 150–220 mAh g^{-1} and NMC-622 from 100–200 mAh g^{-1} when cycled up to 4.3 V). This was probably caused by a lower stability for such cathode materials. Notably, in most cases, the first cycles (and consequently, the indicated initial discharge capacity values) were performed at low C-rates (between 0.05 and 0.1C).

Overall, the initial discharge capacity increases when higher cut-off potentials of the cell are employed, as higher degrees of lithiation are achieved. In particular, the capacity of LCO is almost doubled when the voltage increases from 4.2 to 4.6 V. In the case of NMC-811, NMC-622, and NMC-532, the capacities can extend beyond 150 mAh g^{-1} with cut-off voltages of 4.3 V. Other studies employing cut-off voltages of 4.5 V with NMC-811[158] and 4.4 V with NMC-622,[296] report even higher initial capacities of approximately 200 mAh g^{-1}. The maximum voltage at which various cathode materials were tested is 5 V for LNMO, 4.8 V for Li-rich cathodes, 4.6 V for LCO, NMC-111, and NMC-532, 4.5 V for NMC-811, LMO, LFMP,[298] and NCA, and 4.4 V for NMC-622. However, in most cases, the maximum energy densities are not achieved when the highest cut-off voltages are used (refer to Figure S1, Supporting Information).

The previous analysis provides an overview of the energy density landscape of cathode–polymer electrolyte systems for HVLP batteries, but the cycling stability is the critical parameter for appropriately selecting the cell chemistry. The studies reporting long-term cycling for more than 500 cycles are presented in **Figure 7**. Among the 186 papers analyzed herein, only 18 studies reported more than 500 cycles, and in particular, no study reported more than 500 cycles with LMO, NMC-532,[299] or Li-rich as cathode materials. For these cathode materials, the cases with the highest cyclability (200, 200, and 85 cycles respectively) were represented in Figure 7.

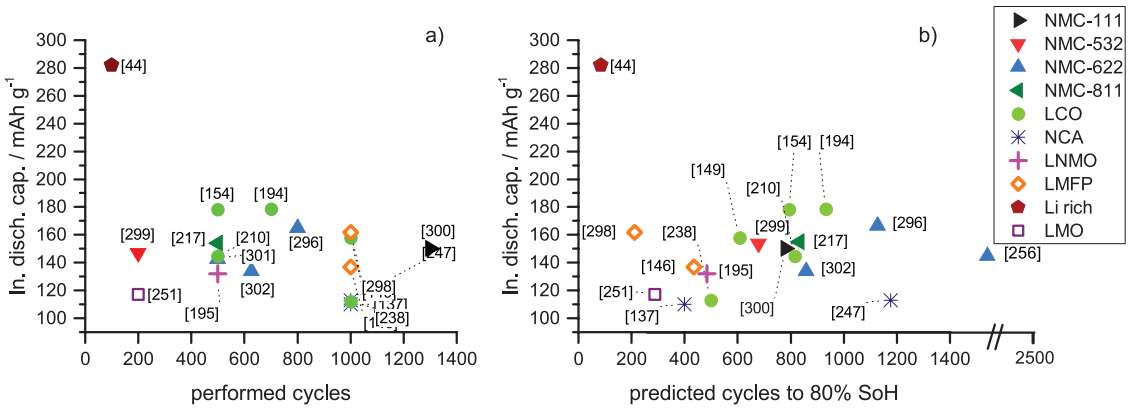

Figure 7. Discharge capacity over cycling from all the screened publications that reports more than 500 cycles: a) initial discharge capacity versus performed cycles and b) initial discharge capacity versus predicted cycles to 80% SoH.

The combination of NMC-111 with ionic plastic crystal polymer materials exhibited the highest number of cycles (1300).[300] Additionally, six HVLP battery combinations achieved cycles >1000.[137,146,149,238,247,298] However, the number of cycles from these batteries to 80% SoH ranges within 400–800 (they were terminated at SoH < 80%). In Figure 7b, the predicted number of cycles to 80% SoH was estimated by linear fitting the data from the initial and final discharge capacity. In particular, only two HVLP cells exhibited an extremely low degradation rate (>1000 predicted cycles to 80% SoH in Figure 7b) and initial discharge capacities over 140 mAh g^{-1}.[296,301] Although both cells employed a GPE electrolyte, the second cell delivered an exceptionally low degradation rate (>2500 cycles to 80% SoH) that was potentially caused by the extremely low active-material loading (<2 mg cm^{-2}). Note that the active material loading of all these HVLP cells performing over 500 cycles is below 3 mg cm^{-2},[44,137,146,149,154,194,195,210,217,238,247,251,298–302] except the study with NMC-622 and polyamide/carbonate electrolyte-based GPE, that uses a loading of 6 mg cm^{-2}.[296] If only capacity decay and specific capacities are considered, 8 out of these 18 HVLP cells delivered initial discharge capacities > 140 mAh g^{-1} and performed over 500 cycles, enabling 400–1200 predicted cycles to 80% SoH.

The relationship between the active material loading of the cathode electrode and the cycling stability of the HVLP cells is illustrated in **Figure 8**. In 50% of the HVLP cells, the active material loading was extremely low, below 2.5 mg cm^{-2}, whereas only 10% of the cases exhibited loadings beyond 8.6 mg cm^{-2}. The low number of HVLP cells with a high quantity of CAM loading is probably related to the inherent challenge of cycling polymer electrolyte-based cells at correspondently high current densities, owing to the sluggish lithium-ion diffusion in the cathode and the accelerated lithium dendrites growth. Overall, half of the studies reported 100 cycles or less, and only 10% of the studies reported more than 400 cycles. Note that no HVLP cell with CAM loading > 10 mg cm^{-2} delivered more than 1000 cycles (death zone top-right corner of Figure 8a). This limit progressively decreased with the increasing CAM loadings, that is, for loadings > 15 mg cm^{-2}, no study reports more than 200 cycles. To date, achieving a suitable cyclability is apparently challenging with practical loading (>15 mg cm^{-2}).

In half of the publications (vertical red line in Figure 8b), the predicted number of cycles to 80% SoH was almost 200 cycles, whereas in only 10% of the studies, the predicted cyclability

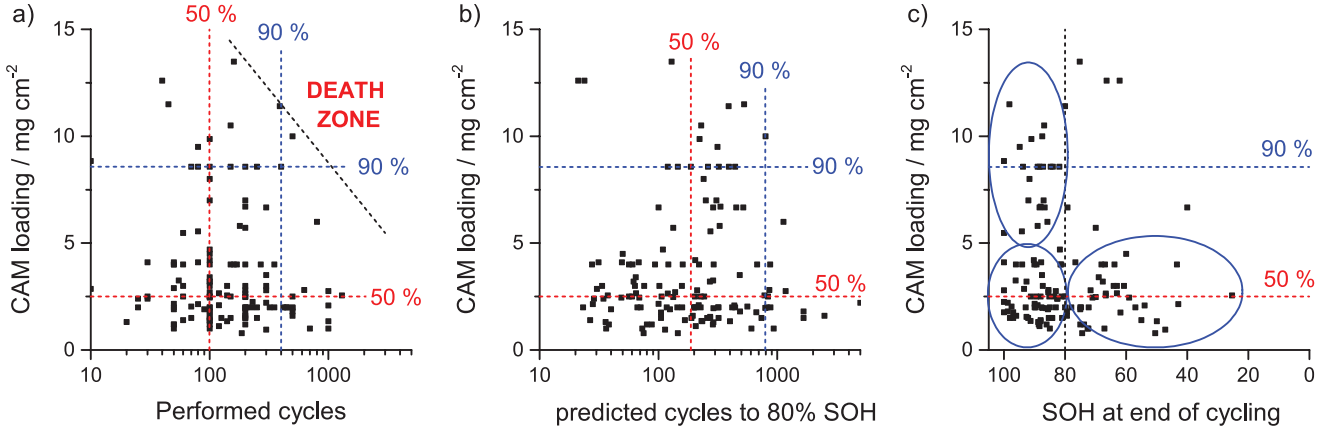

Figure 8. Cathode loading, number of performed cycles, and predicted cyclability (until 80% capacity retention) of HVLP cells. a) Cathode loadings versus the corresponding performed cycles. Red and blue dotted lines represent the values of 50 % and 90 % percentiles, respectively; b) Cathode loadings versus the corresponding predicted cycles at 80% capacity retention. The latter was calculated by linear fitting of the discharge capacity profiles; c) Performed cycles versus predicted cyclability.

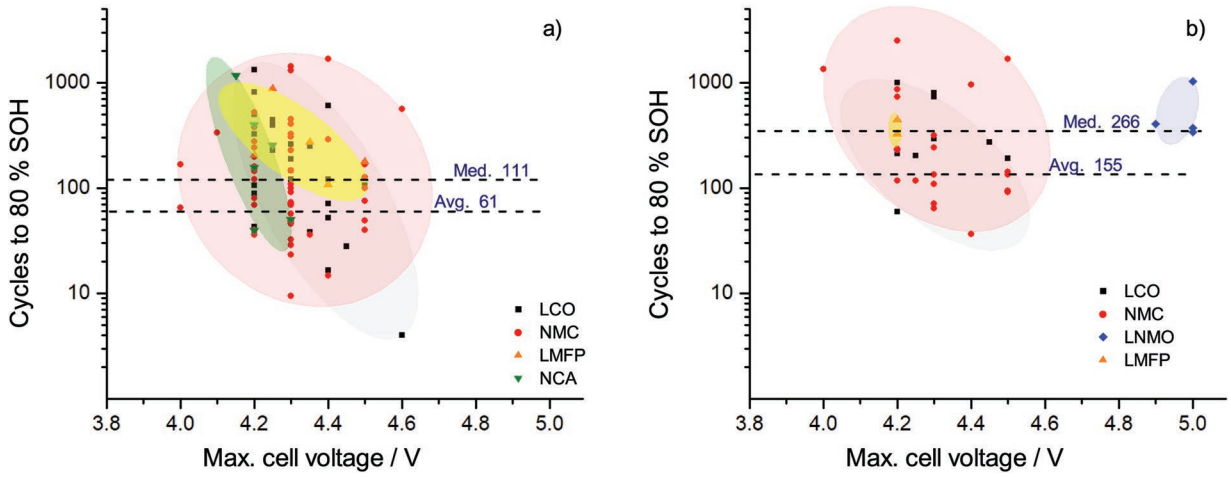

Figure 9. Predicted cycles to 80% capacity retention in the publication utilizing a) PEO or PEG and b) PVdF or P(VdF-HFP) as main polymer or the polymer facing the cathode side (in multilayer systems).

was greater than 800 cycles (vertical blue line in Figure 8b). In general, the predicted cyclability is greater than the actually performed cycles (e.g., median of performed cycles is 100, vertical red line in Figure 8a). More specifically, this case refers to cycling at high loadings, which is mostly terminated before the SoH reaches 80% (Figure 8c). In contrast, several studies at low CAM loadings are conducted until a low SoH is achieved. The discrepancy between the predicted cyclability and performed cycles can be explained by either a) a long experimental period hindering further cycling, or b) the occurrence of sudden capacity decay or shorts. At high loadings, both reasons may account for influence as cycling is forcibly conducted at low C-rates, and the probability of shorts and degradation is higher than that at low loadings.

Overall, considering the large variability of polymer types employed in the HVLP cells (Figure 7), no clear trend was observed regarding the polymer type and its cyclability. To further analyze the degradation of polyether-based electrolytes, their cycle life was compared with that of the second-most common type, PVdF-based electrolytes. Accordingly, the variations in the cycling stability with the upper cut-off voltage are presented in **Figure 9**. As observed, the variation follows an exponential trend, but considerable variations (up to 2 orders of magnitude in case of polyethers) were observed by employing the same cut-off voltage and the same cathode material. This can be explained by the various mass loading, C-Rate, and temperature employed, among other factors.

Overall, the average capacity loss of polyether-based electrolytes is three-times greater than that of PVdF-based electrolytes (analysis from 97 and 34 data entries, respectively). Within the group of polyether-based electrolytes, the reduction in the cycle life with the cut-off voltage (slope in Figure 9a) follows this trend: NCA > LCO > LFMP. On the contrary, PVdF degradation is apparently independent of the voltage (Figure 9b), as capacity deterioration values for LNMO-PVdF cells were similar for a cut-off voltage of 4.8 or 5 V, and those are less than the capacity losses obtained with NMC or LCO, cycled up to lower cut-off voltages (≈4.3 V). With PVdF-based systems (typically GPEs), the capacity deterioration is driven by the degradation of the liquid electrolyte or plasticizer.

Owing to the low room-temperature ionic conductivity of polymer electrolytes, ca. half of the long-term cycle stability studies were performed at temperatures over 40 °C (**Figure 10**). Specifically, with PEO-based electrolytes, most publications presented data between 50 and 60 °C, and the PEO studies performed at room temperature constituted only 30% of the total number of studies. Based on these, one-third of the PEO studies conducted at room temperature considered GPEs and another third contains inorganic particles (hybrid polymer electrolytes). In PVdF-based electrolytes, the operating conditions primarily involved room temperature (31 out of 39). In most PVdF and P(VdF-HFP) publications (17 out of 34), the polymer electrolyte is employed along with liquid electrolytes forming a gel polymer. This is because of the porous structure that can absorb and fix liquid electrolytes.[303] However, with other polymer electrolyte types, several publications present cycling data at room temperature.

Although the stability of the SPE interface is expected to decrease at higher temperatures, the capacity decay of PEO and PEG-based HVLP cells was less at 60 °C than that at 25 °C. This was reported in two distinct studies with LCO and LFMP as the cathode material and an upper cut-off voltage of 4.3 and 4.25 V, respectively.[189,227] In both cases, the C-Rate employed at 25 °C was equal to or similar to that at 60 °C (0.2 and 0.3C, respectively), signifying that the effect of the electrolyte diffusion overpotential at room temperatures is more detrimental toward the battery life than the increased electrolyte oxidation or the structural degradation of the cathode at 60 °C. However, the variations in capacity fade with temperature in high voltage lithium metal–PEO cells might not follow a diminishing trend. For instance, in the study by Homann et al. with Li-PEO/LiTFSI–NMC battery, a 30% capacity loss was observed after 50 cycles at 0.1 C at 60 °C, whereas no loss was observed at 40 °C.[103]

Most scholars selected the operation at high temperature (T > 40 °C) possibly because of the higher discharge capacities compared to room temperature conditions,[103,189,227,250] that is,

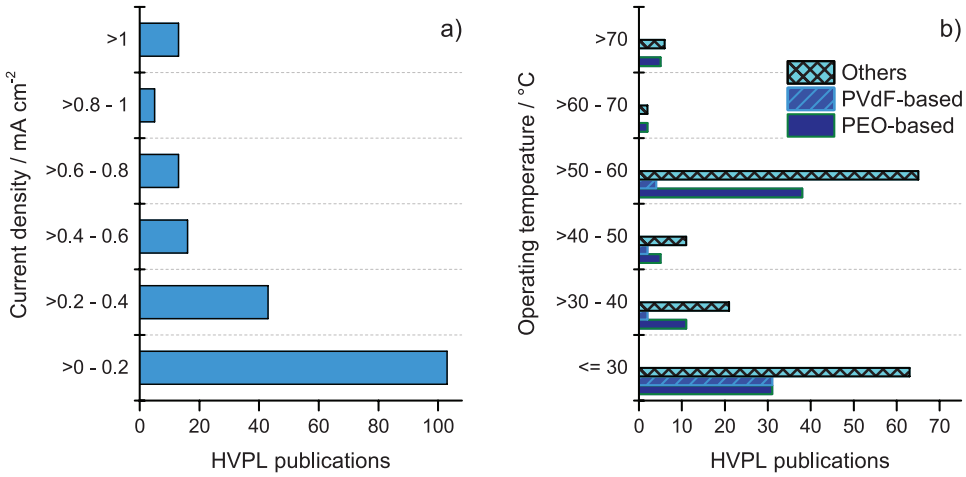

Figure 10. a) Current density from all the data inputs. b) Operating temperature range of the different polymer electrolytes.

up to 35% less at 25 °C than at 60 °C.[189] This variation in the discharge capacity is caused by the higher electrolyte overpotential at room temperature. Although there are exceptions, certain publications using GPEs reported similar or even higher discharge capacities at RT than at higher temperatures.[200,211,251] The highest operating temperature reported in the 186 reviewed papers was 100 °C, where an anion-anchored conjugated microporous polymer with ionic liquid and LiTFSI was cycled in LCO and NMC-111/Li metal cells.[304] In this case, the initial discharge capacities were reduced considerably, despite the low C-rate employed.

Conclusively, the first results indicated that the degradation rate of HVLP batteries using PEO-based electrolytes is greater at room temperature than at 60 °C. However, the optimum operating temperature for maximizing the life expectancy is situated in between, as high temperature accelerates the side reactions. Thus, further studies are required for each electrolyte system at varying temperatures to identify the most critical degradation mechanisms at each temperature.

Despite significant progress in solid and quasisolid-state battery technology over the recent years, the utilization of high mass loading and high current densities are crucial for achieving high energy and power density batteries. Around 20% of existing studies do not reveal information on the active material loading of the cathode or the current density at which cells are cycled; only the C-rate is indicated. As reported, these two factors crucially affect the degradation rate. In papers that did not directly cite the current density, the mass loading and theoretical capacity of the cathode material were calculated based on the C-rate, (except in papers that indicated 1C = specific capacity mAh g^{-1}, for which this value was employed). As displayed in Figure 10, the cyclability study in most publications was performed utilizing low current densities (57% of the publications under 0.2 mA cm^{-2}). In 28 out of 186 publications, the cells were cycled at either moderate current densities (>0.5 mA cm^{-2}) and/or CAM loading (>5 mg cm^{-2}), and only in 9 out of 186 studies, both criteria were fulfilled. The cycling performance of the HVLP cells obtained from these 29 publications is summarized in **Table 7**.

4. Characterization Techniques for Degradation Phenomena

As summarized in previous sections, a deep understanding of the unique degradation mechanisms in HVLP batteries is required to improve its life expectancy. This section describes the techniques used to date for reviewing and characterizing the degradation phenomena of HVPL batteries. A brief overview is also provided for the basic characterization techniques for HVLP battery characterization.

4.1. Electrochemical Methods

CV is commonly used for determining the electrochemical behavior of selected electrodes in contact with various electrolytes and analyzing the reversibility of the system.[316] CV is useful for determining the electrolyte stability window. Although CV measurements are often employed to extract the entire ESW of the electrolyte, CV poses several limitations: i) any oxidation/reduction during the first half scan can influence the electrochemical behavior during the following reverse scan owing to the reaction of the decomposition products produced in the first place, ii) Li plating and stripping delivers much higher current densities than the electrolyte decomposition process, and therefore, weak decomposition processes may be masked, resulting in an overestimation of the electrochemical stability. In this case, the reduction stability could be evaluated by comparing the intensity of the plating/stripping peaks in consecutive scans, for example, a progressive reduction in the intensity may indicate a progressive degradation of the electrolyte, iii) it is necessary to operate at an extremely slow scan rate (0.1 mV s^{-1}),[105] which is translated in large measurement times. Altogether, the stability towards the reduction and oxidation should be evaluated in separated experiments, and CV is more useful for evaluating stability at low voltages. LSV is more appropriate for evaluating the high-voltage stability, because the reverse scan and following CV scans provide less insights. LSV is the standard method to determine the oxidation potential of the electrolyte, where the current is measured

Table 7. Cell performances in long-term cycling studies, achieved with high cathode loadings (>5 mg cm^{-2}) and/or high current densities (>0.5 mA cm^{-2}). Greyed cells indicate whether the cathode loading and/or the current density comply with these two criteria. Greyed cells in the cycle number column highlight the two publications reporting 500 cycles or more.

Electrolyte	Cathode	$m_{cath\ act}$/mg cm^{-2}	I/mA cm^{-2}	n_{cycle}	Cap $_{disch.\ in}$ mAh g^{-1}	Cap loss per cycle/%	Ref.
PEO/LiTFSI/ LIBOB/ $LiPF_6$	LCO	8.5	0.62	400	131	0.045	[227]
PDOL/LiDFOB	NMC-811	13.5	0.62	160	167	0.15	[198]
PEO/Ionic Liquid/LiFSI	NMC-111	6.66	2	300	148	0.039	[135]
Polyamide/LiTFSI/LiBOB/EC/EMC[a)]	NMC-622	6	0.96	800	200	0.018	[296]
Pyrd-PVA-CN[b)] gel/$LiPF_6$	NMC-622	9.87	1.35	100	178	0.09	[272]
SICPE/LiBFMB[c)]	NCA	5.2	0.7	200	151	0.195	[120]
PDOL/LiFSI	NMC-111	10.7	2.9	400	120	0.0475	[305]
PEO/LiTFSI	NMC	8	0.66	100	156	0.083	[203]
PEGDA/LiTFSI	NMC-811	10.5	0.5	100	200	0.12	[191]
P(VdF-HFP)/$LiPF_6$	LMO	10.8	0.32	100	95	0.084	[270]
PEO/PAN/LiTFSI	NMC-811	21	0.35	100	177	0,22	[306]
PEGMA/LiTFSI	NMC-532	8.836	0.24	10	120	0	[307]
PDADMATFSI/ LiFSI	NCA	8	0.04	20	150	1.4	[165]
PMMA/LiTFSI/LIBOB	NMC-111	11.4	0.21	390	136	0.051	[308]
PMMA/LiBOB	LCO	12.6	0.43	40	140	0.94	[309]
	NMC	12.6	0.43	40	131	0.83	
P(VdF-HFP)/LiBOB	$Li_3V_2(PO_4)_3$	10	0.39	500	130	0.025	[310]
PVdF/LiFSI	NMC-532	9.5	0.26	80	161	0.063	[43]
P(VdF-HFP)/LiTFSI	NMC-532	10.5	0.17	15	147	0.087	[168]
PEO/LiTFSI	LCO	5.5	0.15	60	140	0	[311]
	NMC-111	5.5	0.15	80	140	0.07	
P(VdF-HFP)/$LiPF_6$	LCO	2.5	0.87	150	150	0.098	[312]
PFEC[d)]/LiDFOB	LCO	3.2	0.87	100	173	0.073	[313]
PDOL/LiTFSI	NMC-111	2.5	1.5	60	153	0.33	[200]
P(VdF-HFP)/$LiPF_6$	NMC-532	4	0.54	50	149	0.21	[198]
PEO/LiFSI	NMC-811	2.5	0.69	150	148	0.049	[282]
PVdF/PMMA/PEO/ $LiPF_6$	NMC-532	4	0.54	167	200	0.029	[314]
P(VdF-HFP)/LiFSI	NMC-111	3.4	0.85	196	100	0.31	[228]
PEO/LiTFSI	NMC-111	2.65	1.44	126	120	0.31	[315]
PVC/PEO/PTFE[e)]/LITFSI	NMC-111	2	0.54	140	100	0.25	[209]
	LCO	2	0.54	120	100	0.1	

[a)]EMC: ethyl methyl carbonate; [b)]Pyrd-PVA-CN: cyanoethyl poly(vinyl alcohol) having pyrrolidone moieties; [c)]LiBFMB: lithium bis(fluoromalonato) borate poly(diallyldimethylammonium); [d)]PFEC: poly(fluoroethylene carbonate); [e)]PTFE: poly(tetrafluoroethylene).

as the potential between the working electrode and reference electrode is swept linearly with respect to time. The onset of oxidation can be detected using an exponential (Butler–Volmer-like) increase in the current.[317,318] Generally, LSV with polymer electrolytes is conducted in a two-electrode configuration with a blocking working electrode (typically composed of stainless steel) and a Li foil used as a reference and counter electrode. A common problem related to LSV (and CV) is the low signal/background ratio caused by slow reaction kinetics. In addition, there is no consensus in the scientific community regarding the determination of the oxidation onset. In particular, two distinct methods have been used: i) to consider the voltage at which an arbitrary current density limit is achieved (current cut-off method), ii) to consider the intersection of the tangent of the LSV profile above the oxidation onset with the *x*-axis, or iii) consider the intersection of tangents of the LSV curves at potentials below and above the onset of electrolyte decomposition (**Figure 11**). The determination of the oxidation onset with the current cut-off method is influenced by the scan rate (current increases with the scan rate, Figure 11a,b) as well as the mass transport limitations, which may be severe with polymer electrolytes. Although the tangent methods (ii and iii) are less affected by the scan rate and mass transport limitations, the selection of the intercept and the determination of the regions for linear fitting (for tangents construction) remain as arbitrary parameters (Figure 11c,d).[319] Following Mousavi et al.,[320] the linear fitting of I versus E profiles should be performed in the LSV regions in which the differential profile dI/dE approaches zero. Generally, the potential respective to the steep increase of the current was selected, corresponding to the final breakdown

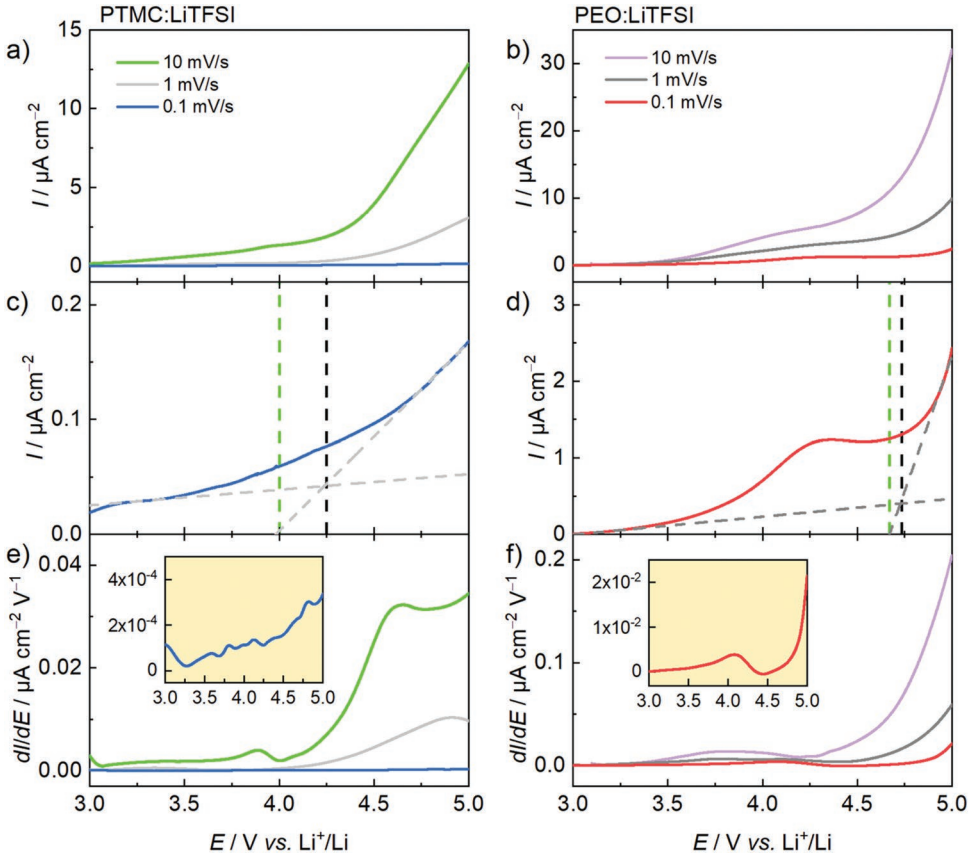

Figure 11. Determination of the oxidative stability by LSV of a,c,e) PTMC/LiTFSI and of b,d,f) PEO/LiTFSI. Panels (a) and (b) show the effect of the scan rate on the shape of the LSV profiles; panels (c) and (d) show the tangent method for the determination of the oxidation onset; panels (e) and (f) show the derivative profiles dI/dE at different scan rates. The insets show magnifications of the derivative profiles at the lowest scan rate. Reproduced under the terms of Creative Commons Attribution 4.0 License.[319] Copyright 2021, The Authors, published by IOP Publishing.

of the electrolyte. Below these limits, all current responses were neglected, possibly resulting in an overestimation of the electrochemical stability of the electrolytes. Furthermore, in certain cases, the inflection points may be difficult to distinguish. The analysis of the derivative profile dI/dE may be useful for detecting the low-intensity faradic processes (Figure 11e,f).

Floating test is an alternative method that determines the oxidative stability limit of electrolytes.[108] In the floating test, the cell is charged at a constant current up to a selected potential, and this voltage is maintained. To explore the oxidative limit of the electrolyte, the cell was progressively placed at higher voltages until the breakdown voltage is achieved. The oxidation stability limit corresponds to the voltage at which the steady-state or leakage current attains a predetermined value, or it represents the voltage at which the leakage current starts to increase with the voltage. This method is a more stringent test of oxidative stability, with respect to LSV or CV, because the electrolyte is maintained at each voltage step for a considerably longer period. This can be performed either with a blocking working electrode or with a cell cathode as working electrode, considering the electrolyte-electrode interaction.[150,197,200,203,246] If aluminum is used as a working electrode, this test indicates the passivation ability of the electrolyte with regard to the current collector corrosion.[321] Similar to other voltammetric methods, the floating test presents certain interpretation issues. In context, abrupt increases in the current may result from ultimate electrolyte decomposition, but this event may be preceded by a more gradual increase of the leakage current at lower voltages. Therefore, the interpretation of the floating test results is challenging in this case, because the last sudden increase of the current may mask the degradation events occurring at lower potentials, which may not be observed distinctly.

Alternative electrochemical methods employed for studying the electrolyte electrochemical stability include i) differential pulse voltammetry (DPV) that is a technique involving the application of amplitude potential pulses on a linear ramp potential. It is faster than CV with an improved signal-to-background ratio;[105] ii) synthetic charge–discharge profile voltammetry (SCPV), which replicates the potential versus time profile of a full cell containing a blocking working electrode;[319,322] iii) reversible/irreversible capacity analysis,[109,318,323] that uses the ratio of anodic versus cathodic capacity in CV as a measure of the irreversibility of the electrochemical process; and iv) cut-off increase cell cycling (CICC),[319] in which a full cell is galvanostatically cycled at progressively increasing cut-off voltages. Moreover, the reversibility of the electrochemical reactions is monitored by the evolution of the coulombic efficiency with the cut-off voltage.

Thus, each technique offers its own merits and limits. The cell setup and experimental conditions impact the stability

of the electrolyte, and the interpretation of the experimental results is often ambiguous, resulting in significant discrepancies in the literature for the electrochemical stability of the same materials.[109] Furthermore, the influence of the specific cathode chemistries and electrode geometries (flat vs porous electrodes) cannot be neglected. The results obtained by standard voltammetric experiments with flat blocking electrodes have to be considered only as orientative, and additional stability tests should be performed with cell setups representing real cell conditions, that is, employing the concerned cathodes as working electrodes. In this activity, the degradation effects related to the anode and dendrites growth must be carefully distinguished. Ultimately, electrolyte degradation can be correctly assessed only by coupling electrochemical techniques with other analytical techniques.

Electrochemical impedance spectroscopy (EIS) is an efficient and nondestructive technique for characterizing the evolution of interfacial degradation or the growth of passivation layers in solid-state batteries.[318]

EIS is routinely used for studying the stability of polymer electrolytes with high-voltage cathodes, and the influence of cathode coating layers (artificial CEI).[168,171,209,210,222–224,227–230,237,240,324,325] An increase in the interface resistance is indicative of the degradation reactions occurring at the interfaces, corresponding typically to a degradation of cell performance. Conversely, the stabilization of the impedance spectrum upon cycling or the reduced impedance after coating is indicative of a higher cell cyclability, owing to either improved electrolyte stability or cathode interface protection.

The degradation of the polymer electrolyte during cycling in a full cell can be determined by following the evolution of the cell impedance, and in particular, the interfacial impedance contribution caused by either the SEI or CEI. Nonetheless, the individual contribution may not be easily distinguished in a two-electrode setup. Note that the EIS spectra of full cells are dependent on the voltage at which they are collected. The monitoring of the EIS spectra at various voltages can be useful for distinguishing the cathode interface impedance from the anode interface resistance. For instance, the EIS spectra of an NMC/Li cell at the end of discharge (3.0 V) and charge (4.3 V) over 200 cycles are presented in **Figure 12**.[171] The cell displays higher impedance at the HV, and an additional impedance contribution that is attributed to the cathode interface. Notably, the cathode interface impedance is inaccessible in the discharged state and completely masked by the anode counterpart.

EIS can be monitored also in other conditions, for instance over a period of time at a fixed voltage.[223] If the impedance spectra are recorded at the end of charge, the high voltage causes oxidative degradation of the electrolyte at the cathode interface. Predictably, this increases the corresponding interface resistance, although the anode interface resistance should remain stable.

Furthermore, the EIS can be utilized to monitor the cathode/electrolyte interface using cathode symmetrical cells.[325] In this setup, the cathode interface resistance is determined without interference from the anode. By measuring EIS over time, the stability of the electrolyte with the cathode material can be evaluated in static conditions. Additionally, if EIS is measured at various temperatures, the activation energy for the charge transfer between the electrolyte and cathode can be determined. The issue with this setup is that it allows measurements only at a fixed voltage. Probably the most beneficial approach to employing EIS with symmetric cathode cells would be with the use of delithiated cathodes (i.e., in their most reactive form), which requires previous activation (delithiation) of the cathodes in a full cell. EIS in three-electrode configuration cells can separate the cathode interface resistances from those at the anode.[326] However, this procedure is more common with liquid electrolytes because of the challenges pertaining to the introduction of a reference electrode in a polymer cell.

Overall, the EIS spectra provide useful information on the evolution of the cell impedance upon cycling, and are

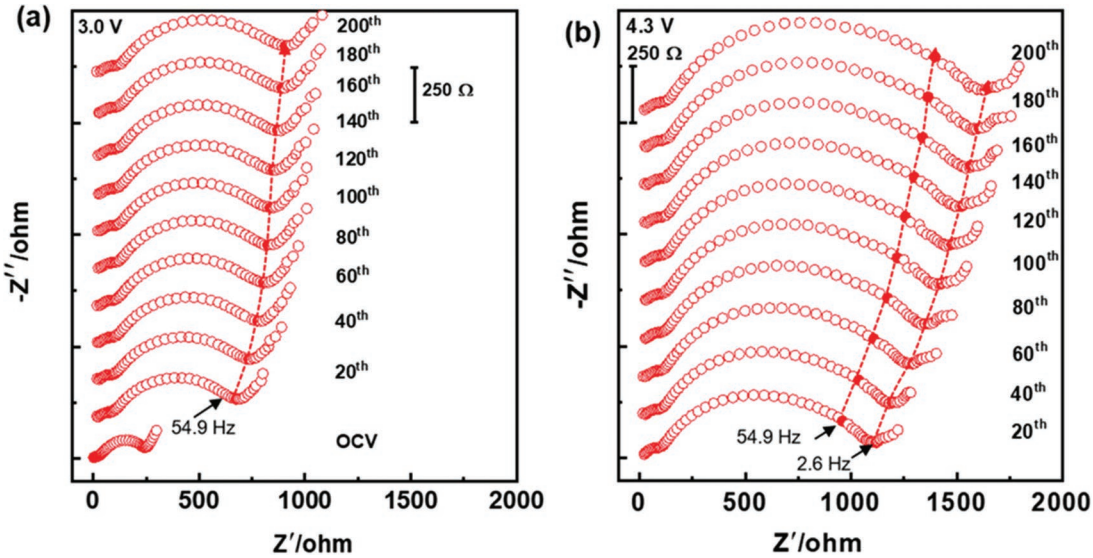

Figure 12. Nyquist plots of a Li/NMC-811 cell measured at a) 3.0 and b) 4.3 V. Adapted under the terms of Creative Commons Attribution 4.0 License.[171] Copyright 2021, The Authors, published by Wiley-VCH.

particularly insightful in the study of electrode/electrolyte interfacial resistances. The standard procedure for the analysis of EIS spectra requires fitting with electrical equivalent circuit models, which is in general straightforward. However, the interpretation of the EIS results is often difficult. The two biggest issues regard the selection of the correct fitting model (most EIS spectra can be perfectly fitted by varying equivalent circuit models) and the physicochemical interpretation of the equivalent circuit elements.[327] Last, care must be implemented to avoid overinterpretation of the EIS spectra, namely, by limiting the minimum number of fitting parameters. The risk of misinterpretation is especially high for EIS spectra of two-electrode cells, as the contributions of various electrochemical phenomena (e.g., SEI impedance, anode, and cathode charge transfer impedances) are often overlapped and cannot be conveniently separated.

4.2. Diffraction and Microscopy Techniques

4.2.1. X-Ray Diffraction (XRD)

X-ray diffraction (XRD) is a non-destructive technique that provides information on the crystallographic structure of a material. The degradation of high voltage cathode materials upon cycling can be accompanied by the variations in the lattice parameters, strain, phase transformation, or by the appearance of new phases.[271,328,329]

XRD can be employed for monitoring variations in the crystallinity of polymer electrolytes.[330,331] An increase in the crystallinity of the polymer electrolyte with storage or cycling is generally related to reduced ionic conductivity. However, the recovery of the aged electrolyte after cycling might hinder this analysis, as nonnegligible amounts of material are required for this technique.

4.2.2. Scanning Electron Microscopy (SEM)

SEM is utilized to identify the variations in the morphology of pristine or cycled electrodes and polymer electrolytes. In addition, SEM is widely employed to characterize lithium metal electrodes after cycling.[43,128,219,240,263,332,333] In this case, SEM enables the determination of the morphology of Li deposits and detect inhomogeneous Li deposition that might result in dendrites formation.[129,151]

SEM analysis on the cathode is more difficult, as it is not always possible to separate the electrode from the polymer electrolyte. In principle, only a small number of studies, usually involving GPEs, conducted SEM analysis on cathodes.[154,187,193,195] Moreover, SEM analysis on the cathodes can detect typical degradation effects such as the presence of extensive CEI on the cathode surface and cracks in the particles.

In situ studies allow the identification of variations in the electrolyte morphology over time (i.e., shrinkage, dendrite growth) and it is an extremely useful technique for identifying the primary source of degradation. A recent study by Kaboli et al. investigated the behavior of an NMC-PEO-Li cell via in situ SEM, observing a continuous reduction in the SPE thickness upon cycling. This could be attributed to the electrolyte chemical degradation facilitated by the electrochemical process at the cathode electrolyte interface.[112] The absence of this type of degradation with an LFP-PEO-Li cell further indicated that this degradation mechanism is specific for NMC. Ultimately, the authors observed similar Li-dendrites formation with both LFP and NMC, implying that Li-dendrites growth is dependent on the experimental conditions but not on the cathode chemistry. However, the electrode setup varies from that used in commercial cells (side-by-side instead of face-to-face), which might cause differences in the electrochemical response, and therefore, the evolution of the aging mechanisms.

4.2.3. Transmission Electron Microscopy (TEM)

Owing to its high resolution, TEM is frequently employed for determining the thickness and uniformity of the CEI. As an extremely thin layer (few nm) cannot be conveniently characterized, the distinct nature of its carbonaceous components with respect to the cathode material is represented by a lighter-colored region at the surface of the cathode particles. Studies have been reported for cells employing GPEs,[135,154,182,201,251] SPEs,[152,183,194,226] and using various cathode materials: LCO,[152,154,183,194,201,222,226] LNMO,[182] LMO,[251] and NMC.[135]

High-resolution TEM comprises the direct imaging of the atomic structure of samples. It can determine whether the structural variations have occurred during cycling in the cathode material. In post-mortem analysis, this technique can determine whether the original morphology is maintained during cycling[194] or if the cathode surface becomes less crystalline, thereby being able to identify the appearance of amorphous layers comprising electrolyte decomposition products.[227] This could be identified by the inorganic particles from composite electrolytes and whether they are participating in the formation of the CEI.[135]

4.3. Spectroscopic Methods

4.3.1. Energy-Dispersive X-Ray Spectroscopy (EDS)

Energy-dispersive X-ray spectroscopy (EDS) is a common characterization technique for materials, often coupled with electron microscopy experiments. Upon excitation by the electron beam of the electron microscope, the sample emits X-rays with characteristic energies corresponding to the particular elements of the sample. EDS is considered relatively bulk-sensitive with X-rays escaping from several tens of micrometers within the sample, and it can be quantitatively used to reasonably determine the composition. EDS can be used for identifying the chemical variations in the components of cycled or aged cells and to aid in the determination of their degradation mechanisms. EDS is particularly useful for detecting transition metal-ion cross-talk in HVLP cells: transition metal ions dissolved from the cathode and deposited on the anode can be detected by conducting the EDS analysis on cycled Li-metal anodes.[143,182]

4.3.2. Gas Analysis

The analysis of gases evolved during battery operation can reveal important information pertaining to the reaction mechanisms of the cell components. This type of analysis is particularly applicable to high voltage processes, during which gas evolution is more likely to be observed. Such techniques, commonly known as DEMS or online electrochemical mass spectrometry, usually require specially produced cells and comprise in-house built equipment.

Upon employing a GPE of cyanoethyl poly(vinyl alcohol) with pyrrolidone moieties (Pyrd-PVA-CN) in 1 M $LiPF_6$ in EC/EMC, Cho et al. measured the gas evolution for a cell with NMC-622 cathode and Li metal anode by maintaining at 70 °C and 4.5 V versus Li/Li^+.[272] Compared with a standard liquid electrolyte, heating of the GPE-containing cell resulted in substantially lower oxygen evolution over a period of 20 h. The authors concluded that the GPE stabilized the cathode material and suppressed the TMD, which has been reported to bear a catalytic effect on the gas evolution because of electrolyte oxidation.

However, the PEO severely decomposed in combination with $LiCoO_2$ versus Li/Li^+. The evolution of gases including H_2 and simple hydrocarbons (e.g., C_2H_2, C_2H_4, C_2H_6) was determined to initiate at ≈4.5 V versus Li/Li^+ (**Figure 13**). Moreover, the $LiCoO_2$ electrode cycled in combination with the SPE yielded a surface catalytic effect, resulting in H_2 evolution at only 4.2 V. This was mitigated by employing a LATP surface coating of $LiCoO_2$, which provided stability to the system up to 4.6 V.[111] Seidl et al. demonstrated H_2 evolution from LiTFSI in PEO when in contact with Li metal, and the evolution of species such as methanol and 2-methoxyethanol during a voltage ramp to 5 V versus Li/Li^+.[105]

Such decomposition and gas evolution can be circumvented by a sandwich-structured HSE, as demonstrated by Li et al.[217] The study employed a PAN-based electrolyte on the cathode side and a PEO-based electrolyte on the anode (Li metal) side. The LLTO nanofibers were used as an inorganic filler in each phase and as a polymer-in-ceramic center layer of the sandwich. In situ DEMS analysis was used to demonstrate that the application of multiple polymer electrolytes on each side of the cell suppresses the side reactions, whereas it typically results in gas evolution if only a single polymer had been used.

4.3.3. X-Ray Photoelectron Spectroscopy (XPS)

A technique now popular in the investigation of battery interfaces is X-ray photoelectron spectroscopy (XPS). This surface-sensitive method can be performed without using large-scale facilities and is used to characterize the interfacial reactions between battery components. For instance, this offers high chemical sensitivity with the ability to determine transition metal oxidation states or to distinguish between the environments of carbon (e.g., carbon black vs PVdF vs SEI components). The use of XPS to study the interfacial reactions in solid-state batteries is already well-reviewed by Sångeland et al.[334] However, the instability of interfaces within the high voltage systems is of paramount importance and can be classified as severe. As XPS is commonly used to study SEI on anode materials from liquid–electrolyte systems, the SEI formed between polymer electrolyte-based systems can reveal their degradation mechanisms. As observed, the SEI chemistry for polymer electrolyte-based systems can substantially differ from that for liquid-based systems.[272,335] This is typically determined through the manifestation of peaks for species only present in the polymer electrolyte or through variations in intensity for certain decomposition products, for instance, Li_2CO_3, $Li_xPO_yF_z$, LiOH, LiF, Li_3N (**Figure 14**). This has been demonstrated using XPS that GPEs can effectively suppress excessive SEI formation at the anode surfaces and CEI formation at the cathode surfaces, compared with that obtained using a liquid Electrolyte.[336–338]

The sample preparation for XPS from polymer electrolyte-based systems is particularly challenging because of the strong adhesion occurring between the electrolyte and the electrodes, which raises the difficulty to access the interfaces of interest. Certain studies determined that dissolving the electrolyte (PEO-based SPE) using acetonitrile could resolve this limitation.[335] However, similar to washing electrodes that have been in contact with liquid electrolytes, the extent of influence of such a dissolution on the interphase under investigation should be clarified.

The ether chain of PEO itself oxidizes at voltages above 3.4 V versus Li^+/Li, as determined by the reduced relative intensity of the hydrocarbon peak, compared to the peak for C—O, in C 1s spectra.[105] However, multiple studies have employed XPS for characterizing hybrid systems with both solid, inorganic electrolytes and SPE/GPE. Consequently, the SPE can be used as a thin protective layer between the solid electrolyte and electrode to enhance interfacial contact.[339] Others use homogeneous mixtures of the inorganic and SPE to create hybrid solid-state electrolytes (HSEs) that can combine the advantages of each mixture to offer high performance.[128,324,340] XPS is used to characterize the electrode/electrolyte interphase formed between the HSE and electrode.

4.3.4. Nuclear Magnetic Resonance (NMR) Spectroscopy

Nuclear magnetic resonance (NMR) spectroscopy is a non-destructive method that is able to characterize materials in the solid state (ss-NMR) and can determine molecular conformation in solution. Operando NMR, as well as XRD, are the two major tools that can be utilized to understand structural variations and phase transformations in cathode materials at high voltages.[341]

For polymer electrolytes, magic angle spinning nuclear magnetic resonance (MAS NMR) provides insight into their transport properties and can aid in identifying preferential Li pathways between polymer, inorganic fillers, or additives.[128,152,183,219,342] A detailed perspective of the use of this technique in solid-state batteries has been proposed by Foran et al.[343]

For investigating the degradation phenomena, MAS-NMR can be employed in ^7Li cathodes to quantify the lithium content after cycling based on the chemical shift of the signal in the paramagnetic region.[344] This can be used for

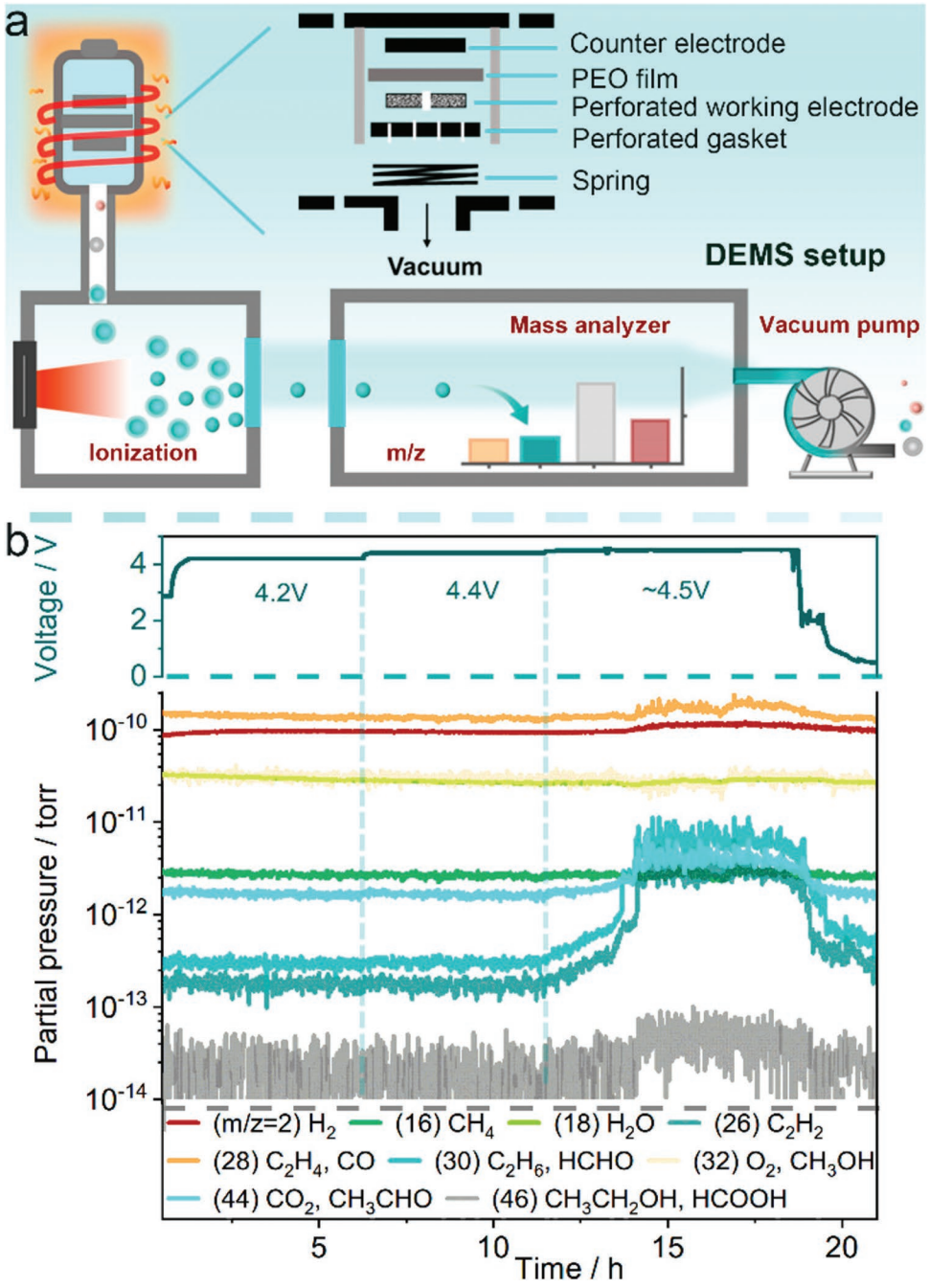

Figure 13. a) Schematic diagram of the experimental setup for DEMS. b) Voltage profile and partial pressures of various gases from the in situ DEMS experiment for the SPE 'half-cell' with active material-free working electrode. Reproduced with permission.[111] Copyright 2021, American Chemical Society.

determining the lithium content at the CEI/SEI of varying cathodes or anodes, based on the region below the peak of the diamagnetic region.[345–347] Other elements such as P or F can be screened for studying the chemical composition of these interfaces.

In lithium metal anodes, ^{7}Li NMR chemical shift imaging (CSI) provides chemical and spatial information on the microstructural growth of Li. Consequently, it has been employed to study dendrite growth in liquid[348,349] and inorganic electrolytes,[350] but not yet in polymer electrolytes. In addition, dynamic nuclear polarization-enhanced NMR has been employed to investigate the SEI on metallic lithium, and in a recent study by Hope et al., this was achieved at room temperature.[351]

To investigate the degradation of multilayer or CPEs, the utilization of ss-NMR can be a powerful tool to elucidate the temporal variations in Li conduction pathways and during cycling, indicating the component that limits the performance.

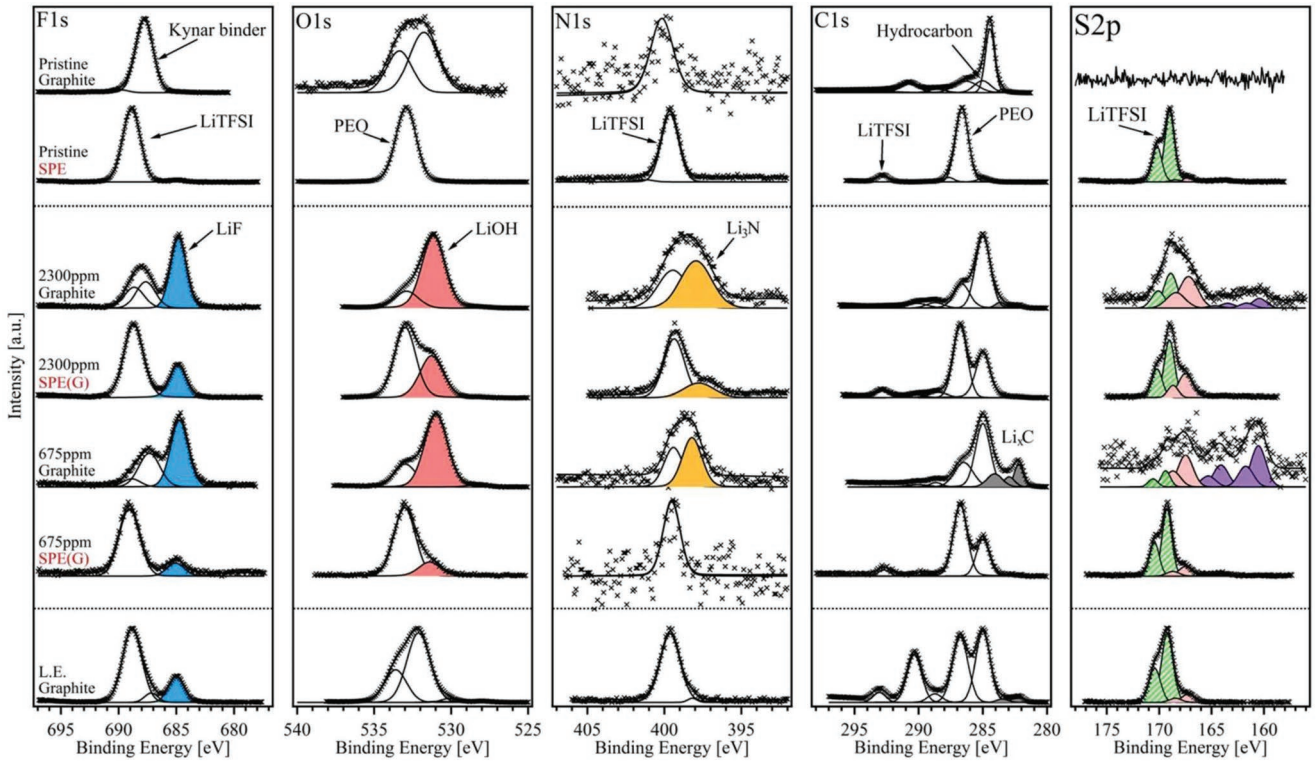

Figure 14. XPS spectra for a pristine graphite electrode (top), a PEO-based SPE, electrode and electrolyte samples from cycled graphite half-cells with various H_2O content, and a graphite electrode from a liquid electrolyte cell (bottom). Reproduced with permission.[335] Copyright 2014, The Royal Society of Chemistry.

4.3.5. Fourier Transform Infrared (FTIR) Spectroscopy

FTIR spectroscopy is extensively used to understand the nature of bonding and functional groups present in the polymer electrolytes. In particular, this technique is used to investigate the interaction between the salt and polymer matrix, study the polymerization process, and determine the structure of GPEs, etc. The degradation or the chemical transformations in the polymer electrolytes after cycling can be ascertained by Fourier transform infrared (FTIR) spectroscopy. Chai et al.[193] reported a high voltage CPE poly(methylethyl α-cyanoacrylate) for LNMO half-cell. The absorption peaks in the FT-IR spectra of the polymer electrolyte before and after 100 cycles remained intact and displayed its excellent electrochemical stability along with interfacial compatibility. Qiu et al.[110] studied the failure mechanisms in LCO/PEO/Li solid-state batteries using FTIR and other techniques. To study the degradation of PEO, electrodes containing Super-P carbon additive and PEO were maintained at varying potentials (3.9–4.4 V) for 48 h, and thereafter, disassembled. The intensity of the FTIR peaks referring to ester species increases when moving from the lower to higher potentials, indicating the degradation of PEO.

Zhao et al.[246] used attenuated total reflectance Fourier-transform infrared spectroscopy (ATR-FTIR) to study the anode and cathode interfaces in NMC/Li cells with PEO/LiTFSI SPE. After cycling, the anode surface did not exhibit variations in the FTIR spectra. In contrast, the cathode interface spectra depicted a new peak at 1000 cm^{-1} in the aged cathode, which could be attributed to the decomposition of PEO at higher potentials, because the original peak of CH_2 from PEO almost disappeared.

In addition, in situ FTIR is an advanced variation of this technique that can be used to decipher the interface chemistry. Wang et al.[152]] employed the in situ FTIR technique to monitor the variations occurring at the electrolyte/cathode interface in the charge–discharge process in a $LiCoO_2$/PDES-CPE/Li cell. Herein, PDES-CPE refers to polymerized deep eutectic solvent–CPE, which is a combination of various molten solid powders and lithium salts. At the cathode–electrolyte interface, a reversible increase or decrease in the anion peaks was observed that corresponded to the charge/discharge process. The in situ FTIR revealed that the $TFSI^-$ salt peaks, C—O—C and C≡N from PCUMA, and SN peak reversibly varied over cycling, whereas all other peaks remain unchanged. Overall, in situ FTIR is a powerful technique that can be used to investigate the degradation of the polymer electrolyte and its contribution to forming stable CEI/SEI layers at the electrodes.

Seidl et al.[105] studied the oxidative stability of PEO/LiTFSI electrolyte, which was subsequently tested in NMC/Li cells. In addition, FTIR spectroscopy was employed in post-mortem analysis to identify the decomposition products of the PEO oxidation. The FTIR was performed on PEO/LiTFSI supported on glass fiber separators, which were previously extracted from Li/SS (stainless steel) cells and maintained at voltages varying from 3.2 to 4.6 V. For the cells maintained at OCV and 3.2 V, the FTIR spectra did not exhibit any variation. After

increasing the voltage to 3.4 V, a reduction in the peak intensity of $C-O_{stretching}$ mode was observed. This mode corresponds to the C—O bond at the terminal C—OH alcohol group of PEO. At voltages greater than 3.6 V, several variations were observed in the entire spectra, especially 1) the peak intensities of the $C-O_{stretching}$ and $C-C_{alcohol}$ almost disappeared after 3.4 V. 2) The asymmetric S—N—S vibration for $TFSI^-$ anion was replaced by HTFSI, which was formed by the reaction of $TFSI^-$ and the protons released during PEO oxidation. 3) A gradual reduction in the peak intensity of C—C, C—O, and H—C—H vibrations was observed, which arises from PEO chain oxidation into smaller fragments. The variations observed in the FTIR spectra were confirmed in the electrochemical techniques performed in the study.

4.3.6. X-Ray Absorption Spectroscopy (XAS)

X-ray absorption spectroscopy (XAS) is a synchrotron technique that is useful for determining the electronic states of elements within a material. In particular, the oxidation states of transition metals can be assessed to evaluate the extent to which a transition metal is still involved in the redox reactions of a battery.

Co K-edge spectra measured by Li et al. for LAGP-coated $LiCoO_2$ (LCO) cathodes, cycled for 50 cycles using a PEO-based SPE, displayed that Co^{3+} was still the predominant oxidation state after discharge (3 V).[227] This is in contrast to uncoated LCO in which the cobalt existed in the 4+ oxidation state after discharge, thereby implying that it had not been reduced as expected on lithiation. This was confirmed through 2D X-ray absorption in the near-edge structure (XANES) mapping, including Co L-edge and O K-edge soft XAS.

Another study on LCO exhibited an incomplete reduction of cobalt after cycling in $LiCoO_2$/PEO-LiTFSI/Li cells.[110] This was inferred from the emergence of weak pre-edge peaks in the O K-edge XAS spectra measured in the total fluorescence yield (TFY) mode. An absorption shoulder after the edge could be attributed to the formation of CoO or Co_3O_4 phases, most probably at the electrode–electrolyte interface. The study demonstrated an improved performance using the same SPE but for $Li_{1.4}Al_{0.4}Ti_{1.6}(PO_4)_3$-coated $LiCoO_2$ and an additional cathode material of $LiMn_{0.7}Fe_{0.3}PO_4$.

Furthermore, Liang et al. investigated various binders including PEO, PVdF, and two carboxyl-rich binders (Na-alginate and CMC) with LCO, a PEO-based SPE, and Li metal anode.[238] The XAS measurements of the O K-edge and Co L-edge spectra for the electrodes with multiple binders before and after cycling demonstrated the various interactions occurring between the binder and LCO particle surfaces. In particular, two XAS modes were used, namely, TFY for more bulk sensitive measurements and total electron yield (TEY) for greater surface sensitivity. Conclusively, the carboxyl-rich binders exhibited a greater degree of interaction with the LCO particles and appropriate coating of the particles, as the PEO exposes the LCO surfaces. They further determined that the CMC/LCO interface provided greater stability during cycling than the PEO/LCO interface.

5. Conclusions and Perspectives

Despite the increasing interest in HVLP batteries for commercial advanced lithium metal batteries, their application is still hindered by the limited oxidative stability, especially of the polyether-based polymer electrolytes. Currently, the ultimate oxidative stability limit of PEO and PEO-based electrolytes is debated, with a few groups reporting stability limits up to 4.5 V versus Li/Li^+, whereas the commonly accepted value for PEO decomposition is below 4.0 V. This discrepancy is exacerbated by the common use of voltammetric methods for determining the electrolyte oxidative stability, which overestimates the polymer electrolyte stability. However, polyether-based electrolytes are now commonly cycled with 4-V-class cathode materials, and they exhibit decent results in terms of cyclability. Nonetheless, up until a few years ago, 3-V-class cathode materials (such as LFP and V_2O_5) were used. This is possibly one of the most important advancements in the field of polymer electrolytes achieved in recent years, resulting from the implementation of diverse strategies, such as passivation of the cathode surface and modification of the electrolyte chemical structure (e.g., multilayered electrolytes, composite, hybrid, and cross-linked electrolytes). Other polymers with higher oxidative stability included polycarbonates, PAN, PMMA, and PVdF, but these were commonly employed in GPEs or using plasticizers, as they have lower ionic conductivities than PEO. In contrast, the GPEs exhibit reduced thermal and mechanical stability compared to SPEs.

Herein, we conducted a statistical analysis considering 186 publications from 2005 to 2022 of HVPL-based lithium batteries (>4 V), with the aim of determining any specific trend in the cyclability and degradation of HVPL batteries. The most popular cathode–electrolyte combination is NMC-PEO, and LiTFSI is the most used salt with these two materials appearing in at least 50% of the publications. As expected, the discharge capacity increased with the cell cut-off voltage. However, very few studies employed an upper cut-off potential over 4.3 V versus Li/Li^+, that is, the common maximum potential attained by cathodes in commercial LIBs. Despite the challenge in analyzing long-term cycling stability, certain trends were detected between the two most employed polymer types (polyether and PVdF-based). Although the degradation rate of HVLP cells with polyethers in the electrolyte increases with the application of a higher cut-off voltage, this was not the case with PVdF systems as LNMO/Li cells cycled up to 5 V exhibited the lowest degradation values. Moreover, on average, the cells with polyether-based electrolytes degraded three times faster than the ones with PVdF-based electrolytes (66 vs 200 cycles to attain 80% SoH). Only 5 out of 186 publications displayed a cycle of over 1000 cycles, which is less than that for current state-of-the-art commercial lithium-ion batteries.

The results of the statistical analysis indicated that the performances of HVPL batteries lagged behind the performance of commercial LIBs. Note that cells employing SPEs generally operate at high temperatures that may further adversely impact cyclability. In most publications, extremely low cathode loadings were employed, further complicating the comparison with commercial LIBs. Among the various types of polymer electrolytes, the comparatively worse performance of polyether-based

electrolytes apparently confirmed the predictions regarding the low oxidative stability of these materials. To date, the most viable solution for HVLP batteries, considering other performance parameters such as the operation temperature, involves the use of non-polyether-based GPEs.

To review the oxidation of polymer electrolytes and the effectiveness of strategies to stabilize them, an increasing number of studies include post-mortem characterization of the electrodes and electrolytes. In most cases, a comparison is performed between the cells cycled with liquid and SPEs. However, the recovery of both electrodes and the separation from the electrolyte is challenging in solid-state cells, which hinders a complete study of the system compared to liquid electrolyte cells. In context, only a handful of operando studies on HVLP batteries have been performed, but they are essential for an improved understanding of the vital factors that limit the cycle life of such systems.

Overall, SPEs (mainly polyether-based electrolytes, polycarbonates, or HSEs with other polymer matrices) have demonstrated significant prospects for use in combination with 4V-class cathode materials. In contrast, the use of polyethers with 5V-class cathode materials will be potentially hindered by the low oxidative stability of these materials over 4.5 V. The operational temperature and rate capability of SPE-based batteries are limited by their poor ionic conductivity, and therefore, GPEs are more suited for applications requiring high power density and low-temperature operation. Furthermore, GPEs typically employ polymer matrices with high voltage stability, such as vinylidene fluoride copolymers, PAN, and PMMA derivatives. Thus, they are promising for application with 5V-class cathode materials. On the downside, most of these polymers exhibit lower stability versus lithium metal, and the introduction of liquid electrolytes reintroduces the safety issues that could be avoided using SPEs. The anode passivation and the use of flame retardant additives may aid in overcoming these problems.

Sufficient cyclability at practical cathode loadings remains to be demonstrated with both GPEs and SPEs, and the issue of lithium dendrites growth, in case lithium metal is used, has not yet been solved. The uneven lithium electrodeposition, which is exacerbated at high current densities, poses a severe limit to the achievable rate capability and cathode loadings of lithium metal batteries. The resolution of this issue will require further advances in lithium interface engineering and considerable enhancement of the electrolyte mechanical properties, for both SPEs and GPEs. For 5V-class lithium batteries, the issue of TMD should be addressed, although the use of polymer electrolytes and the introduction of metal-ion trapping moieties appear to be beneficial in this sense.

Thus, we suggest the following research directions for further improving the performance of HVLP batteries:

- With both SPEs and GPEs, the enhancement of the mechanical properties is required to hinder the growth of lithium dendrites. The cross-linking and addition of inorganic fillers are beneficial strategies, but not yet adequate to ensure the safety requirements for commercial application.
- For SPEs, a reduced thickness—possibly down to 5 μm—may compensate the low ionic conductivity, thereby improving the rate capability and diminishing the operational temperature of SPE-based cells. Thus, again, further improvement is required in terms of the mechanical properties and processability of SPE membranes.
- The introduction of inorganic ionic conductors in HSEs, especially in the form of nanowires and nanofibers, has proved to enhance the electrochemical stability and ionic conductivity of SPEs. This could potentially create an avenue for utilizing SPEs with high-voltage polymer hosts (e.g., PAN, PVdF, and others) in combination with 5V-class cathode materials. However, the ionic conductivity of HSEs is still inadequate for practical room-temperature operation. Thus, the addition of plasticizer or liquid electrolytes is necessary also in this case.
- Despite recent studies reporting oxidative stability for polyethers up to 4.5 V versus Li/Li^+, we observed that polyether-based HVLP cells have lower cyclability, by average, than non-polyether cells. Therefore, we consider the application of high-voltage stable polymer electrolyte interlayers as the safest option for using polyether-based electrolytes with high-voltage cathode materials. Moreover, this appears to be the only solution for their use with 5V-class cathode materials.
- Further efforts should be devoted for the development of cells based on GPEs with 5V-class cathode materials. This combination offers the potential of outperforming the corresponding cells with liquid electrolytes, as they are probably a safer option and might suppress the migration of transition metal ions to the anode.
- Regarding the HVLP cell performances, the focus should be on achieving appropriate cyclability with practical cathode loadings (≈2 mAh cm^{-2}). This will require concurrent enhancement of the electrolyte transport properties and hindering of lithium dendrites growth. Considering the current development stage of this technology, cathode loadings of at least 1 mAh cm^{-2} should be used when cycling HVLP cells, otherwise, the resulting cell performances may have little relevance for practical applications.
- The oxidation stability of the electrolytes is still debated, and the use of complementary operando techniques, coupled with electrochemical methods, will shed light on this issue. In this regard, specific post-mortem protocols should be employed to systematically analyze aged electrodes and electrolytes based on the challenges of recovering all the components in these solid or quasisolid systems.

Overall, the prospects for polymer-based high-voltage cells are highly encouraging. In the last few years, cycling with HVLP cells has been reported in an increasing number of studies, marking a striking improvement in the field. Although several challenges require addressal, further research on the main gaps identified in this review should enable the development of HVLP cells for overperforming Li-ion technology.

Supporting Information

Supporting Information is available from the Wiley Online Library or from the author.

Acknowledgements

M.A.C.M. and N.B. contributed equally to this work. The authors are grateful to the European Commission for the support of the work performed within the EU H2020 projects CoFBAT (Grant Agreement 875126) and SafeLimove (Grant Agreement 875189). After initial publication, a spelling mistake in the surname of F.P. was rectified on August 25, 2022.

Conflict of Interest

The authors declare no conflict of interest.

Keywords

degradation, high-voltage cathodes, lithium batteries, polymer electrolytes, solid-state batteries

Received: April 14, 2022
Revised: June 17, 2022
Published online: July 14, 2022

[1] A. Masias, J. Marcicki, W. A. Paxton, *ACS Energy Lett.* **2021**, *6*, 621.
[2] S. Jiao, X. Ren, R. Cao, M. H. Engelhard, Y. Liu, D. Hu, D. Mei, J. Zheng, W. Zhao, Q. Li, N. Liu, B. D. Adams, C. Ma, J. Liu, J.-G. Zhang, W. Xu, *Nat. Energy* **2018**, *3*, 739.
[3] X. Ren, L. Zou, X. Cao, M. H. Engelhard, W. Liu, S. D. Burton, H. Lee, C. Niu, B. E. Matthews, Z. Zhu, C. Wang, B. W. Arey, J. Xiao, J. Liu, J.-G. Zhang, W. Xu, *Joule* **2019**, *3*, 1662.
[4] K. Wang, J. Wan, Y. Xiang, J. Zhu, Q. Leng, M. Wang, L. Xu, Y. Yang, *J. Power Sources* **2020**, *460*, 228062.
[5] Y. Gao, J. Jiang, C. Zhang, W. Zhang, Z. Ma, Y. Jiang, *J. Power Sources* **2017**, *356*, 103.
[6] J. Wen, Y. Yu, C. Chen, *Mater. Express* **2012**, *2*, 197.
[7] C. Cui, C. Yang, N. Eidson, J. Chen, F. Han, L. Chen, C. Luo, P. Wang, X. Fan, C. Wang, *Adv. Mater.* **2020**, *32*, 1906427.
[8] J. Li, C. Ma, M. Chi, C. Liang, N. J. Dudney, *Adv. Energy Mater.* **2015**, *5*, 1401408.
[9] F. Zheng, M. Kotobuki, S. Song, M. O. Lai, L. Lu, *J. Power Sources* **2018**, *389*, 198.
[10] J. Y. Song, Y. Y. Wang, C. C. Wan, *J. Power Sources* **1999**, *77*, 183.
[11] X. Cheng, J. Pan, Y. Zhao, M. Liao, H. Peng, *Adv. Energy Mater.* **2018**, *8*, 1702184.
[12] J.-M. Tarascon, A. S. Gozdz, C. Schmutz, F. Shokoohi, P. C. Warren, *Solid State Ionics* **1996**, *86–88*, 49.
[13] W. Liu, N. Liu, J. Sun, P.-C. Hsu, Y. Li, H.-W. Lee, Y. Cui, *Nano Lett.* **2015**, *15*, 2740.
[14] M. Keller, A. Varzi, S. Passerini, *J. Power Sources* **2018**, *392*, 206.
[15] F. Croce, G. B. Appetecchi, L. Persi, B. Scrosati, *Nature* **1998**, *394*, 456.
[16] N. Boaretto, L. Meabe, M. Martinez-Ibañez, M. Armand, H. Zhang, *J. Electrochem. Soc.* **2020**, *167*, 070524.
[17] K. Xu, *Chem. Rev.* **2014**, *114*, 11503.
[18] J. R. Nair, L. Imholt, G. Brunklaus, M. Winter, *Electrochem. Soc. Interface* **2019**, *28*, 55.
[19] J. W. Fergus, *J. Power Sources* **2010**, *195*, 4554.
[20] R. Miao, B. Liu, Z. Zhu, Y. Liu, J. Li, X. Wang, Q. Li, *J. Power Sources* **2008**, *184*, 420.
[21] X. Zuo, X.-M. Liu, F. Cai, H. Yang, X.-D. Shen, G. Liu, *J. Power Sources* **2013**, *239*, 111.
[22] L. Porcarelli, C. Gerbaldi, F. Bella, J. R. Nair, *Sci. Rep.* **2016**, *6*, 19892.
[23] H. M. J. C. Pitawala, M. A. K. L. Dissanayake, V. A. Seneviratne, B.-E. Mellander, I. Albinson, *J. Solid State Electrochem.* **2008**, *12*, 783.
[24] L.-Z. Fan, X.-L. Wang, F. Long, X. Wang, *Solid State Ionics* **2008**, *179*, 1772.
[25] L.-Z. Fan, J. Maier, *Electrochem. Commun.* **2006**, *8*, 1753.
[26] L.-Z. Fan, Y.-S. Hu, A. J. Bhattacharyya, J. Maier, *Adv. Funct. Mater.* **2007**, *17*, 2800.
[27] J. Shin, W. A. Henderson, S. Passerini, *Electrochem. Commun.* **2003**, *5*, 1016.
[28] J.-H. Shin, W. A. Henderson, S. Passerini, *J. Electrochem. Soc.* **2005**, *152*, A978.
[29] D. Brogioli, F. Langer, R. Kun, F. La Mantia, *ACS Appl. Mater. Interfaces* **2019**, *11*, 11999.
[30] W. Wu, Z. Wei, J. Wang, J. Shang, M. Wang, S.-S. Chi, Q. Wang, L. Du, T. Zhang, Z. Zheng, Y. Deng, *Chem. Eng. J.* **2021**, *424*, 130335.
[31] V. Bocharova, A. P. Sokolov, *Macromolecules* **2020**, *53*, 4141.
[32] Z. Gadjourova, Y. G. Andreev, D. P. Tunstall, P. G. Bruce, *Nature* **2001**, *412*, 520.
[33] Z. Stoeva, I. Martin-Litas, E. Staunton, Y. G. Andreev, P. G. Bruce, *J. Am. Chem. Soc.* **2003**, *125*, 4619.
[34] A. M. Christie, S. J. Lilley, E. Staunton, Y. G. Andreev, P. G. Bruce, *Nature* **2005**, *433*, 50.
[35] C. Zhang, S. Gamble, D. Ainsworth, A. M. Z. Slawin, Y. G. Andreev, P. G. Bruce, *Nat. Mater.* **2009**, *8*, 580.
[36] J. Lopez, D. G. Mackanic, Y. Cui, Z. Bao, *Nat. Rev. Mater.* **2019**, *4*, 312.
[37] D. Grazioli, O. Verners, V. Zadin, D. Brandell, A. Simone, *Electrochim. Acta* **2019**, *296*, 1122.
[38] C. Monroe, J. Newman, *J. Electrochem. Soc.* **2005**, *152*, A396.
[39] D. Cao, X. Sun, Q. Li, A. Natan, P. Xiang, H. Zhu, *Matter* **2020**, *3*, 57.
[40] S.-D. Tao, J. Li, R. Hu, L. Wang, Z. Chi, T. Li, *Appl. Surf. Sci.* **2021**, *536*, 147794.
[41] C. Wang, Y. Yang, X. Liu, H. Zhong, H. Xu, Z. Xu, H. Shao, F. Ding, *ACS Appl. Mater. Interfaces* **2017**, *9*, 13694.
[42] X. Judez, M. Piszcz, E. Coya, C. Li, I. Aldalur, U. Oteo, Y. Zhang, W. Zhang, L. M. Rodriguez-Martinez, H. Zhang, M. Armand, *Solid State Ionics* **2018**, *318*, 95.
[43] J. Hu, P. He, B. Zhang, B. Wang, L.-Z. Fan, *Energy Storage Mater.* **2020**, *26*, 283.
[44] Q. Wang, W.-L. Song, L.-Z. Fan, Y. Song, *J. Membr. Sci.* **2015**, *492*, 490.
[45] X. Li, Y. Zheng, Y. Duan, M. Shang, J. Niu, C. Y. Li, *Nano Lett.* **2020**, *20*, 6914.
[46] X.-X. Zeng, Y.-X. Yin, N.-W. Li, W.-C. Du, Y.-G. Guo, L.-J. Wan, *J. Am. Chem. Soc.* **2016**, *138*, 15825.
[47] T. N. T. Phan, S. Issa, D. Gigmes, *Polym. Int.* **2019**, *68*, 7.
[48] K. J. Harry, X. Liao, D. Y. Parkinson, A. M. Minor, N. P. Balsara, *J. Electrochem. Soc.* **2015**, *162*, A2699.
[49] N. Wu, Y.-R. Shi, S.-Y. Lang, J.-M. Zhou, J.-Y. Liang, W. Wang, S.-J. Tan, Y.-X. Yin, R. Wen, Y.-G. Guo, *Angew. Chem., Int. Ed. Engl.* **2019**, *58*, 18146.
[50] K. Deng, J. Qin, S. Wang, S. Ren, D. Han, M. Xiao, Y. Meng, *Small* **2018**, *14*, 1801420.
[51] M. Martinez-Ibañez, E. Sanchez-Diez, L. Qiao, Y. Zhang, X. Judez, A. Santiago, I. Aldalur, J. Carrasco, H. Zhu, M. Forsyth, M. Armand, H. Zhang, *Adv. Funct. Mater.* **2020**, *30*, 2000455.
[52] W. Zhou, S. Wang, Y. Li, S. Xin, A. Manthiram, J. B. Goodenough, *J. Am. Chem. Soc.* **2016**, *138*, 9385.
[53] X. Yang, X. Gao, C. Zhao, Q. Sun, Y. Zhao, K. Adair, J. Luo, X. Lin, J. Liang, H. Huang, L. Zhang, S. Lu, R. Li, X. Sun, *Energy Storage Mater.* **2020**, *27*, 198.
[54] C. Zhang, S. Liu, G. Li, C. Zhang, X. Liu, J. Luo, *Adv. Mater.* **2018**, *30*, 1801328.

[55] K. Yan, B. Sun, P. Munroe, G. Wang, *Energy Storage Mater.* **2018**, *11*, 127.
[56] D. Sharon, P. Bennington, S. N. Patel, P. F. Nealey, *ACS Energy Lett.* **2020**, *5*, 2889.
[57] S. Li, L. Fan, Y. Lu, *Energy Storage Mater.* **2019**, *18*, 205.
[58] M. Liu, C. Wang, Z. Cheng, S. Ganapathy, L. A. Haverkate, S. Unnikrishnan, M. Wagemaker, *ACS Mater. Lett.* **2020**, *2*, 665.
[59] H. Zhang, G. G. Eshetu, X. Judez, C. Li, L. M. Rodriguez-Martínez, M. Armand, *Angew. Chem., Int. Ed.* **2018**, *57*, 15002.
[60] A. Santiago, X. Judez, J. Castillo, I. Garbayo, A. Sáenz de Buruaga, L. Qiao, G. Baraldi, J. A. Coca-Clemente, M. Armand, C. Li, H. Zhang, *J. Phys. Chem. Lett.* **2020**, *11*, 6133.
[61] A. Varzi, K. Thanner, R. Scipioni, D. Di Lecce, J. Hassoun, S. Dörfler, H. Altheus, S. Kaskel, C. Prehal, S. A. Freunberger, *J. Power Sources* **2020**, *480*, 228803.
[62] I. Gracia, M. Armand, D. Shanmukaraj, In *Solid Electrolytes For Advanced Applications* (Eds: R. Murugan, W. Weppner), Springer International Publishing, Cham **2019**, pp. 347–373.
[63] W. Zhao, J. Yi, P. He, H. Zhou, *Electrochem. Energy Rev.* **2019**, *2*, 574.
[64] S. Xia, X. Wu, Z. Zhang, Y. Cui, W. Liu, *Chem* **2019**, *5*, 753.
[65] Q. Zhao, S. Stalin, C.-Z. Zhao, L. A. Archer, *Nat. Rev. Mater.* **2020**, *5*, 229.
[66] D. Zhou, D. Shanmukaraj, A. Tkacheva, M. Armand, G. Wang, *Chem.* **2019**, *5*, 2326.
[67] Y. An, X. Han, Y. Liu, A. Azhar, J. Na, A. K. Nanjundan, S. Wang, J. Yu, Y. Yamauchi, *Small* **2022**, *18*, 2103617.
[68] G. Xi, M. Xiao, S. Wang, D. Han, Y. Li, Y. Meng, *Adv. Funct. Mater.* **2021**, *31*, 2007598.
[69] J. Wu, L. Yuan, W. Zhang, Z. Li, X. Xie, Y. Huang, *Energy Environ. Sci.* **2021**, *14*, 12.
[70] M. Li, C. Wang, Z. Chen, K. Xu, J. Lu, *Chem. Rev.* **2020**, *120*, 6783.
[71] Y. Zheng, Y. Yao, J. Ou, M. Li, D. Luo, H. Dou, Z. Li, K. Amine, A. Yu, Z. Chen, *Chem. Soc. Rev.* **2020**, *49*, 8790.
[72] X. Yu, A. Manthiram, *Energy Storage Mater.* **2021**, *34*, 282.
[73] S. Tang, W. Guo, Y. Fu, *Adv. Energy Mater.* **2021**, *11*, 2000802.
[74] F. Baskoro, H. Q. Wong, H.-J. Yen, *ACS Appl. Energy Mater.* **2019**, *2*, 3937.
[75] P. M. Ketkar, T. H. Epps, *Acc. Chem. Res.* **2021**, *54*, 4342.
[76] H. Zhang, C. Li, M. Piszcz, E. Coya, T. Rojo, L. M. Rodriguez-Martinez, M. Armand, Z. Zhou, *Chem. Soc. Rev.* **2017**, *46*, 797.
[77] J. Zhu, Z. Zhang, S. Zhao, A. S. Westover, I. Belharouak, P. Cao, *Adv. Energy Mater.* **2021**, *11*, 2003836.
[78] J. Mindemark, M. J. Lacey, T. Bowden, D. Brandell, *Prog. Polym. Sci.* **2018**, *81*, 114.
[79] B. Sun, J. Mindemark, K. Edström, D. Brandell, *Solid State Ionics* **2014**, *262*, 738.
[80] A. S. Shaplov, R. Marcilla, D. Mecerreyes, *Electrochim. Acta* **2015**, *175*, 18.
[81] J. Liang, J. Luo, Q. Sun, X. Yang, R. Li, X. Sun, *Energy Storage Mater.* **2019**, *21*, 308.
[82] X. Yu, A. Manthiram, *Energy Environ. Sci.* **2018**, *11*, 527.
[83] N. Boaretto, I. Garbayo, S. Valiyaveettil-SobhanRaj, A. Quintela, C. Li, M. Casas-Cabanas, F. Aguesse, *J. Power Sources* **2021**, *502*, 229919.
[84] Y. Chen, K. Wen, T. Chen, X. Zhang, M. Armand, S. Chen, *Energy Storage Mater.* **2020**, *31*, 401.
[85] S. Lou, F. Zhang, C. Fu, M. Chen, Y. Ma, G. Yin, J. Wang, *Adv. Mater.* **2021**, *33*, 2000721.
[86] X.-B. Cheng, C.-Z. Zhao, Y.-X. Yao, H. Liu, Q. Zhang, *Chem* **2019**, *5*, 74.
[87] R. Wang, W. Cui, F. Chu, F. Wu, *J. Energy Chem.* **2020**, *48*, 145.
[88] X. Wang, R. Kerr, F. Chen, N. Goujon, J. M. Pringle, D. Mecerreyes, M. Forsyth, P. C. Howlett, *Adv. Mater.* **2020**, *32*, 1905219.
[89] Q. Zhou, J. Ma, S. Dong, X. Li, G. Cui, *Adv. Mater.* **2019**, *31*, 1902029.
[90] H. Zhang, J. Zhang, J. Ma, G. Xu, T. Dong, G. Cui, *Electrochem. Energy Rev.* **2019**, *2*, 128.
[91] H. Xu, H. Zhang, J. Ma, G. Xu, T. Dong, J. Chen, G. Cui, *ACS Energy Lett.* **2019**, *4*, 2871.
[92] Z. Li, H. Zhang, X. Sun, Y. Yang, *ACS Energy Lett.* **2020**, *5*, 3244.
[93] F. Croce, F. S. Fiory, L. Persi, B. Scrosati, *Electrochem. Solid-State Lett.* **2001**, *4*, A121.
[94] M. Wetjen, G.-T. Kim, M. Joost, G. B. Appetecchi, M. Winter, S. Passerini, *J. Power Sources* **2014**, *246*, 846.
[95] K. Yoshida, M. Nakamura, Y. Kazue, N. Tachikawa, S. Tsuzuki, S. Seki, K. Dokko, M. Watanabe, *J. Am. Chem. Soc.* **2011**, *133*, 13121.
[96] F. Faglioni, B. v. Merinov, W. A. Goddard, B. Kozinsky, *Phys. Chem. Chem. Phys.* **2018**, *20*, 26098.
[97] S. Pandian, S. P. Adiga, P. Tagade, K. S. Hariharan, K. S. Mayya, Y.-G. Lee, *J. Power Sources* **2018**, *393*, 204.
[98] L. Chen, S. Venkatram, C. Kim, R. Batra, A. Chandrasekaran, R. Ramprasad, *Chem. Mater.* **2019**, *31*, 4598.
[99] C. F. N. Marchiori, R. P. Carvalho, M. Ebadi, D. Brandell, C. M. Araujo, *Chem. Mater.* **2020**, *32*, 7237.
[100] Y. Xia, T. Fujieda, K. Tatsumi, P. P. Prosini, T. Sakai, *J. Power Sources* **2001**, *92*, 234.
[101] S. Sylla, J.-Y. Sanchez, M. Armand, *Electrochim. Acta* **1992**, *37*, 1699.
[102] G. Homann, L. Stolz, J. Nair, I. C. Laskovic, M. Winter, J. Kasnatscheew, *Sci. Rep.* **2020**, *10*, 4390.
[103] G. Homann, L. Stolz, M. Winter, J. Kasnatscheew, *iScience* **2020**, *23*, 101225.
[104] G. Homann, L. Stolz, K. Neuhaus, M. Winter, J. Kasnatscheew, *Adv. Funct. Mater.* **2020**, *30*, 2006289.
[105] L. Seidl, R. Grissa, L. Zhang, S. Trabesinger, C. Battaglia, *Adv. Mater. Interfaces* **2022**, *9*, 2100704.
[106] Z. Du, X. C. Chen, R. Sahore, X. Wu, J. Li, N. J. Dudney, *J. Electrochem. Soc.* **2021**, *168*, 050549.
[107] X. Yang, M. Jiang, X. Gao, D. Bao, Q. Sun, N. Holmes, H. Duan, S. Mukherjee, K. Adair, C. Zhao, J. Liang, W. Li, J. Li, Y. Liu, H. Huang, L. Zhang, S. Lu, Q. Lu, R. Li, C. V. Singh, X. Sun, *Energy Environ. Sci.* **2020**, *13*, 1318.
[108] Z. Fang, Y. Luo, H. Liu, Z. Hong, H. Wu, F. Zhao, P. Liu, Q. Li, S. Fan, W. Duan, J. Wang, *Adv. Sci.* **2021**, *8*, 2100736.
[109] Z. Li, Y. Zhao, W. E. Tenhaeff, *Chem. Mater.* **2021**, *33*, 1927.
[110] J. Qiu, X. Liu, R. Chen, Q. Li, Y. Wang, P. Chen, L. Gan, S. Lee, D. Nordlund, Y. Liu, X. Yu, X. Bai, H. Li, L. Chen, *Adv. Funct. Mater.* **2020**, *30*, 1909392.
[111] K. Nie, X. Wang, J. Qiu, Y. Wang, Q. Yang, J. Xu, X. Yu, H. Li, X. Huang, L. Chen, *ACS Energy Lett.* **2020**, *5*, 826.
[112] S. Kaboli, H. Demers, A. Paolella, A. Darwiche, M. Dontigny, D. Clément, A. Guerfi, M. L. Trudeau, J. B. Goodenough, K. Zaghib, *Nano Lett.* **2020**, *20*, 1607.
[113] L. Yang, J. Zhang, W. Xue, J. Li, R. Chen, H. Pan, X. Yu, Y. Liu, H. Li, L. Chen, X. Huang, *Adv. Funct. Mater.* **2022**, *32*, 2200096.
[114] D. Lin, W. Liu, Y. Liu, H. R. Lee, P.-C. Hsu, K. Liu, Y. Cui, *Nano Lett.* **2016**, *16*, 459.
[115] H. Xu, M. Jing, J. Li, Z. Huang, T. Wang, W. Yuan, B. Ju, X. Shen, *ACS Sustainable Chem. Eng.* **2021**, *9*, 11118.
[116] C. Park, *Solid State Ionics* **2003**, *159*, 111.
[117] Y.-C. Jung, S.-M. Lee, J.-H. Choi, S. S. Jang, D.-W. Kim, *J. Electrochem. Soc.* **2015**, *162*, A704.
[118] S. H.-S. Cheng, K.-Q. He, Y. Liu, J.-W. Zha, M. Kamruzzaman, R. L.-W. Ma, Z.-M. Dang, R. K. Y. Li, C. Y. Chung, *Electrochim. Acta* **2017**, *253*, 430.
[119] T. A. Zegeye, W.-N. Su, F. W. Fenta, T. S. Zeleke, S.-K. Jiang, B. J. Hwang, *ACS Appl. Energy Mater.* **2020**, *3*, 11713.
[120] K. Liu, X. Li, J. Cai, Z. Yang, Z. Chen, B. Key, Z. Zhang, T. L. Dzwiniel, C. Liao, *ACS Energy Lett.* **2021**, *6*, 1315.

[121] A. Orue, M. Arrese-Igor, R. Cid, X. Júdez, N. Gómez, J. M. López del Amo, W. Manalastas, M. Srinivasan, C. Rojviriya, M. Armand, F. Aguesse, P. López-Aranguren, *J. Mater. Chem. A* **2022**, *10*, 2352.
[122] S. Wang, Q. Sun, W. Peng, Y. Ma, Y. Zhou, D. Song, H. Zhang, X. Shi, C. Li, L. Zhang, *J. Energy Chem.* **2021**, *58*, 85.
[123] S. Mu, W. Huang, W. Sun, N. Zhao, M. Jia, Z. Bi, X. Guo, *J. Energy Chem.* **2021**, *60*, 162.
[124] H. Zhang, X. An, Y. Long, H. Cao, Z. Cheng, H. Liu, Y. Ni, *Chem. Eng. J.* **2021**, *425*, 130632.
[125] R. Fan, C. Liu, K. He, S. Ho-Sum Cheng, D. Chen, C. Liao, R. K. Y. Li, J. Tang, Z. Lu, *ACS Appl. Mater. Interfaces* **2020**, *12*, 7222.
[126] F. Chen, D. Yang, W. Zha, B. Zhu, Y. Zhang, J. Li, Y. Gu, Q. Shen, L. Zhang, D. R. Sadoway, *Electrochim. Acta* **2017**, *258*, 1106.
[127] Y. Wang, J. Ju, S. Dong, Y. Yan, F. Jiang, L. Cui, Q. Wang, X. Han, G. Cui, *Adv. Funct. Mater.* **2021**, *31*, 2101523.
[128] H. Xu, P.-H. Chien, J. Shi, Y. Li, N. Wu, Y. Liu, Y.-Y. Hu, J. B. Goodenough, *Proc. Natl. Acad. Sci. USA* **2019**, *116*, 18815.
[129] H. Huo, B. Wu, T. Zhang, X. Zheng, L. Ge, T. Xu, X. Guo, X. Sun, *Energy Storage Mater.* **2019**, *18*, 59.
[130] F. Han, Y. Zhu, X. He, Y. Mo, C. Wang, *Adv. Energy Mater.* **2016**, *6*, 1501590.
[131] Y. Zhu, X. He, Y. Mo, *ACS Appl. Mater. Interfaces* **2015**, *7*, 23685.
[132] O. Borodin, X. Ren, J. Vatamanu, A. von Wald Cresce, J. Knap, K. Xu, *Acc. Chem. Res.* **2017**, *50*, 2886.
[133] I. Shaji, D. Diddens, N. Ehteshami, M. Winter, J. R. Nair, *Energy Storage Mater.* **2022**, *44*, 263.
[134] D. E. Ciurduc, N. Boaretto, J. P. Fernández-Blázquez, R. Marcilla, *J. Power Sources* **2021**, *506*, 230220.
[135] H. Wu, Y. Xu, X. Ren, B. Liu, M. H. Engelhard, M. S. Ding, P. Z. El-Khoury, L. Zhang, Q. Li, K. Xu, C. Wang, J. Zhang, W. Xu, *Adv. Energy Mater.* **2019**, *9*, 1902108.
[136] H. Wu, P. Gao, H. Jia, L. Zou, L. Zhang, X. Cao, M. H. Engelhard, M. E. Bowden, M. S. Ding, J. Hu, D. Hu, S. D. Burton, K. Xu, C. Wang, J.-G. Zhang, W. Xu, *ACS Appl. Mater. Interfaces* **2021**, *13*, 31583.
[137] V. Vijayakumar, D. Diddens, A. Heuer, S. Kurungot, M. Winter, J. R. Nair, *ACS Appl. Mater. Interfaces* **2020**, *12*, 567.
[138] K. Kimura, J. Motomatsu, Y. Tominaga, *J. Polym. Sci., Part B: Polym. Phys.* **2016**, *54*, 2442.
[139] K. Kimura, Y. Tominaga, *ChemElectroChem* **2018**, *5*, 4008.
[140] X. Jiao, X. Pan, *J. Electroanal. Chem.* **2021**, *882*, 114995.
[141] M. Matsumoto, T. Uno, M. Kubo, T. Itoh, *Ionics* **2013**, *19*, 615.
[142] P. N. Didwal, Y. N. Singhbabu, R. Verma, B.-J. Sung, G.-H. Lee, J.-S. Lee, D. R. Chang, C.-J. Park, *Energy Storage Mater.* **2021**, *37*, 476.
[143] J. Zhao, J. Zhang, P. Hu, J. Ma, X. Wang, L. Yue, G. Xu, B. Qin, Z. Liu, X. Zhou, G. Cui, *Electrochim. Acta* **2016**, *188*, 23.
[144] J. Li, S. Dong, C. Wang, Z. Hu, Z. Zhang, H. Zhang, G. Cui, *J. Mater. Chem. A* **2018**, *6*, 11846.
[145] C. Sångeland, B. Sun, D. Brandell, E. J. Berg, J. Mindemark, *Batteries Supercaps* **2021**, *4*, 785.
[146] J. Chai, Z. Liu, J. Zhang, J. Sun, Z. Tian, Y. Ji, K. Tang, X. Zhou, G. Cui, *ACS Appl. Mater. Interfaces* **2017**, *9*, 17897.
[147] J. Chai, Z. Liu, J. Ma, J. Wang, X. Liu, H. Liu, J. Zhang, G. Cui, L. Chen, *Adv. Sci.* **2017**, *4*, 1600377.
[148] J. Ju, Y. Wang, B. Chen, J. Ma, S. Dong, J. Chai, H. Qu, L. Cui, X. Wu, G. Cui, *ACS Appl. Mater. Interfaces* **2018**, *10*, 13588.
[149] Z. Lv, Q. Zhou, S. Zhang, S. Dong, Q. Wang, L. Huang, K. Chen, G. Cui, *Energy Storage Mater.* **2021**, *37*, 215.
[150] Y. Xie, H. Gao, J. Gim, A. T. Ngo, Z.-F. Ma, Z. Chen, *J. Phys. Chem. Lett.* **2019**, *10*, 589.
[151] P. Wang, J. Chai, Z. Zhang, H. Zhang, Y. Ma, G. Xu, H. Du, T. Liu, G. Li, G. Cui, *J. Mater. Chem. A* **2019**, *7*, 5295.
[152] C. Wang, H. Zhang, S. Dong, Z. Hu, R. Hu, Z. Guo, T. Wang, G. Cui, L. Chen, *Chem. Mater.* **2020**, *32*, 9167.
[153] R. Hu, H. Qiu, H. Zhang, P. Wang, X. Du, J. Ma, T. Wu, C. Lu, X. Zhou, G. Cui, *Small* **2020**, *16*, 1907163.
[154] X. Li, X. Han, H. Zhang, R. Hu, X. Du, P. Wang, B. Zhang, G. Cui, *ACS Appl. Mater. Interfaces* **2020**, *12*, 51374.
[155] Z. Lin, X. Guo, Z. Wang, B. Wang, S. He, L. A. O'Dell, J. Huang, H. Li, H. Yu, L. Chen, *Nano Energy* **2020**, *73*, 104786.
[156] Y. Wang, L. Wu, Z. Lin, M. Tang, P. Ding, X. Guo, Z. Zhang, S. Liu, B. Wang, X. Yin, Z. Chen, K. Amine, H. Yu, *Nano Energy* **2022**, *96*, 107105.
[157] Y. Kuai, F. Wang, J. Yang, H. Lu, Z. Xu, X. Xu, Y. NuLi, J. Wang, *Mater. Chem. Front.* **2021**, *5*, 6502.
[158] Y. Wang, S. Chen, Z. Li, C. Peng, Y. Li, W. Feng, *Energy Storage Mater.* **2022**, *45*, 474.
[159] Z. Lin, X. Guo, R. Zhang, M. Tang, P. Ding, Z. Zhang, L. Wu, Y. Wang, S. Zhao, Q. Zhang, H. Yu, *Nano Energy* **2022**, *98*, 107330.
[160] M. M. Rao, J. S. Liu, W. S. Li, Y. Liang, D. Y. Zhou, *J. Membr. Sci.* **2008**, *322*, 314.
[161] P. Sun, Y. Liao, H. Xie, T. Chen, M. Rao, W. Li, *J. Power Sources* **2014**, *269*, 299.
[162] H. Xie, Y. Liao, P. Sun, T. Chen, M. Rao, W. Li, *Electrochim. Acta* **2014**, *127*, 327.
[163] X. Luo, Y. Liao, H. Xie, Y. Zhu, Q. Huang, W. Li, *Electrochim. Acta* **2016**, *220*, 47.
[164] X. Wang, G. M. A. Girard, H. Zhu, R. Yunis, D. R. MacFarlane, D. Mecerreyes, A. J. Bhattacharyya, P. C. Howlett, M. Forsyth, *ACS Appl. Energy Mater.* **2019**, *2*, 6237.
[165] G. M. A. Girard, X. Wang, R. Yunis, P. C. Howlett, M. Forsyth, *J. Solid State Electrochem.* **2020**, *24*, 2479.
[166] C. Fu, G. Homann, R. Grissa, D. Rentsch, W. Zhao, T. Gouveia, A. Falgayrat, R. Lin, S. Fantini, C. Battaglia, *Adv. Energy Mater.* **2022**, 2200412.
[167] P. Yao, B. Zhu, H. Zhai, X. Liao, Y. Zhu, W. Xu, Q. Cheng, C. Jayyosi, Z. Li, J. Zhu, K. M. Myers, X. Chen, Y. Yang, *Nano Lett.* **2018**, *18*, 6113.
[168] B. Zhang, L. Chen, J. Hu, Y. Liu, Y. Liu, Q. Feng, G. Zhu, L.-Z. Fan, *J. Power Sources* **2019**, *442*, 227230.
[169] K. Liu, M. Wu, H. Jiang, Y. Lin, T. Zhao, *J. Mater. Chem. A* **2020**, *8*, 18802.
[170] M. Jia, Z. Bi, C. Shi, N. Zhao, X. Guo, *ACS Appl. Mater. Interfaces* **2020**, *12*, 46231.
[171] Z. Chen, G.-T. Kim, J.-K. Kim, M. Zarrabeitia, M. Kuenzel, H.-P. Liang, D. Geiger, U. Kaiser, S. Passerini, *Adv. Energy Mater.* **2021**, *11*, 2101339.
[172] M. Yao, Q. Ruan, T. Yu, H. Zhang, S. Zhang, *Energy Storage Mater.* **2022**, *44*, 93.
[173] K. Z. Walle, L. Musuvadhi Babulal, S. H. Wu, W.-C. Chien, R. Jose, S. J. Lue, J.-K. Chang, C.-C. Yang, *ACS Appl. Mater. Interfaces* **2021**, *13*, 2507.
[174] Y. Zhang, H. Fei, Y. An, C. Wei, J. Feng, *ChemistrySelect* **2020**, *5*, 1214.
[175] K. Xu, *Chem. Rev.* **2004**, *104*, 4303.
[176] T. A. Barnes, J. W. Kaminski, O. Borodin, T. F. Miller, *J. Phys. Chem. C* **2015**, *119*, 3865.
[177] S. P. Ong, O. Andreussi, Y. Wu, N. Marzari, G. Ceder, *Chem. Mater.* **2011**, *23*, 2979.
[178] X. Fan, L. Chen, O. Borodin, X. Ji, J. Chen, S. Hou, T. Deng, J. Zheng, C. Yang, S.-C. Liou, K. Amine, K. Xu, C. Wang, *Nat. Nanotechnol.* **2018**, *13*, 715.
[179] J. Wu, X. Wang, Q. Liu, S. Wang, D. Zhou, F. Kang, D. Shanmukaraj, M. Armand, T. Rojo, B. Li, G. Wang, *Nat. Commun.* **2021**, *12*, 5746.
[180] Q. Zheng, Y. Yamada, R. Shang, S. Ko, Y.-Y. Lee, K. Kim, E. Nakamura, A. Yamada, *Nat. Energy* **2020**, *5*, 291.
[181] X. Cui, H. Zhang, S. Li, Y. Zhao, L. Mao, W. Zhao, Y. Li, X. Ye, *J. Power Sources* **2013**, *240*, 476.

[182] S. Wang, C. Wei, W. Ding, L. Zou, Y. Gong, Y. Liu, L. Zang, X. Xu, *Polymers* **2019**, *11*, 1306.
[183] X. Yu, L. Wang, J. Ma, X. Sun, X. Zhou, G. Cui, *Adv. Energy Mater.* **2020**, *10*, 1903939.
[184] R. Chen, F. Liu, Y. Chen, Y. Ye, Y. Huang, F. Wu, L. Li, *J. Power Sources* **2016**, *306*, 70.
[185] Q. Wang, X. Liu, Z. Cui, X. Shangguan, H. Zhang, J. Zhang, K. Tang, L. Li, X. Zhou, G. Cui, *Electrochim. Acta* **2020**, *337*, 135843.
[186] X. Zuo, X. Ma, J. Wu, X. Deng, X. Xiao, J. Liu, J. Nan, *Electrochim. Acta* **2018**, *271*, 582.
[187] Z. Chen, D. Steinle, H.-D. Nguyen, J.-K. Kim, A. Mayer, J. Shi, E. Paillard, C. Iojoiu, S. Passerini, D. Bresser, *Nano Energy* **2020**, *77*, 105129.
[188] H.-D. Nguyen, G.-T. Kim, J. Shi, E. Paillard, P. Judeinstein, S. Lyonnard, D. Bresser, C. Iojoiu, *Energy Environ. Sci.* **2018**, *11*, 3298.
[189] Z. Wei, Z. Zhang, S. Chen, Z. Wang, X. Yao, Y. Deng, X. Xu, *Energy Storage Mater.* **2019**, *22*, 337.
[190] F. Fu, Y. Liu, C. Sun, L. Cong, Y. Liu, L. Sun, H. Xie, *Energy Environ. Mater.* **2022**, https://doi.org/10.1002/eem2.12367.
[191] M. J. Lee, J. Han, K. Lee, Y. J. Lee, B. G. Kim, K.-N. Jung, B. J. Kim, S. W. Lee, *Nature* **2022**, *601*, 217.
[192] P. Hu, J. Zhao, T. Wang, C. Shang, J. Zhang, B. Qin, Z. Liu, J. Xiong, G. Cui, *Electrochem. Commun.* **2015**, *61*, 32.
[193] J. Chai, J. Zhang, P. Hu, J. Ma, H. Du, L. Yue, J. Zhao, H. Wen, Z. Liu, G. Cui, L. Chen, *J. Mater. Chem. A* **2016**, *4*, 5191.
[194] T. Dong, J. Zhang, G. Xu, J. Chai, H. Du, L. Wang, H. Wen, X. Zang, A. Du, Q. Jia, X. Zhou, G. Cui, *Energy Environ. Sci.* **2018**, *11*, 1197.
[195] Y. Ma, J. Ma, J. Chai, Z. Liu, G. Ding, G. Xu, H. Liu, B. Chen, X. Zhou, G. Cui, L. Chen, *ACS Appl. Mater. Interfaces* **2017**, *9*, 41462.
[196] K. Khan, Z. Tu, Q. Zhao, C. Zhao, L. A. Archer, *Chem. Mater.* **2019**, *31*, 8466.
[197] Q. Zhao, X. Liu, S. Stalin, K. Khan, L. A. Archer, *Nat. Energy* **2019**, *4*, 365.
[198] Q. Zhao, X. Liu, S. Stalin, L. Archer, *Cell Rep. Phys. Sci.* **2020**, *1*, 100146.
[199] S. Wen, C. Luo, Q. Wang, Z. Wei, Y. Zeng, Y. Jiang, G. Zhang, H. Xu, J. Wang, C. Wang, J. Chang, Y. Deng, *Energy Storage Mater.* **2022**, *47*, 453.
[200] C. Zhao, Q. Zhao, X. Liu, J. Zheng, S. Stalin, Q. Zhang, L. A. Archer, *Adv. Mater.* **2020**, *32*, 1905629.
[201] H. Wu, B. Tang, X. Du, J. Zhang, X. Yu, Y. Wang, J. Ma, Q. Zhou, J. Zhao, S. Dong, G. Xu, J. Zhang, H. Xu, G. Cui, L. Chen, *Adv. Sci.* **2020**, *7*, 2003370.
[202] J. Luo, Q. Sun, J. Liang, X. Yang, J. Liang, X. Lin, F. Zhao, Y. Liu, H. Huang, L. Zhang, S. Zhao, S. Lu, R. Li, X. Sun, *Nano Energy* **2021**, *90*, 106566.
[203] W. Choi, Y. Kang, I.-J. Kim, B.-G. Seong, W.-R. Yu, D. W. Kim, *ACS Appl. Mater. Interfaces* **2021**, *13*, 35664.
[204] Y.-C. Jung, M.-S. Park, D.-H. Kim, M. Ue, A. Eftekhari, D.-W. Kim, *Sci. Rep.* **2017**, *7*, 17482.
[205] W. He, Z. Cui, X. Liu, Y. Cui, J. Chai, X. Zhou, Z. Liu, G. Cui, *Electrochim. Acta* **2017**, *225*, 151.
[206] Y. Sun, X. Zhang, C. Ma, N. Guo, Y. Liu, J. Liu, H. Xie, *J. Power Sources* **2021**, *516*, 230686.
[207] T. Itoh, K. Fujita, K. Inoue, H. Iwama, K. Kondoh, T. Uno, M. Kubo, *Electrochim. Acta* **2013**, *112*, 221.
[208] X. Pan, H. Sun, Z. Wang, H. Huang, Q. Chang, J. Li, J. Gao, S. Wang, H. Xu, Y. Li, W. Zhou, *Adv. Energy Mater.* **2020**, *10*, 2002416.
[209] J. Bae, X. Zhang, X. Guo, G. Yu, *Nano Lett.* **2021**, *21*, 1184.
[210] J. Lu, J. Zhou, R. Chen, F. Fang, K. Nie, W. Qi, J.-N. Zhang, R. Yang, X. Yu, H. Li, L. Chen, X. Huang, *Energy Storage Mater.* **2020**, *32*, 191.
[211] K. Wen, X. Tan, T. Chen, S. Chen, S. Zhang, *Energy Storage Mater.* **2020**, *32*, 55.
[212] M. Arrese-Igor, M. Martinez-Ibañez, E. Pavlenko, M. Forsyth, H. Zhu, M. Armand, F. Aguesse, P. López-Aranguren, *ACS Energy Lett.* **2022**, *7*, 1473.
[213] W. Zhou, Z. Wang, Y. Pu, Y. Li, S. Xin, X. Li, J. Chen, J. B. Goodenough, *Adv. Mater.* **2019**, *31*, 1805574.
[214] X. Yu, J. Li, A. Manthiram, *ACS Mater. Lett.* **2020**, *2*, 317.
[215] H. Duan, M. Fan, W.-P. Chen, J.-Y. Li, P.-F. Wang, W.-P. Wang, J.-L. Shi, Y.-X. Yin, L.-J. Wan, Y.-G. Guo, *Adv. Mater.* **2019**, *31*, 1807789.
[216] J.-Y. Liang, X.-X. Zeng, X.-D. Zhang, T.-T. Zuo, M. Yan, Y.-X. Yin, J.-L. Shi, X.-W. Wu, Y.-G. Guo, L.-J. Wan, *J. Am. Chem. Soc.* **2019**, *141*, 9165.
[217] B. Li, Q. Su, C. Liu, Q. Wang, M. Zhang, S. Ding, G. Du, B. Xu, *J. Power Sources* **2021**, *496*, 229835.
[218] N. Wu, P. Chien, Y. Qian, Y. Li, H. Xu, N. S. Grundish, B. Xu, H. Jin, Y. Hu, G. Yu, J. B. Goodenough, *Angew. Chem.* **2020**, *132*, 4160.
[219] N. Wu, P.-H. Chien, Y. Li, A. Dolocan, H. Xu, B. Xu, N. S. Grundish, H. Jin, Y.-Y. Hu, J. B. Goodenough, *J. Am. Chem. Soc.* **2020**, *142*, 2497.
[220] K. Liu, M. Wu, H. Jiang, Y. Lin, J. Xu, T. Zhao, *J. Power Sources* **2022**, *526*, 231172.
[221] D. Cai, X. Wu, J. Xiang, M. Li, H. Su, X. Qi, X. Wang, X. Xia, C. Gu, J. Tu, *Chem. Eng. J.* **2021**, *424*, 130522.
[222] Y. Kobayashi, S. Seki, A. Yamanaka, H. Miyashiro, Y. Mita, T. Iwahori, *J. Power Sources* **2005**, *146*, 719.
[223] S. Seki, Y. Kobayashi, H. Miyashiro, Y. Mita, T. Iwahori, *Chem. Mater.* **2005**, *17*, 2041.
[224] Y. Kobayashi, S. Seki, M. Tabuchi, H. Miyashiro, Y. Mita, T. Iwahori, *J. Electrochem. Soc.* **2005**, *152*, A1985.
[225] H. Miyashiro, Y. Kobayashi, S. Seki, Y. Mita, A. Usami, M. Nakayama, M. Wakihara, *Chem. Mater.* **2005**, *17*, 5603.
[226] Q. Yang, J. Huang, Y. Li, Y. Wang, J. Qiu, J. Zhang, H. Yu, X. Yu, H. Li, L. Chen, *J. Power Sources* **2018**, *388*, 65.
[227] Z. Li, A. Li, H. Zhang, R. Lin, T. Jin, Q. Cheng, X. Xiao, W.-K. Lee, M. Ge, H. Zhang, A. Zangiabadi, I. Waluyo, A. Hunt, H. Zhai, J. J. Borovilas, P. Wang, X.-Q. Yang, X. Chuan, Y. Yang, *Nano Energy* **2020**, *72*, 104655.
[228] S. K. Singh, D. Dutta, R. K. Singh, *Electrochim. Acta* **2020**, *343*, 136122.
[229] J. Liang, Y. Sun, Y. Zhao, Q. Sun, J. Luo, F. Zhao, X. Lin, X. Li, R. Li, L. Zhang, S. Lu, H. Huang, X. Sun, *J. Mater. Chem. A* **2020**, *8*, 2769.
[230] H. Zhai, T. Gong, B. Xu, Q. Cheng, D. Paley, B. Qie, T. Jin, Z. Fu, L. Tan, Y.-H. Lin, C.-W. Nan, Y. Yang, *ACS Appl. Mater. Interfaces* **2019**, *11*, 28774.
[231] J. Liang, S. Hwang, S. Li, J. Luo, Y. Sun, Y. Zhao, Q. Sun, W. Li, M. Li, M. N. Banis, X. Li, R. Li, L. Zhang, S. Zhao, S. Lu, H. Huang, D. Su, X. Sun, *Nano Energy* **2020**, *78*, 105107.
[232] J. H. Kim, H. Kim, W. Choi, M.-S. Park, *ACS Appl. Mater. Interfaces* **2020**, *12*, 35098.
[233] Y.-J. Kim, R. Rajagopal, S. Kang, K.-S. Ryu, *Chem. Eng. J.* **2020**, *386*, 123975.
[234] J. S. Lee, Y. J. Park, *ACS Appl. Mater. Interfaces* **2021**, *13*, 38333.
[235] H. Kim, D. Byun, W. Chang, H.-G. Jung, W. Choi, *J. Mater. Chem. A* **2017**, *5*, 25077.
[236] G. Lu, W. Peng, Y. Zhang, X. Wang, X. Shi, D. Song, H. Zhang, L. Zhang, *Electrochim. Acta* **2021**, *368*, 137639.
[237] T. Kobayashi, Y. Kobayashi, M. Tabuchi, K. Shono, Y. Ohno, Y. Mita, H. Miyashiro, *ACS Appl. Mater. Interfaces* **2013**, *5*, 12387.
[238] J. Liang, D. Chen, K. Adair, Q. Sun, N. G. Holmes, Y. Zhao, Y. Sun, J. Luo, R. Li, L. Zhang, S. Zhao, S. Lu, H. Huang, X. Zhang, C. V. Singh, X. Sun, *Adv. Energy Mater.* **2021**, *11*, 2002455.

[239] T. Dong, P. Mu, S. Zhang, H. Zhang, W. Liu, G. Cui, *Electrochem. Energy Rev.* **2021**, *4*, 545.
[240] J. Ma, Z. Liu, B. Chen, L. Wang, L. Yue, H. Liu, J. Zhang, Z. Liu, G. Cui, *J. Electrochem. Soc.* **2017**, *164*, A3454.
[241] J. Qiu, L. Yang, G. Sun, X. Yu, H. Li, L. Chen, *Chem. Commun.* **2020**, *56*, 5633.
[242] S. Choudhury, Z. Tu, A. Nijamudheen, M. J. Zachman, S. Stalin, Y. Deng, Q. Zhao, D. Vu, L. F. Kourkoutis, J. L. Mendoza-Cortes, L. A. Archer, *Nat. Commun.* **2019**, *10*, 3091.
[243] M. Arrese-Igor, M. Martinez-Ibañez, J. M. López del Amo, E. Sanchez-Diez, D. Shanmukaraj, E. Dumont, M. Armand, F. Aguesse, P. López-Aranguren, *Energy Storage Mater.* **2022**, *45*, 578.
[244] H. Markusson, H. Tokuda, M. Watanabe, P. Johansson, P. Jacobsson, *Polymer* **2004**, *45*, 9057.
[245] S. Li, Y.-M. Chen, W. Liang, Y. Shao, K. Liu, Z. Nikolov, Y. Zhu, *Joule* **2018**, *2*, 1838.
[246] Q. Zhao, P. Chen, S. Li, X. Liu, L. A. Archer, *J. Mater. Chem. A* **2019**, *7*, 7823.
[247] W. Liang, Y. Shao, Y.-M. Chen, Y. Zhu, *ACS Appl. Energy Mater.* **2018**, *1*, 6064.
[248] C. Wang, T. Wang, L. Wang, Z. Hu, Z. Cui, J. Li, S. Dong, X. Zhou, G. Cui, *Adv. Sci.* **2019**, *6*, 1901036.
[249] L. Qiao, Z. Cui, B. Chen, G. Xu, Z. Zhang, J. Ma, H. Du, X. Liu, S. Huang, K. Tang, S. Dong, X. Zhou, G. Cui, *Chem. Sci.* **2018**, *9*, 3451.
[250] Q. Wang, Z. Cui, Q. Zhou, X. Shangguan, X. Du, S. Dong, L. Qiao, S. Huang, X. Liu, K. Tang, X. Zhou, G. Cui, *Energy Storage Mater.* **2020**, *25*, 756.
[251] P. Jaumaux, Q. Liu, D. Zhou, X. Xu, T. Wang, Y. Wang, F. Kang, B. Li, G. Wang, *Angew. Chem., Int. Ed.* **2020**, *59*, 9134.
[252] S. Liu, J. Su, J. Zhao, X. Chen, C. Zhang, T. Huang, J. Wu, A. Yu, *J. Power Sources* **2018**, *393*, 92.
[253] J. Li, F. Huo, T. Chen, H. Yan, Y. Yang, S. Zhang, S. Chen, *Energy Storage Mater.* **2021**, *40*, 394.
[254] C. Zhan, T. Wu, J. Lu, K. Amine, *Energy Environ. Sci.* **2018**, *11*, 243.
[255] D. H. Jang, Y. J. Shin, S. M. Oh, *J. Electrochem. Soc.* **1996**, *143*, 2204.
[256] Y. Xia, Y. Zhou, M. Yoshio, *J. Electrochem. Soc.* **1997**, *144*, 2593.
[257] C. Zhan, J. Lu, A. Jeremy Kropf, T. Wu, A. N. Jansen, Y.-K. Sun, X. Qiu, K. Amine, *Nat. Commun.* **2013**, *4*, 2437.
[258] B. Aktekin, M. J. Lacey, T. Nordh, R. Younesi, C. Tengstedt, W. Zipprich, D. Brandell, K. Edström, *J. Phys. Chem. C* **2018**, *122*, 11234.
[259] C. Bolli, A. Guéguen, M. A. Mendez, E. J. Berg, *Chem. Mater.* **2019**, *31*, 1258.
[260] D. Aurbach, M. D. Levi, K. Gamulski, B. Markovsky, G. Salitra, E. Levi, U. Heider, L. Heider, R. Oesten, *J. Power Sources* **1999**, *81–82*, 472.
[261] W. Choi, A. Manthiram, *J. Electrochem. Soc.* **2006**, *153*, A1760.
[262] G. Amatucci, *Solid State Ionics* **1996**, *83*, 167.
[263] Q. Liu, B. Cai, S. Li, Q. Yu, F. Lv, F. Kang, Q. Wang, B. Li, *J. Mater. Chem. A* **2020**, *8*, 7197.
[264] D. Aurbach, B. Markovsky, G. Salitra, E. Markevich, Y. Talyossef, M. Koltypin, L. Nazar, B. Ellis, D. Kovacheva, *J. Power Sources* **2007**, *165*, 491.
[265] J. A. Gilbert, I. A. Shkrob, D. P. Abraham, *J. Electrochem. Soc.* **2017**, *164*, A389.
[266] I. Buchberger, S. Seidlmayer, A. Pokharel, M. Piana, J. Hattendorff, P. Kudejova, R. Gilles, H. A. Gasteiger, *J. Electrochem. Soc.* **2015**, *162*, A2737.
[267] D. Huang, C. Engtrakul, S. Nanayakkara, D. W. Mulder, S.-D. Han, M. Zhou, H. Luo, R. C. Tenent, *ACS Appl. Mater. Interfaces* **2021**, *13*, 11930.
[268] A. Blyr, A. Du Pasquier, G. Amatucci, J.-M. Tarascon, *Ionics* **1997**, *3*, 321.
[269] J.-H. Cho, J.-H. Park, M.-H. Lee, H.-K. Song, S.-Y. Lee, *Energy Environ. Sci.* **2012**, *5*, 7124.
[270] A. Banerjee, B. Ziv, Y. Shilina, S. Luski, I. C. Halalay, D. Aurbach, *Adv. Energy Mater.* **2017**, *7*, 1601556.
[271] M. Zhu, J. Wu, W. H. Zhong, J. Lan, G. Sui, X. Yang, *Adv. Energy Mater.* **2018**, *8*, 1702561.
[272] Y.-G. Cho, S. H. Jung, J. Jeong, H. Cha, K. Baek, J. Sung, M. Kim, H. T. Lee, H. Kong, J. Cho, S. J. Kang, J. M. Park, H.-K. Song, *ACS Appl. Mater. Interfaces* **2021**, *13*, 9965.
[273] T. Zhao, Y. Meng, R. Ji, F. Wu, L. Li, R. Chen, *J. Alloys Compd.* **2019**, *811*, 152060.
[274] T. Dong, H. Zhang, Y. Ma, J. Zhang, X. Du, C. Lu, X. Shangguan, J. Li, M. Zhang, J. Yang, X. Zhou, G. Cui, *J. Mater. Chem. A* **2019**, *7*, 24594.
[275] F. Bigoni, F. de Giorgio, F. Soavi, C. Arbizzani, *J. Electrochem. Soc.* **2017**, *164*, A6171.
[276] N. P. W. Pieczonka, V. Borgel, B. Ziv, N. Leifer, V. Dargel, D. Aurbach, J.-H. Kim, Z. Liu, X. Huang, S. A. Krachkovskiy, G. R. Goward, I. Halalay, B. R. Powell, A. Manthiram, *Adv. Energy Mater.* **2015**, *5*, 1501008.
[277] D. W. McOwen, D. M. Seo, O. Borodin, J. Vatamanu, P. D. Boyle, W. A. Henderson, *Energy Environ. Sci.* **2014**, *7*, 416.
[278] H. Yang, K. Kwon, T. M. Devine, J. W. Evans, *J. Electrochem. Soc.* **2000**, *147*, 4399.
[279] Q. Li, N. Imanishi, Y. Takeda, A. Hirano, O. Yamamoto, *Ionics* **2002**, *8*, 79.
[280] D. T. Hallinan, A. Rausch, B. McGill, *Chem. Eng. Sci.* **2016**, *154*, 34.
[281] K. Matsumoto, K. Inoue, K. Nakahara, R. Yuge, T. Noguchi, K. Utsugi, *J. Power Sources* **2013**, *231*, 234.
[282] C.-Z. Zhao, Q. Zhao, X. Liu, J. Zheng, S. Stalin, Q. Zhang, L. A. Archer, *Adv. Mater.* **2020**, *32*, 1905629.
[283] T. Kawamura, T. Tanaka, M. Egashira, I. Watanabe, S. Okada, J. I. Yamaki, *Electrochem. Solid-State Lett.* **2005**, *8*, A459.
[284] B. Garcia, M. Armand, *J. Power Sources* **2004**, *132*, 206.
[285] L. J. Krause, W. Lamanna, J. Summerfield, M. Engle, G. Korba, R. Loch, R. Atanasoski, *J. Power Sources* **1997**, *68*, 320.
[286] K. Kanamura, *J. Power Sources* **1999**, *81–82*, 123.
[287] H.-B. Han, S.-S. Zhou, D.-J. Zhang, S.-W. Feng, L.-F. Li, K. Liu, W.-F. Feng, J. Nie, H. Li, X.-J. Huang, *J. Power Sources* **2011**, *196*, 3623.
[288] J. Wang, Y. Yamada, K. Sodeyama, C. H. Chiang, Y. Tateyama, A. Yamada, *Nat. Commun.* **2016**, *7*, 3623.
[289] L. Qiao, U. Oteo, M. Martinez-Ibañez, A. Santiago, R. Cid, E. Sanchez-Diez, E. Lobato, L. Meabe, M. Armand, H. Zhang, *Nat. Mater.* **2022**, *21*, 455.
[290] T. M. Nguyen, J. Suk, Y. Kang, *J. Electrochem. Sci. Technol.* **2019**, *10*, 250.
[291] K. Karthik, R. Murugan, *J. Solid State Electrochem.* **2018**, *22*, 2989.
[292] G. Liang, V. K. Peterson, K. W. See, Z. Guo, W. K. Pang, *J. Mater. Chem. A* **2020**, *8*, 15373.
[293] Q. Li, Y. Wang, X. Wang, X. Sun, J.-N. Zhang, X. Yu, H. Li, *ACS Appl. Mater. Interfaces* **2020**, *12*, 2319.
[294] Y. Zhao, Y. Bai, W. Li, A. Liu, M. An, Y. Bai, G. Chen, *Chem. Eng. J.* **2020**, *394*, 124847.
[295] Q. Wang, W.-L. Song, L.-Z. Fan, Y. Song, *J. Membr. Sci.* **2015**, *486*, 21.
[296] M. Chen, C. Ma, Z. Ding, L. Zhou, L. Chen, P. Gao, W. Wei, *ACS Energy Lett.* **2021**, *6*, 1280.
[297] J. R. Nair, I. Shaji, N. Ehteshami, A. Thum, Di. Diddens, A. Heuer, M. Winter, *Chem. Mater.* **2019**, *31*, 3118.
[298] L. Li, J. Wang, L. Zhang, H. Duan, Y. Deng, G. Chen, *Energy Storage Mater.* **2022**, *45*, 1062.
[299] M. Zhu, J. Wu, B. Liu, W.-H. Zhong, J. Lan, X. Yang, G. Sui, *J. Membr. Sci.* **2019**, *588*, 117194.

[300] Y. Zhou, X. Wang, H. Zhu, M. Armand, M. Forsyth, G. W. Greene, J. M. Pringle, P. C. Howlett, *Energy Storage Mater.* **2018**, *15*, 407.
[301] F. Xu, S. Deng, Q. Guo, D. Zhou, X. Yao, *Small Methods* **2021**, *5*, 2100262.
[302] S. L. Beshahwured, Y.-S. Wu, T. B. Truong, R. Jose, C.-C. Yang, *Chem. Eng. J.* **2021**, *426*, 131850.
[303] F. Chen, M. Jing, H. Yang, W. Yuan, M. Liu, Y. Ji, S. Hussain, X. Shen, *Ionics* **2021**, *27*, 1101.
[304] M. Wu, Z. Shan, B. Xu, G. Zhang, *Chem. Eng. J.* **2022**, *427*, 131728.
[305] P. Cheng, H. Zhang, Q. Ma, W. Feng, H. Yu, X. Huang, M. Armand, Z. Zhou, *Electrochim. Acta* **2020**, *363*, 137198.
[306] F. He, W. Tang, X. Zhang, L. Deng, J. Luo, *Adv. Mater.* **2021**, *33*, 2105329.
[307] M. Jia, P. Wen, Z. Wang, Y. Zhao, Y. Liu, J. Lin, M. Chen, X. Lin, *Adv. Funct. Mater.* **2021**, *31*, 2101736.
[308] A. Hosseinioun, E. Paillard, *J. Membr. Sci.* **2020**, *594*, 117456.
[309] M. Z. Kufian, M. F. Aziz, M. F. Shukur, A. S. Rahim, N. E. Ariffin, N. E. A. Shuhaimi, S. R. Majid, R. Yahya, A. K. Arof, *Solid State Ionics* **2012**, *208*, 36.
[310] S. Yu, S. Schmohl, Z. Liu, M. Hoffmeyer, N. Schön, F. Hausen, H. Tempel, H. Kungl, H.-D. Wiemhöfer, R.-A. Eichel, *J. Mater. Chem. A* **2019**, *7*, 3882.
[311] Z. Xie, Z. Wu, X. An, X. Yue, P. Xiaokaiti, A. Yoshida, A. Abudula, G. Guan, *J. Membr. Sci.* **2020**, *596*, 117739.
[312] W. Xiao, Z. Wang, Y. Zhang, R. Fang, Z. Yuan, C. Miao, X. Yan, Y. Jiang, *J. Power Sources* **2018**, *382*, 128.
[313] J. Liu, X. Shen, J. Zhou, M. Wang, C. Niu, T. Qian, C. Yan, *ACS Appl. Mater. Interfaces* **2019**, *11*, 45048.
[314] Z. Wang, K. Yang, Y. Song, H. Lin, K. Li, Y. Cui, L. Yang, F. Pan, *Nano Res.* **2020**, *13*, 2431.
[315] M.-J. Lee, S. Lee, V. Roev, D. Im, W. Choi, M.-S. Kang, *Ionics* **2020**, *26*, 4795.
[316] F. Marken, A. Neudeck, A. M. Bond, in *Electroanalytical methods: Guide to experiments and applications* (Eds: F. Scholz), Springer Berlin, Heidelberg, Germany **2010**, Ch. II.1.
[317] J. Kasnatscheew, B. Streipert, S. Röser, R. Wagner, I. Cekic Laskovic, M. Winter, *Phys. Chem. Chem. Phys.* **2017**, *19*, 16078.
[318] K. Xu, S. P. Ding, T. R. Jow, *J. Electrochem. Soc.* **1999**, *146*, 4172.
[319] G. Hernández, I. L. Johansson, A. Mathew, C. Sångeland, D. Brandell, J. Mindemark, *J. Electrochem. Soc.* **2021**, *168*, 100523.
[320] M. P. S. Mousavi, A. J. Dittmer, B. E. Wilson, J. Hu, A. Stein, P. Bühlmann, *J. Electrochem. Soc.* **2015**, *162*, A2250.
[321] T. Ma, G. L. Xu, Y. Li, L. Wang, X. He, J. Zheng, J. Liu, M. H. Engelhard, P. Zapol, L. A. Curtiss, J. Jorne, K. Amine, Z. Chen, *J. Phys. Chem. Lett.* **2017**, *8*, 1072.
[322] A. Mathew, M. J. Lacey, D. Brandell, *J. Power Sources Adv.* **2021**, *11*, 100071.
[323] K. Xu, M. S. Ding, T. Richard Jow, *Electrochim. Acta* **2001**, *46*, 1823.
[324] S. H.-S. Cheng, C. Liu, F. Zhu, L. Zhao, R. Fan, C.-Y. Chung, J. Tang, X. Zeng, Y.-B. He, *Nano Energy* **2021**, *80*, 105562.
[325] X. Li, L. Cong, S. Ma, S. Shi, Y. Li, S. Li, S. Chen, C. Zheng, L. Sun, Y. Liu, H. Xie, *Adv. Funct. Mater.* **2021**, *31*, 2010611.
[326] J. Song, *J. Power Sources* **2002**, *111*, 255.
[327] A. Lasia, *Electrochemical Impedance Spectroscopy and its Applications*, Springer New York, New York, NY, USA **2014**.
[328] T. Waldmann, A. Iturrondobeitia, M. Kasper, N. Ghanbari, F. Aguesse, E. Bekaert, L. Daniel, S. Genies, I. J. Gordon, M. W. Löble, E. De Vito, M. Wohlfahrt-Mehrens, *J. Electrochem. Soc.* **2016**, *163*, A2149.
[329] J. R. Nair, F. Colò, A. Kazzazi, M. Moreno, D. Bresser, R. Lin, F. Bella, G. Meligrana, S. Fantini, E. Simonetti, G. B. Appetecchi, S. Passerini, C. Gerbaldi, *J. Power Sources* **2019**, *412*, 398.
[330] A. K. Łasińska, M. Marzantowicz, J. R. Dygas, F. Krok, Z. Florjańczyk, A. Tomaszewska, E. Zygadło-Monikowska, Z. Żukowska, U. Lafont, *Electrochim. Acta* **2015**, *169*, 61.
[331] G. Chen, F. Zhang, Z. Zhou, J. Li, Y. Tang, *Adv. Energy Mater.* **2018**, *8*, 1801219.
[332] X. Liu, Y. Ren, L. Zhang, S. Zhang, *Front. Chem.* **2019**, *7*, 421.
[333] S. Wang, Q. Li, M. Bai, J. He, C. Liu, Z. Li, X. Liu, W. Lai, L. Zhang, *Electrochim. Acta* **2020**, *353*, 136604.
[334] C. Sångeland, J. Mindemark, R. Younesi, D. Brandell, *Solid State Ionics* **2019**, *343*, 115068.
[335] C. Xu, B. Sun, T. Gustafsson, K. Edström, D. Brandell, M. Hahlin, *J. Mater. Chem. A* **2014**, *2*, 7256.
[336] P. Wang, W. Qu, W. Song, H. Chen, R. Chen, D. Fang, *J. Mater. Chem. A* **2014**, *2*, 7256.
[337] Y. Ma, Q. Sun, Z. Wang, S. Wang, Y. Zhou, D. Song, H. Zhang, X. Shi, C. Li, L. Zhang, L. Zhu, *J. Mater. Chem. A* **2021**, *9*, 3597.
[338] H. Jia, H. Onishi, N. von Aspern, U. Rodehorst, K. Rudolf, B. Billmann, R. Wagner, M. Winter, I. Cekic-Laskovic, *J. Power Sources* **2018**, *397*, 343.
[339] F. J. Simon, M. Hanauer, A. Henss, F. H. Richter, J. Janek, *ACS Appl. Mater. Interfaces* **2019**, *11*, 42186.
[340] Q. Liu, Y. Liu, X. Jiao, Z. Song, M. Sadd, X. Xu, A. Matic, S. Xiong, J. Song, *Energy Storage Mater.* **2019**, *23*, 105.
[341] B. Hu, X. Lou, C. Li, F. Geng, C. Zhao, J. Wang, M. Shen, B. Hu, *J. Power Sources* **2019**, *438*, 226954.
[342] S. Munoz, S. Greenbaum, *Membranes* **2018**, *8*, 120.
[343] G. Foran, N. Verdier, D. Lepage, C. Malveau, N. Dupré, M. Dollé, *Polymers* **2021**, *13*, 1207.
[344] J. Bareño, N. Dietz Rago, F. Dogan, D. G. Graczyk, Y. Tsai, S. R. Naik, S.-D. Han, E. Lee, Z. Du, Y. Sheng, J. Li, D. L. Wood, L. A. Steele, J. Lamb, S. Spangler, C. Grosso, K. Fenton, I. Bloom, *J. Power Sources* **2018**, *385*, 165.
[345] M. Cuisinier, J.-F. Martin, P. Moreau, T. Epicier, R. Kanno, D. Guyomard, N. Dupré, *Solid State Nucl. Magn. Reson.* **2012**, *42*, 51.
[346] J. Lee, N. Dupre, M. Avdeev, B. Kang, *Sci. Rep.* **2017**, *7*, 6728.
[347] S. Haber, M. Leskes, *Adv. Mater.* **2018**, *30*, 1706496.
[348] H. J. Chang, N. M. Trease, A. J. Ilott, D. Zeng, L.-S. Du, A. Jerschow, C. P. Grey, *J. Phys. Chem. C* **2015**, *119*, 16443.
[349] H. J. Chang, A. J. Ilott, N. M. Trease, M. Mohammadi, A. Jerschow, C. P. Grey, *J. Am. Chem. Soc.* **2015**, *137*, 15209.
[350] L. E. Marbella, S. Zekoll, J. Kasemchainan, S. P. Emge, P. G. Bruce, C. P. Grey, *Chem. Mater.* **2019**, *31*, 2762.
[351] M. A. Hope, B. L. D. Rinkel, A. B. Gunnarsdóttir, K. Märker, S. Menkin, S. Paul, I. V Sergeyev, C. P. Grey, *Nat. Commun.* **2020**, *11*, 2224.

Maria Angeles Cabañero Martínez is a postdoctoral researcher at CIC energiGUNE. She was awarded her Ph.D. in electric engineering by the University of Ulm in 2019, and has previously worked as a researcher at Fraunhofer ISC and ICT, focused on the degradation of commercial Li-ion batteries and planning a pilot plant for the production of new lithium technologies. Her main research interests are the study of degradation mechanisms and electrochemical processes in Li-ion batteries. She has over 10 years of experience working in the R&D battery field, with a focus on the development of new battery materials and systems.

Nicola Boaretto is a postdoctoral researcher at CIC energiGUNE. He obtained a Ph.D. in Materials Science and Engineering (2016) at the University of Padua, in collaboration with the Fraunhofer Institute of Silicate Research. Between 2008 and 2010 he worked on the development of proton exchange membranes for fuel cells. In 2012, he started his Ph.D. project on polymer electrolytes for lithium metal batteries. In 2018 he moved to the IMDEA Energy Institute, where he developed flexible, multifunctional lithium-ion batteries. Finally, in 2019 he joined the CIC energiGUNE, where he is currently working on lithium polymer batteries.

Andrew J. Naylor is a researcher at the Department of Chemistry–Ångström and the Ångström Advanced Battery Centre at Uppsala University. He was awarded his Ph.D. in Chemistry by the University of Southampton in 2014 and went on to perform postdoctoral studies at the University of St Andrews and University of Oxford. Andy's main interests are in studying the chemistry of interfaces within energy storage devices, predominantly lithium-ion batteries as well as next-generation technologies. A particular focus is on the use and development of surface analysis characterization techniques, especially in the investigation of new materials and electrolytes.

Francisco Alcaide holds a Ph.D. in Chemistry (Electrochemistry) from the University of Barcelona. He has more than 25 years of experience in electrochemical technologies, especially in batteries, fuel cells & hydrogen technologies. He is specialized in electronics and electrocatalysis at the electrochemical interfaces. He has led many R&I projects (national, European, and international) and contracts with companies, in addition to technology transfer and innovation. Invited expert and advisor for several (inter)national public bodies, currently, he is involved in the European projects: DEFACTO, CoFBAT, BIG-MAP, and Battery 2030PLUS. Dr. Alcaide works as Principal Investigator – Project manager at CIDETEC Energy Storage.

Girish D. Salian received his Ph.D. in 2018 from Aix-Marseille University, Marseille, France in the field of Li-ion microbatteries. Prior to starting his Ph.D., he worked as a Research Engineer for the battery pilot line facility at National University of Singapore (NUS). After his Ph.D. he worked as a postdoctoral researcher at Ångström Advanced Battery Centre (ÅABC), Uppsala University, Sweden. His main area of work at Uppsala University was electrolytes for high-voltage cathode materials. Currently, he is working as a Business Development Engineer at ALTRIS. His interests include electrolytes (polymer and liquid), high-voltage cathode materials, and nanostructures for Li-ion microbatteries.

Flavia Palombarini holds a master's in Electrochemistry provided by both the Autonomous University of Barcelona (UAB) and the National Microelectronic Institute (Spain, CNM-CSIC). Her research has been focused on the study and improvement of energy storage devices such as lithium-sulfur batteries and redox flow batteries. Since 2017, she is working in the R&D department of LEITAT in the areas of surface treatments, material science, nanotechnology, and energies with deep knowledge and experience in technological transfers to several industrial sectors. She has also started developing her Ph.D. in Physics at CIC energiGUNE, University of Basque country (UPV) and LEITAT.

Elixabete Ayerbe obtained a degree in Chemical Engineering at the University of Zaragoza and a Master's in Industrial Mathematics at the Universidad Politécnica de Madrid. After several years working in research centers, in 2007 she started as a project manager at CIDETEC. Currently, she leads the modeling and post-mortem group of the energy unit, focused on the development of models, characterization, and post-mortem analysis of batteries. She is coordinator of the European project DEFACTO, on digitization of battery manufacturing processes, and is strongly involved in the BIG-MAP project and the Battery2030+ initiative, in the latter as Thematic Leader of Manufacturability.

Mateu Borràs Argemí has a degree in Chemistry from the University Autónoma de Barcelona-UAB (2012–2016). He courses a Master's Degree in Electrochemistry at the Universidad Autónoma de Madrid-UAM (2016–2017). There he was an intern in the Electrochemistry research group where he worked in LI-ion and Al-Air batteries for. Afterwards, he follows his career at LEITAT, as a R&D Researcher in the Energy Storage group. Specialized in post Li batteries and Supercapacitors focusing research on the development of new materials, processes, and electrochemical characterization. Since October 2021 he is working at Arkyne Technologies (Bioo) developing Soil Microbial Fuel Cells (SMFC).

Montse Casas-Cabanas is the scientific coordinator of the Electrochemical Energy Storage Area and group leader of the Advanced Electrode Materials group at CIC energiGUNE. Her research interests focus on the design of battery materials and the understanding of phenomena that occur in energy storage devices through a multidisciplinary approach, with a focus on crystal chemistry. She has about 20 years of experience in several battery technologies (Li-ion, Na-ion, solid state batteries, Ni-MH, etc.). She has been recently awarded the 2021 Young Researcher award from the Spanish Royal Society of Chemistry.